DISSECTING THE SPATIOTEMPORAL REGULATION OF NODAL SIGNALING AND ITS ROLE AS A MORPHOGENETIC CUE

By

Angela M. Halstead

Dissertation

Submitted to the Faculty of the

Graduate School of Vanderbilt University

in partial fulfillment of the requirements

for the degree of

DOCTOR OF PHILOSOPHY

in

Cell and Developmental Biology

December, 2014

Nashville, Tennessee

Approved:

Chin Chiang, Ph.D.

Guoqiang Gu, Ph.D.

Doug Mortlock, Ph.D.

Christopher V. E. Wright, D.Phil.

ACKNOWLEDGEMENTS

I would like to thank Chris for serving as my mentor, providing a rigorous academic environment in which to study, and not allowing me to get away with anything less than my best effort. I would also like to thank the members of my thesis committee, Chin Chiang, Guoqiang Gu, Doug Mortlock, Josh Gamse, and Trish Labosky, and members of the Wright Lab, especially Mike Ray. Finally, to family and friends, whose support has never wavered during this process.

TABLE OF CONTENTS

Page

LIST OF FIGURES

LIST OF TABLES

CHAPTER I

INTRODUCTION

Embryonic development involves precise regulation and coordination of multiple patterning events that are directed by a core set of signaling pathways, one of which is Nodal signaling. Essential to development, Nodal signaling participates in early embryonic patterning and body axis formation. Nodal was first identified during a genetic screen of transgenic mice with retrovirally induced genetic mutations designed to identify genes required for embryonic development (Conlon et al., 1991). Embryos harboring the 413-d insertional mutation failed to develop past gastrulation due to defects in cell lineage allocation and mesendoderm specification. The 413-d insertion site was later identified to encode *Nodal,* so named for its expression in the node (Zhou et al., 1993). Identification of Nodal homologs in other species made it clear that Nodal and its importance in germ layer specification, gastrulation, anterior-posterior (A-P) axis formation, and left-right (L-R) patterning was highly conserved among vertebrates (Erter et al., 1998; Jones et al., 1995; Levin et al., 1995; Long et al., 2003; Sampath et al., 1998). Nodal orthologs have even been identified in the non-chordate deuterostome sea urchin, where Nodal signaling patterns the oral and aboral axis, and the non-chordate species *Lottia gigantea* and *Biomphalaria glabrata*. In these two species of snails, *Nodal* expression is linked to the chirality of the shell, with *Nodal* expressed on the right side of dextral (rightward shell coiling) species (*L. gigantea*) and on the left side of sinistral (leftward shell coiling) species (*B. glabrata*) (Grande and Patel, 2009). While great strides have been made in deciphering the Nodal pathway over the past 20 years, many mysteries remain. The work presented here

focuses on two under-studied aspects of Nodal signaling: the transcriptional repression of *Nodal* and the role of Nodal signaling as a morphogenetic cue during asymmetric morphogenesis.

Nodal signaling pathway

TGF-β superfamily ligands and receptors

Nodal is a member of the transforming growth factor-β (TGF-β) superfamily, which consists of over 30 members including, in addition to Nodal, bone morphogenetic proteins (BMPs), growth and differentiation factors (GDFs), TGF-β proteins, Activin, Leftys, and anti-Müllerian hormone (AMH) (Shi and Massagué, 2003). TGF-β superfamily ligands participate in an array of diverse processes in both the developing embryo and in adult homeostasis. Specific processes regulated by TGF-β family members include differentiation, morphogenesis, cell proliferation and migration, apoptosis, and disease in both vertebrates and non-vertebrates alike (reviewed in Wu and Hill, 2009).

TGF-β ligands are translated as proproteins, which are cleaved into a prodomain and mature ligand by SPC-class convertases (Furin and PACE4 cleave Nodal) (Constam and Robertson, 2000). Members of the TGF-β family are also characterized by the presence of multiple cysteines capable of forming intramolecular and intermolecular disulfide bounds. Internal disulfide bounds form a cystine knot (3 disulfide bridges) in the mature ligand polypeptide, a hallmark of TGF-β ligands. Intermolecular disulfide bridges support and stabilize the formation of dimers (Derynck and Miyazono, 2008). Lefty proteins, however, only have six cysteines and are not able to form an intermolecular bridge and, therefore, exist only as monomers

(Moustakas and Heldin, 2009). TGF-β family members primarily form homodimers; however, heterodimerization between Nodal and Gdf1 has been reported under conditions of overexpression in *Xenopus* embryos (Tanaka et al., 2007). A Nodal-Gdf1 interaction is further suggested by the lack of *Nodal* expression in the LPM and defects in organ situs in Gdf1$^{-/-}$ embryos (Rankin et al., 2000). In an assay for Nodal long-range activity, only lipofection of *Nodal* and *Gdf1* expression vectors together, and not separately, into the R LPM of *Gdf1*$^{-/-}$ embryos restored *Lefty1* expression in the midline, suggesting that Nodal-Gdf1 dimerization is required for long-range Nodal signaling during L-R patterning (Tanaka et al., 2007).

TGF-β members are roughly divided by co-receptor interactions and downstream signal transducer activation into two subfamilies: BMP (encompassing GDFs and AMH) and TGF-β/Activin/Nodal. All TGF-β superfamily ligands interact with type I and type II serine/threonine kinase receptors, of which there are a total of twelve: seven type I receptors, and five type II receptors (Shi and Massagué, 2003). The mammalian type I receptors are activin-like kinase receptor (ALK) 1-7. For simplicity, the BMP subfamily is usually quoted as signaling through ALK1/2/3/6 while the TGF-β/Activin/Nodal subfamily signals through ALK4/5/7, with ALK4 and ALK7 being the primary receptors for Nodal (Moustakas and Heldin, 2009; Reissmann et al., 2001). Ligand and receptor pairings, however, are not this straightforward, as most type I receptors can bind ligands from either subfamily depending on the developmental/tissue context. Binding to type II receptors is not as promiscuous, but some overlap does exist. For example, Activin and Nodal specifically interact with the type II receptors ActRIIA and ActRIIB, which also bind members of the BMP subfamily ligands, although BMPs primarily signal through the type II receptor BMPRII. In TGF-β/Activin/Nodal signaling receptor activation begins with

the binding of ligands to a pair of type II receptors. This interaction then recruits dimerized type I receptors to the ligand-type II receptor complex, prompting phosphorylation and activation of the cytoplasmic kinase domain of the type I receptor by the type II receptor (Moustakas and Heldin, 2009).

In order to fully engage the cell surface receptors, Nodal, but for some unknown reason not Activin, requires the aid of the epidermal growth factor-Cripto/FRL-1/Cryptic (EGF-CFC) co-receptor family (Shen and Schier, 2000). EGF-CFC co-receptors bind the type I receptor to facilitate binding between Nodal and the type I/II receptor complex (Yan et al., 2002; Yeo and Whitman, 2001). The two EGF-CFC members in mouse, Cryptic and Cripto, display non-overlapping expression patterns, with *Cripto* being expressed similar to *Nodal* in the epiblast (first uniform than proximal distal gradient, primitive streak) during gastrulation and A-P pattering. *Cryptic* is also expressed in the primitive streak and axial mesoderm during gastrulation, but is later expressed in the node and then symmetrically in the lateral plate mesoderm (LPM) during stages of L-R patterning (Shen and Schier, 2000). Disruption of *Cripto* causes defects in A-P patterning (Ding et al., 1998; Xu et al. 1999), while deletion of *Cryptic* causes L-R patterning defects (Gaio et al. 1999; Yan et al., 1999). The requirement for a co-receptor is conserved across vertebrate species as evidenced by the identification of *one-eye-pinhead* in fish, *FRL-1* in frog, and *Cripto* in chicken (Yeo and Whitman, 2001).

Nodal signal transduction through Smads

Activated type I receptors phosphorylate and activate Smads, the downstream signal transducers for the TGF-β superfamily. There are three types of Smad proteins: co-Smad

(Smad4), regulatory (R) Smads (Smad1/2/3/5/8), and inhibitory (I) Smads (Smad6/7). Only R-Smads contain the phosphorylatable C-terminal motif, SSXS. Smads1/5/8 are considered the downstream effectors of the BMP subfamily and are only phosphorylated by type I receptors ALK1/2/3/6. Smads2/3 are the downstream effector for the TGF-β/Activin/Nodal subfamily and are phosphorylated by ALK4/5/7 (reviewed in Attisano and Wrana, 2000). Recruitment of Smad2/3 to the type I/II receptor complex is facilitated by SARA (Smad anchor for receptor activation). SARA simultaneously binds unphosphorylated Smad2/3 and the cell membrane, bringing the R-Smads into close vicinity of the receptor complex. Phosphorylation of the C-terminal SSXS motif triggers SARA to release the now phosphorylated Smad (pSmad), which then forms a complex with the co-Smad, Smad4. R- and co-Smads exist as a heterotrimeric complex consisting of two R-Smads and one Smad4. This complex translocates to the nucleus where it can modify the open and closed state of chromatin by recruiting co-activators or repressors to the desired locus (Attisano and Wrana, 2000) (Fig. 1.1). Activation of R-smads and formation of the R-Smad/Smad4 complex can be inhibited by the I-Smads, Smad6 and Smad7, which interfere with R-Smad-receptor and Smad-Smad interactions (Massagué et al., 2005). Smad7 can inhibit both TGF-β/Activin/Nodal and BMP subfamily receptors, while Smad6 is thought to be specific to BMP subfamily receptors (Attisano and Wrana, 2000).

Smad interactions are mediated by two conserved domians, an N-terminal Mad-homology (MH) 1 domain and a C-terminal MH2 domain. These domains are separated by a less-conserved linker region, which contains phosphorylation and ubiquitin-binding sites that facilitate cross-talk with other signaling pathways and degradation, respectively (Massagué et al., 2005). The MH1 domain can bind directly to DNA and DNA-binding proteins. It also contains a nuclear-

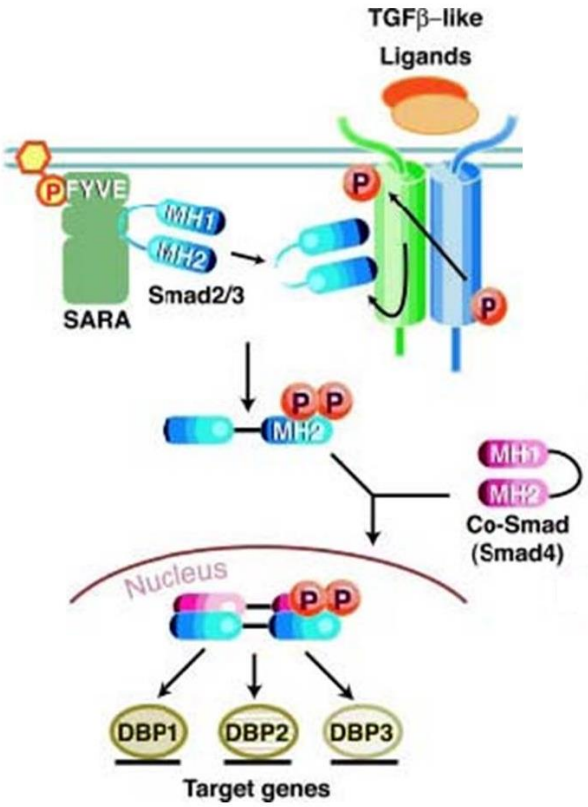

Fig. 1.1 TGF-β/Smad2/3 signaling pathway.
Adapted from Attisano and Wrana, 2002.

localization sequence (NLS). The MH2 domain mediates protein-protein interactions with the type I/II receptor complex, SARA, Smad4, transcription factors, and transcriptional co-factors (Attisano and Wrana, 2000).

All Smads, with the exception of full-length Smad2, can bind DNA directly through the MH1 domain, but they do so with low specificity and affinity. Smads bind the canonical Smad-binding element (SBE) sequence GTCT or its complement AGAC, but degenerate sequences (GNCN) can also be recognized. The inability of full-length Smad2, the most abundant splice variant of Smad2, to bind DNA is due to an insertion in the MH1 domain encoded by exon 3. A naturally occurring splice variant in which exon 3 is deleted has its DNA-binding ability restored. Because the SBE is common throughout the genome, and Smads weakly bind it, most Smads are recruited to specific regions of DNA through interactions with other transcription factors (reviewed in Massagué).

Although both Smad2 and Smad3 are capable of transducing TGF-β/Activin/Nodal signaling from cell-surface receptors to the nucleus, it is unknown if they have an equal propensity to do so. Global deletion of *Smad2* (Waldrip et al., 1998) in the developing mouse embryo results in embryonic lethality caused by defects similar to, but definitively not as severe as those seen in embryos lacking *Nodal* (Conlon et al., 1994; Zhou et al., 1993). Deletion of *Smad3*, however, does not result in developmental defects (Datto et al., 1999; Zhu et al., 1998), suggesting that either Smad2 compensates for loss of Smad3 during development, or that Smad3 is not a primary transducer of Nodal signaling. Although these results suggest that Nodal primarily signals through Smad2, the ability of Smad3 to participate in Nodal signaling has not been fully

excluded. Therefore, signal transduction of Foxh1-dependent Nodal signaling is assumed to occur through pSmad2 and pSmad3, which will be collectively referred to as "pSmad2"from here onward.

In the nucleus, the pSmad2/Smad4 complex interacts with several binding partners in response to Nodal signaling. Such partners include members of the Mix family, Mixer and Milk (*Xenopus*) and Bon (zebrafish), which are involved in mesendoderm induction , but this role may not be conserved as the mouse homolog, Mixl1, has not been shown to interact with pSmad2 (Germain et al., 2000; Kunwar et al., 2003; Randall et al., 2002). The first transcriptional partner identified for pSmad2 was Foxh1, and it remains the most well characterized transcription factor in Nodal signaling (Liu et al., 1999; Osada et al., 2000). Formerly called FAST1 (forkhead activin signal transducer), Foxh1 was first identified in *Xenopus* because of its ability to bind to the activin response element (ARE) of the gene *Mix.2*, which is induced in response to Nodal signaling (or Activin signaling as a surrogate) during mesendoderm formation (Chen et al., 1996). Foxh1 belongs to the winged-helix family of transcription factors. It consists of three domains: a winged-helix or forkhead box DNA binding domain, an Engrailed homology-1 (EH1) domain for facilitating interactions with the Groucho family of co-repressors, and a Smad interaction domain (SID) (Yaklichkin et al., 2007a) (see Fig. 5.3A). Only the DNA-binding domain shows similarity to other winged-helix transcription factors (Liu et al., 1999).

Together with pSmad2 and Smad4, Foxh1 forms the Activin response factor (ARF), which binds the Foxh1 consensus sequence TGT G/T T/G ATT contained within the ARE of all target genes (Attisano et al., 2001). A similar *cis*-regulatory element termed the asymmetric enhancer (ASE)

is the mammalian equivalent of the frog ARE. In the ARF, only pSmad2 directly binds Foxh1, an interaction facilitated through the MH2 domain and SID of pSmad2 and Foxh1, respectively. While Smad4 does not directly contact Foxh1, Smad4 DNA binding sites have been identified adjacent to the Foxh1-binding consensus sequence in the ARE of *Goosecoid* and *Mix.*2 in *Xenopus* (Chen et al., 1996), and also in the ASE of mouse *Nodal* and *Lefty2* (Saijoh et al., 2000). Smad4-DNA interactions near Foxh1 binding sites are thought to help stabilize the ARF, but unlike Foxh1-pSmad2 binding, these interactions are not required for transcriptional activation of target genes (Labbé et al., 1998; Yeo et al., 1999). Genes targeted by Nodal/Smad2/Foxh1 signaling include *Mix.2*, *Goosecoid*, *Foxa2*, *Nodal* itself, *Lefty2*, and *Pitx2* (Whitman, 2001). Much work has been done to elucidate the role of Foxh1 in the transcriptional activation of Nodal target genes through its interaction with pSmad2, but it has recently been proposed that Foxh1 may also repress transcription by interacting with co-repressors through the EH1 motif. This concept is discussed in more detail in Chapter V.

Nodal signaling in development and adult homeostasis

Germ layer specification, gastrulation, A-P axis formation

Nodal is a key regulator of body axis formation and patterning in the developing vertebrate embryo. Specifically, Nodal signaling is essential during two distinct developmental time points: (1) early patterning events that consist of germ layer specification, gastrulation, and anterior-posterior (A-P) axis formation, and (2) a later patterning event that establishes left-right (L-R) asymmetry across the embryo (Lu et al., 2001; Schier and Shen, 1999). Nodal was first identified during a screen of retrovirally-induced insertional mutations in mouse embryos to

identify novel genes essential for early development (Zhou et al., 1993). Nodal-related proteins have since been identified in chick (Cnr1) (Levin et al., 1995), frog (Xnr1, 2, 3, 4, 5, 6) (Jones et al., 1995; Joseph and Melton 1997; Takahashi et al. 2000), and zebrafish (Squint, Cyclops, Southpaw) (Erter et al., 1998; Long et al., 2003; Sampath et al., 1998). The presence of multiple Nodal paralogs in *Xenopus* and zebrafish is attributed to genome duplication events in these species. These Nodal-related proteins have evolved different functional capacities during development, divvying the multiple activities performed by one mouse gene among the paralogs. For example, in zebrafish, *Squint* and *Cyclops* are active during early patterning events, while *Southpaw* is the primary *Nodal*-related gene expressed during L-R specification. Similarly, in *Xenopus*, *Xnr1*, *2*, *4*, *5*, *6* (note not *Xnr3*) are involved in germ layer formation and gastrulation, but only *Xnr1* is expressed later, to then participate in the establishment of L-R asymmetry (reviewed in Schier, 2009). The involvement of *Xnr1* in early axis patterning, gastrulation, and L-R patterning makes it most like mouse Nodal. Xnr3 does not function like the other Xnrs as it lacks mesoderm-inducing potential and specifies neural tissue in animal caps (Hansen et al., 1997). Xnr3 activity may also promote morphogenesis, as *Xnr3* expression in *Xenopus* animal pole cells resulted in the projection of tube-like extensions from the animal cap (Smith et al., 1995). Because my thesis work was performed in both mouse and *Xenopus*, the developmental role of Nodal signaling in both of these species is briefly summarized below. Axis specification in mouse begins at embryonic day (E) 5.0 with the induction of *Nodal* expression in the epiblast by signals emanating from the adjacent extraembryonic ectoderm (ExE). Nodal proprotein translated from *Nodal* transcripts in the epiblast can induce expression of the convertase *Furin* in the ExE, resulting in the cleavage and activation of the Nodal ligand in

the neighboring epiblast. Nodal signaling then activates BMP4, also localized in the ExE, which activates Wnt3 in the epiblast. Wnt signaling feeds back onto *Nodal*, activating its expression through the Wnt-responsive proximal epiblast enhancer (PEE). This feedback between the epiblast and ExE, as well as the subsequent activation of a feed-forward loop through which Nodal induces its own expression, causes expansion of the *Nodal* expression territory throughout the epiblast. In the tip of the epiblast, Nodal signals to the distal visceral endoderm (DVE), where it induces the expression of *Lefty1* and *Cerl*, two feedback inhibitors of Nodal signaling. The graded expression of Lefty1 and Cer1 terminate *Nodal* expression progressively from the tip of the epiblast toward the epiblast-ExE boundary, establishing a proximal-distal gradient of *Nodal* expression across the embryo, thus establishing the proximal-distal (P-D) axis (Fig. 1.2A).

At E6.0, the cells constituting the DVE migrate to the future anterior side of the embryo where it establishes the anterior visceral endoderm (AVE) and continues to express *Lefty1* and *Cer1*. This rotation further suppresses *Nodal* expression, restricting it to the proximal and future posterior side of the embryo, and is now understood as a critical role in establishing the A-P axis. It is in this proximal-posterior region where Nodal signaling initiates the formation of the primitive streak, and the cells in this region are responsible for a pioneer role in commencing gastrulation. As gastrulation proceeds, the primitive streak, while expressing *Nodal*, elongates to the distal tip of the embryo (Fig. 1.2A) as lateral epiblast cells migrate towards the streak, and undergo epithelial-to-mesenchymal transition (EMT). The location of the ingression point, and the time elapsing before ingression occurs, determines the amount of exposure to Nodal signaling, and thus determines future germ-layer cell lineage. Cells that ingress first through

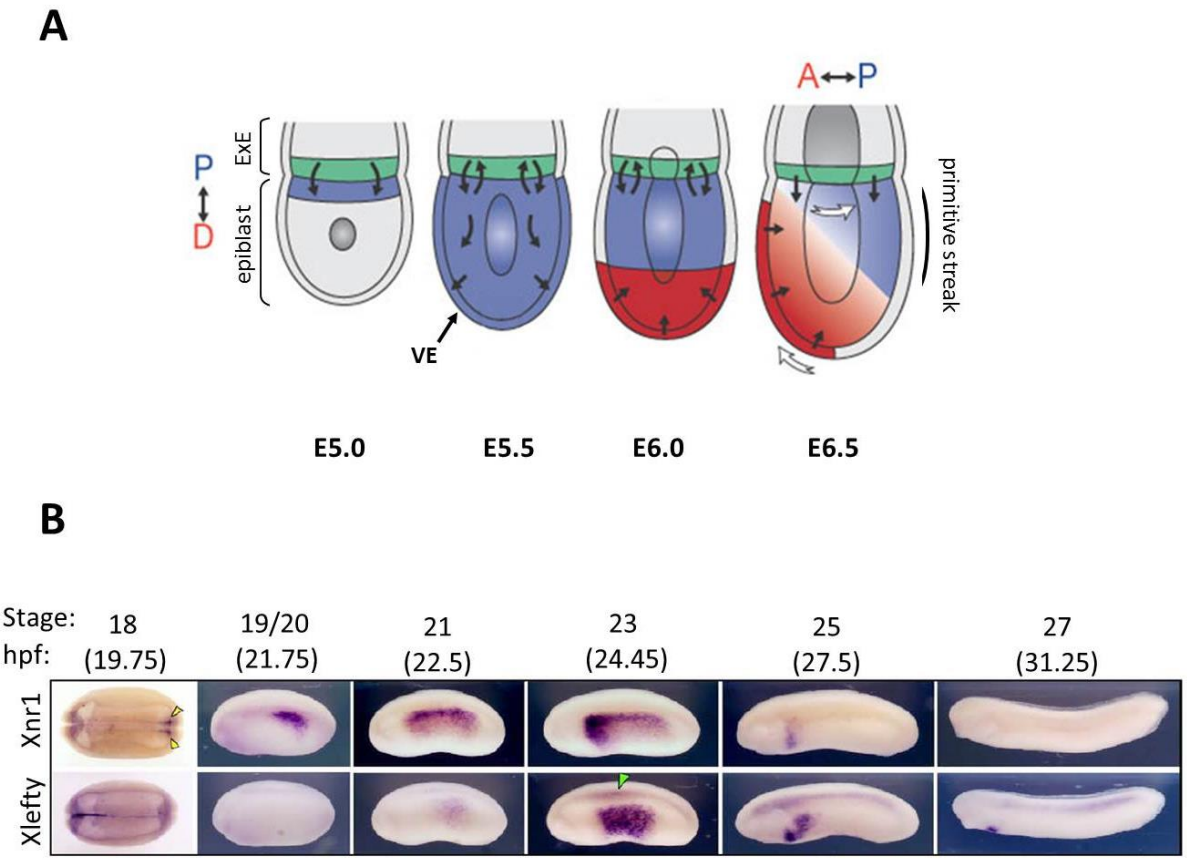

Fig. 1.2 Nodal expression during development. (A) Nodal expression during gastrulation and A-P patterning in the mouse. **E5.0:** *Nodal* (blue) induced in epiblast by signals coming from extraembryonic tissue (green; ExE). **E5.5:** *Nodal* amplifies itself by positive feedback loop, patterns visceral endoderm (VE). **E6.0:** Proximal-distal (P-D) polarity established by *Nodal* and VE signals (red). **E6.5:** *Nodal* regresses, patterns primitive streak; distal VE moves anteriorly as proximal epiblast moves posteriorly (arrows), establishing A-P axis. (B) *Nodal* and *Lefty* expression in *Xenopus* during L-R patterning. **St. 18:** *Xnr1* (frog *Nodal*) bilaterally expressed in posterior "L-R organizer." **St 19/20**: *Xnr1* induced in left lateral plate mesoderm (L LPM). **St. 23:** *Xnr1*, amplified by positive feedback loop, spreads through L LPM. **St. 25:** Expression shut down in anterior LPM by inhibitors and/or lack of tissue competence. Adapted from Brennan et al., 2001 and Ohi and Wright, 2007.

the posterior end of the “early “streak are farthest from the most intense Nodal source and become extraembryonic tissue (chorion, visceral yolk SAC mesoderm, blood islands), while cells that ingress through the slightly “intermediate” streak become mesoderm (lateral plate, paraxial, and cardiac). When the streak is more fully extended, cells entering through the most anterior streak give rise to midline axial mesendoderm tissues (notochord, node, prechordal plate, definitive endoderm). With much experimental support, the current model is that the highest (most perdurant) levels of *Nodal* expression instruct the formation of endoderm and induce the expression of mesendodermal markers such as *Goosecoid* (*Gsc*). Intermediate *Nodal* levels instruct the specific formation and fates of node cells, and the lower levels of *Nodal* expression induce mesoderm and the expression of the mesodermal marker *Brachyury* (*T*) (early patterning and gastrulation in mouse reviewed in Arnold and Robertson, 2009). This dose-dependent response to Nodal signaling is further exemplified in *Nodal* null mutants and hypomorphs (Robertson, 2014). As already discussed above, in *Nodal* null embryos, cells do not differentiate into mesoderm, leading to a failure in gastrulation and developmental arrest (Conlon et al., 1994; Zhou et al., 1993). The ability to induce mesoderm is still present in mutants with reduced *Nodal* expression, but definitive endoderm still fails to be specified (Norris et al., 2002; Vincent et al., 2003). In addition to inducing the expression of *Gsc* and *T*, Nodal signaling also induces the expression of one of its principal feedback inhibitors, *Lefty2*. By E7.5, gastrulation has concluded, the A-P axis has been established, and *Nodal* expression becomes terminated in the embryo through inhibition by Lefty2.

Early patterning events in *Xenopus* might be expected to show significant qualitative differences from mouse based simply upon the variation in developmental strategy. In *Xenopus*

embryos, which develop outside the mother, the lack of extraembryonic tissue and multiple *Nodal*-related genes lead to differences in the earliest phases of *Nodal* induction. Overall, however, the role of Nodal signaling in mesoderm induction and axial patterning is conserved. Expression of *Xnrs* in *Xenopus* is first initiated after the mid-blastula transition (the point at which zygotic transcription begins) by the maternally deposited T-box transcription factor VegT, the Tgf-β family member Vg1, and β-catenin. *Xnr5* and *Xnr6* are the first *Nodal*-related genes to be expressed, followed by *Xnr1*, *Xnr2*, and *Xnr4*. *VegT* and *Vg1* are expressed vegetally, while nuclear β-catenin is found in a dorsal-ventral gradient (higher levels dorsally, across the entire animal-to-vegetal extent (Henry and Melton, 1998; Zhang et al., 1998). The area of overlap of VegT, Vg1, and β-catenin is where the highest expression level of *Xnrs* is located. This creates a dorsal-ventral gradient of Nodal signaling across the vegetal and marginal cells as seen by the localization pattern of pSmad2. In the dorsal marginal zone, Nodal signaling induces dorsal mesoderm, or Spemann's organizer, which secretes factors that further refine the dorsal-ventral axis. As in mouse, the level of Nodal signaling dictates cell lineage, with high levels of signaling in and near the organizer giving rise to dorsal mesoderm, intermediate levels give rise to lateral mesoderm, and low levels give rise to ventral mesoderm. Again, different levels of Nodal signaling induce different mesendodermal markers, with high levels inducing the expression of *Gsc* in the organizer and lower levels inducing *Xenopus Brachyury* (*xbra*) (patterning of the early *Xenopus* embryos is reviewed in DeRobertis, et al., 2000).

Left-right patterning

The second patterning event for which Nodal signaling is essential is L-R specification and asymmetric internal anatomy. Visceral organs are asymmetric with respect to the midline (i.e. heart, stomach, pancreas), the number of appendages in paired organs (right lung has more lobes than the left), and/or looping of the organ (gut, developing heart tube). These asymmetries are thought to in the packing of organs into the body cavity and for generating unidirectional blood flow. Arrangement of visceral organs can diverge from normal *situs solitus* in three ways: (1) isomerism where asymmetrical paired organs such as the lungs become symmetrical, (2) *situs ambiguous* where the position of one or more, but not all of the organs is flipped with respect to the midline, and (3) *situs inversus totalis* where the positioning of all visceral organs is the mirror image of *situs solitus*. Although the magnitude of organ disruption is greater in *situs inversus totalis*, more clinical complications arise from isomerisms or heterotaxia, especially if the heart is affected, which presents more commonly with situs defects than other organs.

There are four steps to the establishment of L-R asymmetry in vertebrates: (1) initial breakage of bilateral symmetry, (2) transfer of L-R asymmetric signals from a specialized signaling structure, the L-R organizer, to the left lateral plate mesoderm (L LPM), (3) establishment and stabilization of side-specific gene domains in the L LPM, and (4) translation of genetic cues into tissue morphogenesis that promotes asymmetric organogenesis (covered in more detail in Chapter IV - *Identifying and Characterizing Tissue Architecture Asymmetries in L vs. R LPM Prior to Gut Looping*). The mechanism by which symmetry is initially broken in the vertebrate

embryo remains controversial, and it is possible that different symmetry-breaking mechanisms have evolved in different species. To date, the earliest break in L-R symmetry identified in most vertebrates centers around nodal flow, and is the most widely accepted theory for how symmetry is broken. Nodal flow is produced in a structure found in all vertebrate model systems termed the L-R organizer (node in mouse and chick, gastrocoel roof plate (GRP) in frog, and Kupffer's vesicle in fish). Despite having a ciliated node, Nodal flow has not been detected in the chicken (Stephen et al., 2014), and, therefore, will not be discussed here. The L-R organizer is composed of monociliated epithelial cells. The cilia on these cells rotate clockwise with a two stroke motion (an effective stroke to the left away from the cell surface and rightward recovery stroke near the cell surface) around an axis that is tilted posteriorly by 40°. This motion combined, with the angle, produces a uniform leftward flow within the L-R organizer that can be visualized by the tracking the movement of small latex beads placed within the organizer (Okada et al., 2005). Disruption of nodal flow, either due to defects in cilia or node formation, in frog, fish, and mouse leads to the loss or randomization of Nodal signaling in the LPM and subsequent defects in asymmetric organogenesis.

Although it is well established that nodal flow is essential for L-R specification events occurring downstream of the L-R organizer, it is debatable as to whether nodal flow acts as the initial symmetry breaking step or if it is the downstream amplifier of an earlier, symmetry-breaking mechanism. Work done primarily in frog [and from one lab] suggests that asymmetries in gap junction localization and serotonin distribution seen as early as the 4-cell stage may be the first break in symmetry. Briefly, maternal mRNAs encoding H^+/K^+-ATPase ion pumps and connexins, which form gap junction channels, are reported to be asymmetrically localized to the ventral

and future right sides of early cleavage-stage embryos (Aw et al., 2010; Fukumoto et al, 2005; Levin et al., 2002). In this theory, which has been termed the "ion-flux" model, asymmetrical localization of ion pumps and gap junctions facilitates the movement and accumulation of serotonin to right-side blastomeres, as seen by immunohistochemistry (Fukumoto et al., 2005). One mechanism by which asymmetrically localized serotonin is proposed to regulate L-R patterning is through modulation of epigenetic marks on the *Xnr1* locus. Serotonin was shown to co-immunoprecipitate with Mad3, a DNA binding protein capable of recruiting HDACs. Through this interaction and its asymmetric localization, serotonin is thought to recruit HDACs to the *Xnr1* intronic asymmetric enhancer (frog equivalent of the mouse ASE) only on the right side of the blastula. This is hypothesized to decrease acetylation at the intronic enhancer, leading to long-term repression of transcription in cells on the right side. Furthermore, pharmacological interference with ion pump, gap junction, serotonin, and HDAC activities in the blastula leads to heterotaxia and *situs inversus*. Despite these data, it is still unclear if the asymmetrical localization and actions of serotonin and ion channels/gap junctions in the early cleavage-stage embryo are the initial break in symmetry. Any role for ion pumps, gap junctions, and serotonin in L-R specification upstream of nodal flow in mammalian embryos has not been identified. Also, immunohistochemistry staining showing asymmetric localization of early determinants, such as serotonin (Fukumoto et al., 2005), have not been successfully repeated.

An alternative model for the role of these early determinants in the breakage of symmetry has been proposed. Ion pumps and serotonin are important for maintaining canonical Wnt signaling in the blastula and gastrula. Wnt signaling is an essential component of the specification process for superficial mesoderm, from which the GRP (left-right organizer) is

derived, and to initiate the expression of *Foxj1*, an essential factor in the formation of motile cilia, in the superficial mesoderm (i.e. GRP). Additionally, gap junctions are proposed to have a fundamental role in transferring the L-R signal from the GRP/node to the L LPM (to be discussed further below). These data argue against a role for serotonin and ion pumps/gap junctions in breaking symmetry independent of nodal flow. Instead, it is suggested that these factors participate in the breakage of symmetry by ensuring the establishment of nodal flow through proper patterning of the GRP.

After the completion of gastrulation and a brief attenuation of *Nodal* expression, *Nodal* expression reinitiates in the L-R organizer. The mouse node is made up of pit cells that are monociliated with the motile cilia. The pit cells are surrounded by crown cells, which have mainly immotile cilia. Nodal is initially symmetrically expressed in the crown cells and then becomes biased towards the left. This increase in expression on the left is established by members of the DAN/Cerberus family (Cerl2 in mouse and Coco in *Xenopus*). *Cerl2* is initially symmetric in the crown cells (Marques et al., 2004), but begins to adopt a rightward bias with the induction of nodal flow. Degradation of *Cerl2* mRNA in the left crown cells is further exacerbated by Wnt signaling (Nakamura et al., 2012). Higher levels of *Cerl2* in the right crown cells leads to greater inhibition of *Nodal* expression in these cells. The small increase in *Nodal* expression in left crown cells is thought to promote the transfer of the Nodal signal from the node to the L LPM, and not the R LPM, by making leftward travel the pathway of least resistance. Loss of *Cerl2* expression in the node leads to randomization of *Nodal* expression in the LPM, demonstrating the importance of right-side inhibition of *Nodal* expression in the node. Furthermore, *Nodal* expression in the node is required for the initiation of Nodal

signaling in the L LPM, as loss of *Nodal* expression in the node results in loss of *Nodal* expression in the L LPM. Exactly what is transferred from the node to the L LPM and the mechanism by which it is transferred remains unclear, although several theories exist.

The "two-cilia" model is the predominant theory as to how a L-R asymmetric signal is transferred from the node to the L LPM. This model suggests that the non-motile cilia on the surrounding crown cells are mechanosensory and can sense either a build-up of an unknown chemical determinant or the mechanical forces (fluid pressure) generated by nodal flow. Support for the chemical determinant model comes from recent studies that localize the Ca^{2+} channel protein Polycystin-2 (Pkd2) to the crown-cell cilia, and show that *Pkd2* deletion specifically from crown cells, and not pit cells, results in L-R patterning defects (Yoshiba et al, 2012). Detection of L-R differences in calcium signaling across the L-R organizer in mouse, frog, chick, and zebrafish, further supports the idea that the chemical determinant being sensed by the non-motile cilia is Ca^{2+}. It is proposed in frog, that the gap junction protein connexin 26 (Cx26), which is expressed in endodermal cells adjacent to the GRP, helps transfer the Ca^{2+} signal from the sensory cells surrounding the left-right organizer to the adjacent endoderm. Calcium signaling has been associated with increased secretion of sulfated glycosaminoglycans (Beyer et al., 2012), components of the extracellular matrix (ECM) with which the Nodal ligand can bind (Marjoram and Wright, 2011; Oki et al., 2007) and are essential for the internal transfer of Nodal from the node to the L LPM (Oki et al., 2007). In mouse, the connexin Cx43, which localizes to the gut endoderm, was found to be important for the establishment of Nodal signaling in the L LPM, most likely by facilitating the transfer an "asymmetric signal" from the node to the L LPM (Viotti et al., 2012). Because essential components of Nodal signaling such

as *Cryptic* and *Foxh1* are not expressed in the tissue between the node and the LPM, it is thought that the transfer of asymmetric signal is not through active Nodal signaling, but rather through transport of the Nodal ligand itself. The data discussed so far allude to the possibility that mechanosensory cilia on crown cells detect an increase abundance of a chemical determinant, perhaps calcium, generated by nodal flow. To the contrary, it was recently reported that only two motile cilia are needed to generate enough nodal flow to maintain proper asymmetrical expression of *Nodal* in the LPM. The authors speculated that Nodal flow produced by two cilia, while slower than what would be seen in wild-type embryos, would still be capable of carrying molecules across the node. However, the rate at which the molecules traverse the node and accumulate on its left side is expected to be greatly reduced compared to wild type, potentially affecting the timing of the transfer of L-R information from the node to the L LPM and causing L-R patterning defects. Because no Nodal signaling phenotype was seen in embryos with only two functional node cilia, the authors state that their results support, but do not definitively prove, the mechanical force model (Shinohara et al., 2012).

Once the L-R signal is transferred from the node, *Nodal* expression first appears in the L LPM by 3-4 somites (stage 19/20 in frog). Expression in the LPM is dynamic and transient, initiating in the posterior LPM adjacent to the node/GRP and then rapidly expanding throughout the L LPM. Expression is extinguished at the anterior boundary of the LPM by 6-8 somites in mouse or by stage 25 in frog, approximately 7-8 hours after first being initiated in the LPM (Fig. 1.2B) (Collignon et al., 1996; Lowe et al., 1996; Meno et al. 1996; Norris et al., 2002; Ohi and Wright, 2007). A principal regulatory influence of this dynamic expression pattern seems to be the self-enhancement and lateral-inhibition (SELI) system. SELI operates through a Nodal

autoregulatory and feedback loop. *Nodal* enhances its own expression (a positive feed-forward loop) and rapidly initiates expression of its feedback antagonist *Lefty2* (Nakamura et al., 2006), which thus mimics the expression of *Nodal* with a temporal delay. Lefty2 inherently travels faster and farther than Nodal, and has greater stability, allowing it to shut off N*odal* expression in the L LPM, as well as prevent the Nodal autoregulatory loop from fully initiating in the R LPM (Marjoram and Wright, 2011; Müller et al., 2012; Nakamura et al., 2006). Also helping to restrict *Nodal* within the L LPM and prevent the initiation of its expression in the R LPM is *Lefty1*, which is expressed in the midline of the embryo.

Aside from initiating the expression of itself and *Lefty2*, Nodal also promotes the expression of *Pitx2*, which encodes a transcription factor widely believed to operate as a principal effector of Nodal signaling. *Pitx2* has three isoforms of which only *Pitx2c* in involved in L-R patterning (for simplicity and matching current literature *Pitx2c* will be called *Pitx2* from here on). L-sided *Pitx2* expression supersedes that of *Nodal* and *Lefty2* in the LPM. *Pitx2* goes on to be expressed asymmetrically in the heart, stomach, intestine, and symmetrically in the head (Schweickert et al., 2000). Establishment of PItx2 as a downstream target of Nodal and as a mediator between L-R signaling and asymmetric morphogenesis was cemented by its ability to alter organ situs without affecting *Nodal* expression when ectopically expressed in the R LPM (Campione et al., 1999; Logan et al., 1998; Piedra et al., 1998; Ryan et al., 1998). Experiments with *Pitx2* revealed a progressive gene-dosage requirement in organ *situs* formation and L-R patterning: lung and gut required the highest level of *Pitx2* expression, followed by the heart, with the stomach requiring the least (Gage et al., 1999; Liu et al., 2001). Exactly how Nodal signaling (acting through Pitx2) influences the alterations in LPM tissue architecture that support asymmetric

organogenesis is not known and will be discussed further in Chapter IV – *Identifying and Characterizing Tissue Architecture Asymmetries in L vs. R LPM Prior to Gut Looping*.

ESCs, germ cells, cancer

The role of Nodal signaling in development extends beyond axis formation and patterning. In the mouse, *Nodal* is first expressed in the preimplantation embryo starting at E3.0 where it plays an important role in maintaining expression of the pluripotency factor *Oct3/4* in the inner cell mass (James et al., 2005; Papanayotou et al., 2014). A similar role is seen in human ESCs, in which low level Nodal signaling is essential for pluripotency and self-renewal. Inhibition of Nodal signaling with small-molecule inhibitors directed against the ALK4/5/7 type I receptors led to reduced proliferation of ESCs and a decrease in markers of the undifferentiated state (reviewed in Watabe and Miyazono, 2009). A similar requirement is seen in mouse epiblast stem cells (EpiSCs), but Nodal signaling does not seem to be essential for maintenance of the undifferentiated state in mESCs (James et al., 2005; Papanayotou et al., 2014). As in the epiblast, Nodal signaling is required for ESCs in culture to differentiate into endoderm and mesoderm (Watabe and Miyazono, 2009).

Recently, Nodal signaling has been implicated in the development of germ cells. Multiple components of Nodal signaling (*Nodal*, *Cripto*, *Lefty1/2*) have been found to be expressed in XY, and not XX, germ cells in E12.5-14.5 mouse embryos. *Cripto* is upregulated in the germ cells in response to *FGF9*, which is expressed by somatic cells of the testis. In turn, Nodal signaling becomes activated and increases *Nodal* expression in germ cells through its positive feedforward loop. Reduction of Nodal signaling causes premature differentiation of XY germ

cells. Elevated levels of *Cripto*, *Nodal*, and *Lefty1* have been detected in testicular germ cell tumors (TGCT). These results led the authors to conclude that, similar to its role in ESCs and the early preimplantation embryo, Nodal signaling helps regulate timing of the transition from proliferation to differentiation (Spiller et al., 2012). The role of Nodal signaling in germ cell development is pertinent to the Foxh1 mutant mouse line described in Chapter V, because mutant male mice are infertile under certain circumstances.

Abnormal reactivation of *Nodal* has been found in various other cancers testicular germ cell tumors. *Nodal* expression has been detected in prostate, breast, and endometrium cancers as well as in melanoma, where it seem to play a role in regulating plasticity, tumorigenicity, and growth. In metastatic melanoma cells, *Nodal* transcription is thought to be triggered by Notch signaling, most likely through the NDE, the Notch-responsive enhancer that was described first for its ability to drive *Nodal* expression in the node during early embryogenesis. Human metastatic melanoma cells do not express *LEFTY*, and the absence of this negative feedback suppressor further allows *NODAL* expression to go unchecked and to increase dramatically once expression is initiated (reviewed in Strizzi et al., 2012).

Regulation of Nodal Signaling

Nodal enhancers

Much evidence supports the idea that proper embryonic patterning depends upon precisely orchestrated dynamic alterations in the level and spatial domains of Nodal ligand distribution. Because Nodal signaling must be so precisely titrated, it is likely that buffered regulatory systems were developed to provide pathway robustness while at the same time providing

rheostat-like level control. Tissue-specific expression of *Nodal* is, in part, accomplished by the combinatorial action of five different *cis*-regulatory domains, or enhancers, that drive expression in the epiblast, node, and LPM (Adachi et al., 1999; Saijoh et al., 2005; Vincent et al., 2003). The PEE, LSE, and NDE enhancers are upstream of the *Nodal* transcriptional start site and the ASE lies in intron 1. The proximal epiblast enhancer (PEE) is a Wnt-responsive enhancer that drives the initial ring of *Nodal* expression at the epiblast-ExE boundary and then eventually in the proximal-posterior region of the epiblast. This initial activation of Nodal signaling then activates transcription through the ASE. Transcription driven by this enhancer is Nodal and Foxh1-dependent. Once this enhancer is activated, a feed-forward loop is established, and Nodal activates its own expression through the ASE. This feed-forward loop causes the *Nodal* expression domain to expand to cover most of the epiblast and visceral endoderm, before fairly rapidly becoming restricted to the prospective posterior side, overlapping slightly with the expression domain driven from the PEE (Fig. 1.2A). On the prospective posterior side, *Nodal i*s expressed within the elongating primitive streak, becoming terminated by approximately E7.25. Starting around E7.5, the node-specific enhancer (NDE), a Notch-responsive and Foxh1-independent enhancer, drives expression in the node. At later stages, the ASE drives *Nodal* expression in only the L LPM (the detection of this function was what first led to its name "asymmetric enhancer"). A second left-sided enhancer (LSE) has been identified that may also function in driving expression in the L LPM, although deletion of the LSE did not significantly alter *Nodal* expression in the LPM and caused no defects in L-R patterning (Saijoh et al., 2005). A fifth, recently identified enhancer termed the highly bound element (HBE) was found to

initiate *Nodal* expression in preimplantation embryos and embryonic stem cells (Papanayotou et al., 2014).

Foxh1

Foxh1 is a major transcription factor regulator of not only *Nodal* transcription, but also that of the Nodal downstream targets *Lefty2* and *Pitx2* (Norris et al., 2002; Saijoh et al., 2000; Shiratori et al., 2001). Transcriptional activation by Foxh1 is currently modeled to depend upon interactions with pSmad2, which recruits potent co-activators to the locus and causes positive activation-type effects on the nearby chromatin structure (Massagué et al., 2005). In mouse, the deletion of Foxh1 binding-sites within the ASE, or deletion of the whole ASE, leads to decreased *Nodal* expression in the epiblast and complete loss of *Nodal*, *Lefty2*, and *Pitx2* expression in the L LPM (Adachi et al., 1999; Norris and Robertson, 1999; Norris et al., 2002; Saijoh et al., 2000; Shiratori et al., 2001). Foxh1 binding sites play a conserved role in the ASE as deletion of these sites in the frog *Xnr1* intronic ASE also attenuated Nodal signaling (Osada et al., 2000). Similar loss of Nodal signaling phenotypes are seen when *Foxh1* is globally deleted. The majority of *Foxh1* null embryos fail to orient the A-P axis appropriately, elongate the primitive streak, or form a node; these major defects together cause embryonic lethality (Hoodless et al., 2001; Yamamoto et al., 2001). Embryos in which *Foxh1* was conditionally inactivated within the L LPM lacked left-sided LPM expression of *Nodal*, *Lefty2*, and *Pitx2*, and exhibited pulmonary right isomerism (Yamamoto et al., 2003). These studies prove that Foxh1 is an essential, positive regulator of Nodal signaling.

ECM interactions

Because Nodal is thought to have many of the properties of the classical morphogen molecule, including the ability to travel long distances in embryonic tissue, its interaction with the ECM is another important regulator of Nodal signaling. Physical interactions between Nodal and the ECM are thought to help shape the spatiotemporal dynamics of Nodal signaling. Studies in mouse have found that chondroitin sulfate proteoglycan (CSPG), a component of the ECM that is enriched around the notochord and ventral neural tube, is needed for the transfer of Nodal signal from the node to the LPM. Mouse embryos cultured in the chemical xyloside, an inhibitor of CSPG synthesis, failed to express *Nodal* in the L LPM (Oki et al.; 2007). In *Xenopus*, a CSPG gradient along the anterior-posterior axis appears to be important for the anterior-ward movement of Xnr1 along the L LPM (Marjoram and Wright, 2011). In older experiments, treatment of *Xenopus* embryos with xyloside had been reported to lead to failure of the heart tube to loop (Yost, 1990). More recent studies have shown that Xnr1 can travel outside the LPM into the endoderm of xyloside-treated embryos (Marjoram and Wright, 2011). The alteration in Nodal localization may be the cause of the heart looping defects seen in the older study.

Aims of Dissertation

The overarching goal of my thesis was to dissect the spatiotemporal regulation of Nodal signaling and its role as a morphogenetic cue in the developing vertebrate embryo with three distinct, yet related, aims: (1) map the intracellular tissue registration of the *Xnr1* expression in the LPM, (2) characterize tissue morphogenesis in the left and right LPM prior to and during gut

looping in *Xenopus*, and (3) dissect the role of Foxh1-Groucho interactions in regulating Nodal signaling. The contribution of repressive transcriptional regulation to the control of Nodal signaling spatiotemporal dynamics, and how this precise control of Nodal signaling is translated into morphogenetic cues for asymmetric morphogenesis is unclear. Attempts to answer these questions are hindered by the inability to detect endogenous Nodal and Lefty ligands. Current detection methods of endogenous Nodal signaling are primarily by *in situ* hybridization analysis of *Nodal*, *Lefty2*, and *Pitx2* expression. It is not known how the *Nodal* expression pattern relates to its protein localization and if active signaling dynamics (perdurance, levels) mimic the transient dynamics of *Nodal* expression. We generated antibodies against pSmad2 to characterize the spatiotemporal dynamics of active Nodal signaling. Generation and characterization of this antibody is discussed in Chapter III.

There is a large gap in our understanding of how Nodal signaling in the LPM initiates or directs chiral organ morphogenesis. A previous graduate student in the lab had begun to characterize the tissue architecture of the LPM and noted possible asymmetries in the actin cytoskeleton between the R and L LPM, with increased F-actin contraction and bundling in the R LPM. In Chapter IV, I verify this asymmetry and identify other ECM or tissue architectural components that potentially display L-R asymmetries in the LPM of *Xenopus*. Our goal was to identify if conserved areas of tissue architecture asymmetries were present in the LPM, and if these areas coincided with regions in the LPM that have been exposed to Nodal signaling as determined by our *Xnr1* expression mapping efforts carried out in aim 1 (Chapter III).

The transcriptional initiation of *Nodal* expression has been well studied; however, very little is known about how transcriptional repression of *Nodal* is mediated. A recent study from our collaborator Dr. Dan Kessler at the University of Pennsylvania suggests that Foxh1 can function as a transcriptional switch, both initiating activating and repressing *Nodal* transcription in *Xenopus*. The ability of Foxh1 to act as a repressor is conveyed through interactions with the Groucho family of co-repressors (Reid et al., 2014 in review). In Chapter V, I describe the derivation and characterization of a mouse model in which the ability of Foxh1 to interact with Groucho proteins is disrupted, testing if the Foxh1 transcriptional switch is conserved in mouse and for the developmental consequences of removing Foxh1-Groucho—mediated repression.

CHAPTER II

MATERIALS AND METHODS

Xenopus embryo manipulations

Oocytes were obtained from *Xenopus laevis* females induced with approximately 600 units human chorionic gonadotropin (hCG). Half of a *Xenopus* male testis was homogenized in 5 mL high salt modified Barth's saline (HS MBS; 7 mL 0.1 M $CaCl_2$, 4 mL 5 M NaCl, 889 mL H_20, 100 mL 10x MBS salts [880 mM NaCl, 10mM KCl, 50 mM HEPES, 25 mM $NaHCO_3$], pH 7.8). The testis slurry was dripped on to oocytes, which were then flooded with 0.1x MBS salts to activate sperm. After at least 30 minutes, and once embryos had turned animal halves upward, embryos were dejellied in 1% thioglycolic acid in 1X Steinburg's solution (SS) pH 6.0 with agitation for 1-2 minutes. Embryos were subsequently cultured in 1X SS (58 mM NaCl, 0.67 mM KCl, 0.34 mM $Ca(NO_3)_2 \cdot 4H_2O$, 0.83 mM $MgSO_4 \cdot 7H_2O$, 4.6 mM Tris, pH 7.4) until the onset of gastrulation (stage 10) when they were transferred to 0.1X SS.

For injections, 1-4 cell-stage embryos were transferred to 5% Ficoll/1X SS and injected with 5-10 nl of total RNA solution using a Narashige nitrogen-driven microinjector glass capillary needles. Injected embryos were allowed to recover at room temperature in 5% Ficoll/1X SS until stage 8 and then transferred into 1x SS until the dorsal lip became evident, at which time embryos were collected and processed.

For animal cap assays, embryos were collected and injected as described above. At stage 8, vitelline membranes were removed and caps were cut using a 400 µM Gastromaster tip. Caps were cultured pigmented side down in 1X SS overnight at room temperature and assayed for elongation the next day.

pSmad2 antibody purification and pSmad1 depletion

Raw pSmad2 anti-serum (8.5 mL) was diluted to 15 mL with TBS Tween 20 (TBSTw). Diluted pSmad2 anti-serum was mixed end-over-end with 1.5 mL of prepared pSmad2 matrix slurry (total of matrix used was 750 µL) for 2 hours at room temperature. A 1:1 matrix slurry was prepared by mixing 1.5 mL pSmad2 matrix with 1.5 mL TBSTw. Slurry was centrifuged in a 15 mL Falcon tube at 500 rpm for 3 minutes at room temperature. The supernatant was removed and the remaining pSmad2 matrix was washed with 10 mL TBSTw, turning end-over-end. Centrifugation and the TBSTw wash was repeated. Supernatant was removed and the pSmad2 matrix was resuspended in 3 mL TBSTw. Using a Pasteur pipet, the anti-serum/matrix mixture was loaded into a 3 mL syringe that had been blocked with 5%BSA/TBSTw for 1 hour and plugged with glass wool at the tip. The matrix was continuously washed with a total volume of 15-20 mL TBSTw. pSmad2 antibodies were eluted from the column with acid (0.15 M glycine pH 2.5) and base (0.1 M CAPS pH 11.5) washes. Eight acid fractions, 0.5 mL each, were collected into 0.5 mL 2M Tris pH 8.0 (neutralizing buffer). The same step was repeated for the base elution. Fractions were tested for pSmad2 reactivity on slot blots. The most reactive fractions were pooled (two pools were collected: acid and base).

Both acid and base fractions were dialyzed. Dialysis tubing (16 mm diameter, 25 mm flat width) was prepared by boiling in 2 L of 0.1 M sodium bicarbonate for 15 minutes, rinsing with distilled water, boiling in 2 L of 0.1 M sodium bicarbonate and 0.01 M EDTA for 15 minutes, and then rinsing in distilled water. Tubing was cut into strips 4-5 cm in length. One end of the tubing was clamped and the acid or base pools were loaded into the tubing with a Pasteur pipet, and then the other end of tubing was clamped. Fractions were dialyzed in 2 L 1x TBS for 4 hours at 4°C while slowly spinning. Fractions were transferred to 4 L fresh 1x TBS overnight at 4°C with spinning. After dialysis, all but 1 mL of the acid pool was aliquoted into 500 µL fractions plus 10% glycerol and stored at -80°C. The same was done for the base pool.

pSmad2 cross-reactivity was depleted from the reserved 1 mL acid and base aliquots by incubating with 1 mL pSmad1 matrix slurry (0.5 mL matrix:0.5 mLTBSTw) plus 3.5 mL TBSTw. Mixture was turned end-over-end for 2 hours at room temperature. Mixture was spun down at 500 rpm for 3 minutes. Supernatant was removed and the spin repeated. Depleted affinity purified antibodies were stored at 4°C.

Antibody labeling on *Xenopus* cryosections

Embryos were fixed in 1xMEMFA (0.1 M MOPS pH 7.4, 2 mM EGTA, 1 mM $MgSO_4$, 3.7% formaldehyde) for 2 hours at room temperature or overnight at 4°C. They were then embedded in a mixture of melted 3% bacto agar/5% sucrose/PBS Tween 20. Blocks were equilibrated in 30% sucrose/PBS Tween 20 overnight at 4°C, and then frozen on 2-Methyl Butane that was supper-chilled in liquid nitrogen. Slides with cryosections were mounted into Sequenza slide racks. Sections were rehydrated in 1x PBS for 1 hour at room temperature,

blocked (2% NDS, 2% 100 mg/mL BSA, PBS) at room temperature for 1 hour, and incubated overnight at 4°C in primary antibody diluted in block. Sections were washed 6x5 minutes with 1x PBS, incubated with secondary antibody for 2 hours at room temperature in block, washed again with 1x PBS, and mounted in ProLong Gold antifade reagent plus DAPI.

Whole-mount immunolabeling (for Technovit embedding)

Embryos (not exceeding 10-12 embryos/vial) were fixed in 1xMEMFA for 30-60 minutes at room temperature on a nutator, then transferred into Dent's fix (4:1 methanol:DMSO) and stored at -20°C for at least two days. Embryos were rehydrated with a MeOH series: 75%MeOH in 1xPBS with 0.1% Tween (PBSTw), 50% MeOH/PBSTw, 25% MeOH/PBSTw, and at least two washes with PBSTw. Each wash was at least 5 minutes on a nutator at room temperature. Embryos were blocked with 500 µL 15% normal donkey serum (NDS) in PBSTw for 2 hours at room temperature on a nutator. Embryos were incubated in primary antibody diluted in 500 µL 15% NDS/PBSTw for 2 days at room temperature on a nutator (see Table 2.1 for compatible primary antibodies), then washed with PBSTw for at least 1.5-2 hours at room temperature on a nutator, changing out PBSTw multiple times (usually 8-10 washes). Embryos were added to secondary antibody (fluorescently-labeled; 1/200, Jackson Immuno) diluted in 500 µL 15% NDS/PBSTw and incubated overnight at 4°C on a nutator. Vials are covered to protect from light for rest of staining protocol and sectioning. PBSTw washes done after primary antibody incubation were repeated. Embryos were fixed in 500 µL 4% PFA for 30 minutes at room

Antibodies used in whole mount						
Antibody	Species	Supplier	Order #	Concentration	Notes	Fixative
B1 integrin	Mouse	DSHB	8C8	1/200	Very strong in all germ layers; st17-23, st33-36	Dent's
B-Catenin	Rabbit	Pierre McCrea		1/200	St23	MEMFA
C-Cadherin	Mouse	DSHB	6B6	1/100	Weak along cell borders; stronger at possible aj; st23	Dent's
E-Cadherin	Mouse	BD Biosciences	610182	1/300	Labels all germ layers, weakest in mesoderm; st17-23, 33-36	Dent's
N-Cadherin	Rabbit	Abcam		1/100	St23	Dent's
CSPG	Mouse			1/100	Around notochord, A-P gradient observed; st23	Dent's
Fibronectin	Mouse	Doug DeSimone	4H2	1/800	Very strong	Dent's
Laminin	Rabbit	Abcam	Ab11575	1/200	Labels LPM borders, weaker than FN; st20-23, 33-36	Dent's

Table 2.1 Antibodies compatible with whole-mount immunolabeling.

temperature on a nutator, and wash twice with PBSTw for 5 minutes each. Embryos were either stored in PBSTw at 4°C or immediately processed for embedding in Technovit 7100.

Technovit 7100 embedding and sectioning

Dehydrate embryos with EtOH series: 25% EtOH/PBSTw, 50% EtOH/PBSTw, 75% EtOH/PBSTw, and 2 washes with 100% EtOH. Each wash is at least 5 minutes on a nutator at room temperature. Prepare Technovit 7100 infiltration mix according to package directions (1 g hardner I [powder]/100 mL Technovit liquid; usually makes 15-20 mL of infiltration mix, which can be stored at 4°C for up to one month). Add 1:1 mixture of 100% EtOH:Technovit infiltration mix to embryos (500 µL total) for 1 hour at 4°C on a nutator. Replace 1:1 EtOH:Technovit mixture with 500 µL 100% Technovit infiltration mix for 1 hour at 4°C on a nutator (can perform this and the previous equilibration step for 30 minutes each at room temperature when short on time). Replace Technovit with fresh 500 µL aliquot of Technovit infiltration mix overnight at 4°C on a nutator (embryos can be stored in this mix for up to 1 month at 4°C).

To embed, take 1 embryo (tissues seem to tear more frequently during sectioning when more than 1 embryo is embedded in the same block) out of vial with a glass Pasteur pipette that has had the tip sawed off to increase boar diameter. Place embryo in a plastic disposable embedding mold (7x7x5 mm – Fisher catalogue #22-363-552). Remove excess liquid around embryo using p200 pipetman. Mix Technovit infiltration mix with hardner II (1 mL hardner II/15 mL Technovit infiltration mix). This embedding mix only stays liquid for a few hours at 4°C before it starts to harden and polymerize, so only make enough for the number of embryos

being embedded (750-1000 µL/embryo). Add enough embedding mix to cover embryo and fill the 7x7x5 mm mold (about 250 µL; return unused mix back to 4°C). Once the Technovit begins to polymerize (15-30 minutes at room temperature depending on how fresh the embedding mix is –mix sitting at 4°C for some time will polymerize faster than mix just prepared), position embryo as desired with dissecting needle and hold until embryo is stationary (once the Technovit starts to polymerize, it usually takes a few minutes until the embryo will maintain its position without assistance). Once stationary, add more embedding mix (500-750 µl) to the mold and position a plastic biopsy cassette (Fisher catalogue #15182702E), with the lid removed, on top of the mold so that the flat part of the cassette sits in the embedding mix and is flush against the embryo block. Make sure no bubbles form between the block and cassette, as this will weaken the connection between the two and likely cause the block to snap off the cassette during sectioning. Let harden overnight at room temperature, protected from light. To add rigidity to and minimize flexing of the biopsy cassette during sectioning, pour approximately 750 µL of Technovit 3040 (harder, yellow plastic; 2:1 powder:liquid) into the open back of the cassette; let harden for at least 10 minutes at room temperature. Carefully pop specimen block attached to cassette out of the plastic embedding mold. If the block does not release from the mold, cut the mold can away with a razor blade. Allow block to dry at least one day before sectioning.

Sectioning was done on a Leica RM2135 microtome outfitted with a universal cassette clamp and knife holder E, which holds disposable metal blades (fisher catalogue #22-030530). Note: glass knives or tungsten carbide blades are recommended for resin sectioning; however, our microtome is not compatible with these options. The angle of the knife was set to 2°. Anything

greater than this causes the sections to rip and curl more frequently. Technovit sections are placed into a room temperature water bath to expand and then are collected on to slides and dried on a slide warmer.

Derivation of Foxh1^{LCA}, Foxh1^{mEH1}, and Foxh1^{F} mice

The *Foxh1*^{LCA}, *Foxh1*^{F}, and *Foxh1*^{mEH1} mouse lines were derived with help from Vanderbilt Transgenic Mouse/Embryonic Stem Cell Shared Resource (TMESCSR). A 129S6 *Foxh1*^{LCA} ES cell line was generated through homologous recombination of a targeting vector that was created by BAC recombineering with the BAC bMQ206P16 (BAC PAC Resources at C.H.O.R.I., Oakland, Ca.). In short, DNA flanking the *Foxh1* locus was subcloned from the BAC into pLCA.71.2272. The BAC and modified pLCA.71.2272 were recombined in recombinant-capable SW106 cells. pBS.DT-A was used to retrieve the modified *Foxh1* locus from the BAC, creating the *Foxh1*^{LCA} targeting vector which was then electroporated into 129 mESCs for homologous recombination with the endogenous *Foxh1* locus. Colonies surviving selection were screened by Southern blotting (described below) and karyotyped. Five out of 317 colonies screened had correct targeting of the *Foxh1* locus. *Foxh1*^{LCA} chimeras were generated to validate germline transmissibility of *Foxh1*^{LCA} ES cell clones. Exchange vectors for the *Foxh1*^{F} and *Foxh1*^{mEH1} alleles were generated by subcloning the *Foxh1* locus from the BAC into phygro66.2272.F. Site-directed mutagenesis was used to mutate the EH1 domain and/or add a FLAG tag. Recombinase-mediated cassette exchange (RMCE) between the *Foxh1*^{LCA} ES cell clone 4B6 and exchange vectors was used to generate *Foxh1*^{F} and *Foxh1*^{mEH1} ES cell lines. Colonies surviving selection were screened with PCR and karyotyped. One clone for each line was injected into

C57BL/6 embryos for generation of chimeras. Following the generation of founder mice for the *Foxh1*^{F} and *Foxh1*^{mEH1} alleles, hygromycin resistance selection cassettes were excised by mating to mice with FLPe (Rodriguez et al., 2000). Flp-mediated deletion was confirmed with the primers 5' AGC TGC CCA TTG TAG TAG C 3' and 5' CAA AGT GAG TTC CAG GAC A 3'.

Southern Blotting

Genomic DNA isolated from targeted ESCs was provided by the Vanderbilt TMESCSR for screening. DNA was digested in a total volume of 60 µL with 4 µL BamHI overnight at 37°C. An additional 2 µL of BamHI was added the following morning, and the digest was continued for two hours. Digested DNA was run on a 0.8% NA agarose gel without ethidium bromide (EtBr) overnight between 30-35 V in 1x TBE buffer. Transfer of DNA to zeta probe membrane and the subsequent processing of the membrane was done according to the lab's genomic Southern blot protocol – July 1998 version. Radioactive probes, approximately 500 base pairs in length, were prepared using the Prime-It Labeling kit (Agilent Technologies) with ^{32}PdATP. Radio-labeled membranes were exposed to film for up to one week at -80°C. The 5' internal probe was amplified from BAC bMQ206P16 with the following primers: 5' AAA AAA ATC GAT AGG GAG GTC TGG CCA ATC GTG 3' and 5' TAT AAG AAT TCT TAT GCT TTG AGA AAG GAT CGC CTC C 3'. Primers for the 3' external probe: 5' AAA AAA ATC GAT AGC CTT TGA GGA GGC CAA GTG 3' and 5' TAT AAG AAT TCG CCT GCA TCA CGG TTG GTT AC 3'.

Mouse husbandry

Animal handling was approved by the Vanderbilt University Medical Center Institutional Animal Care and Use Committee. Mice were purposefully maintained on a mixed ICR/129 background to minimize the chance that a potential phenotype is controlled by a genetic modifier. Mice were maintained as homozygotes for the respective alleles. *Foxh1*^{mEH1} and *Foxh1*^{F} animals were genotyped by PCR (primers 5' ACT TGG GAA ACC ACT TGG TC 3' and 5' TTG ACT CTT GAA CCT CCA GG 3'). Experimental embryos resulted from crosses between mice homozygous for the *Foxh1*^{mEH1}, *Foxh1*^{F}, or wild-type *Foxh1* allele.

Microinjection of *Foxh1* variants into *Xenopus*

Plasmids for generating RNA in vitro were generated by inserting cDNAs encoding Foxh1^{F} or Foxh1^{mEH1} into pCS2+ (from Dr. Dave Turner, University of Michigan). An injection construct encoding Myc-tagged *Xenopus* Grg4 (^{Myc}Grg4) was a gift from Dr. Daniel Kessler, University of Pennsylvania. Capped RNA was produced using the mMessage mMachine kit (Ambion). RNA encoding Foxh1^{F} or Foxh1^{mEH1} (2 ng) was injected alone or in combination with ^{Myc}Grg4 (2 ng) into the animal caps of 1-2 cell *Xenopus* embryos. Embryos were cultured in 1x SS until stage 10, when they were frozen and stored at -20°C for use in co-immunoprecipitations (co-IPs). Embryos were staged according to (Nieuwkoop and Faber, 1967).

Foxh1-Groucho co-immunoprecipitation and immunoblotting

Ten *Xenopus* embryos were used in each co-IP. Embryos were homogenized 10 µL homogenization buffer per embryo (buffer: 20 mM Tris pH8.0, 2.0 mM EDTA, 5.0 mM EGTA, 0.5% NP-40, 1x protease inhibitor cocktail [Roche]), incubated on ice 10 minutes, and centrifuged at 2,000 x g for 5 minutes at 4°C. Centrifuged lysates were removed from the pellet and pellicle and incubated with 4 µg rabbit anti-Foxh1 (ab49133, Abcam) overnight at 4°C mixing end-over-end on a hematological mixer. Lysate-antibody mixtures were then incubated with 50 µL magnetic Dynabeads Protein G (Life Technologies) for 4-5 hours at 4°C on a hematological mixer. After incubation, beads were boiled in 4x sample reducing buffer (0.125 M Tris-Cl pH6.8, 4% SDS, 20% v/v glycerol, 0.2 M DTT, 0.02% bromophenol blue) for 7 minutes. Samples were separated on NuPage 10% Bis-Tris gels (Life Technologies), transferred onto PVDF (0.45 µM, Millipore), and blocked with 7-10% non-fat dry milk dissolved in TBS-Tween (0.1%) for 30-45 minutes at room temperature. Membranes were incubated with monoclonal mouse anti-FLAG M2 (1:3,000; 200472, Agilent Technologies) or rabbit anti-Myc (1:3,000; 06-549, Millipore) in blocking solution overnight at 4°C. Membranes were washed with 0.1% TBS Tween 20 2x5 minutes, 1x10 minutes, and 1x15 minutes. Specifically bound primary antibodies were detected with HRP-conjugated goat anti-mouse IgG_1 (1:7,500; sc2969, Santa Cruz Biotechnology) or Clean-Blot IP detection reagent HRP (1:4,000; 21230, Thermo Scientific) for 45 minutes at room temperature. TBS Tween 20 washes were repeated. Amersham ECL Prime western blotting detection reagent (GE Healthcare) was used for chemiluminescence and membranes were exposed to film (GenHunter) for various time periods.

pSmad immunoblotting

Immunoblotting with the pSmad1 and pSmad2 antibodies was performed as described above except for the following differences. Five *Xenopus* embryos per condition were homogenized with a motorized pestle in 50 µL homogenization buffer containing the phosphatase inhibitors NaF (100 mM), Calyculin A (20 nM), and sodium pyrophosphate (10 mM). Approximately 20 µL of the lysate was used for western blotting. Membranes were blocked in 5% BSA diluted in 0.1% TBS Tween 20. This solution was also used to dilute the primary and secondary antibodies. HRP-conjugated goat anti-rabbit secondary antibody was used (1:5,000; Cell Signaling).

Mouse in situ hybridizations

Embryos were staged based on morphology according to (Downs and Davies, 1993). Whole-mount *in situ* hybridization was as described (Belo et al., 1997), except antibody was used at 1:5,000, with DIG labeled *Nodal, Lefty2, Pitx2, Foxh1, Otx2, Brachyury/T, Gsc, and Foxa2* RNA probes (probes were gifts from Trish Labosky and Yukio Saijoh). All steps were carried out in 24-well tissue culture dishes. Embryos were kept in mesh baskets (Eppendorf tube, tip and cap removed, melted on to mesh of a transwell filter) to facilitate easy transfer from well-to-well. Embryos were prehybridized and hybridized at 68°C, in an incubator, for all probes. Color reaction was done with BM Purple (Roche). Developed embryos were imaged with a Leica M165 FC microscope.

qRT-PCR

RNA was isolated from *Xenopus* animal caps (approximately 10) or E8.25 mouse embryos (1-6) using Trizol (Invitrogen) and RNA pellets were resuspended in 30 µL DEPC water. DNA contamination was removed with the DNA-free kit (Ambion). cDNA was synthesized with the iScript cDNA synthesis kit (Bio-Rad), and qRT-PCR performed using the SsoFast EvaGreen supermix (Bio-Rad). qRT-PCR was performed twice on each cDNA sample to determine ΔC_T. qRT-PCR primers were as follows: *Gsc* 5' ACAACTGGAAGCACTGGA 3' and 5' TCTTATTCCAGAGGAACC 3'; *xBra* 5' GGATCGTTATCACCTCTG 3' and 5' GTGTAGTCTGTAGCAGCA 3'; *Xnr1* 5' AGG AAG CAT CCC TTC CA 3' and 5' GGT ACA ACT TGA CCA CAC T 3'; *Lefty2* 5' ACC AAA GTA CCC CTT GTC TC 3' and 5' GCG ATA TTG TCC ATT GTG CA 3'; *Muscle actin* 5' GCT GAC AGA ATG CAG AAG 3' and 5' TTG CTT GGA GGA GTG TGT 3'; *Epidermal keratin* 5' CAC CAG AAC ACA GAG TAC 3' and 5' CAA CCT TCC CAT CAA CCA 3'; *ODC* 5' GGA GCT GCA AGT TGG AGA 3' and 5' TCA GTT GCC AGT GTG GTC 3'; mouse *Nodal* 5' TGA GCC TCT ACC GAG ACC 3' and 5' ATG TCA ATG GTG AGT GGG C 3'; mouse *Lefty2* 5' ACA AGT TGG TCC GTT TCG C 3' and 5' ACA TTC ATA CGT CAG GAA CCC 5'; mouse *Pitx2* 5' AGG ACT CAT TTC ACT AGC CAG 3' and 5' AGC CAT TCT TGC ACA GCT C 3'; and *GAPDH* 5' AAC TTT GGC ATT GTG GAA GG 3' and 5' GGA TGC AGG GAT GAT GTT CT 3'.

Latex injections

Ventricles of E15.5 embryos were injected with colored, liquid latex (Connecticut Valley Biological Supply) as described (Oh and Li, 1997), using the same microinjection setup used for

injecting *Xenopus* embryos. Hearts were allowed to beat several times to help circulate the latex before fixing whole embryos in 4% paraformaldehyde at 4°C. Embryos were imaged with a Leica M165 FC microscope.

Whole-mount immunolabeling for YFP (detection of *ASE-YFP* transgene)

Embryos were fixed in 4% PFA overnight, then transferred to a 1.5mL Eppendorf tube in which they were washed 3x5 minutes with wash buffer (0.02% PBS Tween 20, 2 % BSA from a 100 mg/mL stock) at room temperature on a nutator. Total volume of each wash was 1.2 - 1.5 mL. Embryos were permeabilized in permeabilization buffer (0.5% PBS Triton) at room temperature on a nutator. Permeabilization times were 15 minutes for E8.25 embryos and 7.5 minutes for E6.5 embryos. Embryos were washed 2x3 minutes with wash buffer at room temperature on a nutator. Embryos were incubated overnight at 4°C in primary antibody, rabbit anti-GFP (1/500), diluted in antibody block (0.1% PBS Tween 20, 2% BSA). The antibody solution was removed and 1 mL wash buffer was added to the embryos. Embryos were allowed to settle and the buffer was removed. Embryos were washed 4x10 minutes with wash buffer at room temperature on a nutator. A fluorophore-conjugated secondary antibody was diluted (1/200, Jackson Immuno) in antibody block. Embryos were incubated with the antibody at room temperature for 1 hour and 45 minutes on a nutator. The antibody solution was removed and 1 mL wash buffer was added. Embryos were allowed to settle and the buffer was removed. Embryos were washed 2x10 minutes with wash buffer at room temperature on a nutator. Embroys were photographed immediately or stored in wash buffer at 4°C in the dark until they were photographed.

CHAPTER III

MAPPING TISSUE REGISTRATION OF *NODAL* EXPRESSION IN *XENOPUS*

Introduction

Interpreting the Nodal signaling gradient

Proper patterning of the vertebrate embryo is highly dependent on the ability of cells to accurately detect and interpret Nodal-signaling levels, which are sometimes very fine quantitative distinctions. How a cell interprets its position within a morphogen gradient has been an intense area of focus in developmental biology for many years. Adoption of a specific cell fate, in some contexts, could be the result of a simple binary decision dependent on whether a signaling source is sensed or not. However, the importance of different levels of Nodal signaling in patterning multiple cell fates suggests that cells are not faced with such an easy "yes" or "no" question, but instead must interpret multiple factors such as perdurance and strength of signal before committing to a particular cell fate.

Most of the knowledge regarding how cells sense the Nodal signaling gradient is extrapolated from experiments performed with Activin, a TGF-β superfamily member that has similar developmental functions to Nodal, but does not require the aid of a co-receptor and is easier to produce and purify. Work primarily from the lab of Sir John Gurdon has suggested that cells respond to Nodal/Activin signaling through a ratchet-like process in which gene expression reflects the highest concentration of morphogen to which cells have been exposed, provided enough time is passed at this upper concentration. In experiments where a bead coated in 1.5

nM Activin (a so-called "weak" bead) was sandwiched between two animal caps (tissue that is naïve to Nodal/Activin signaling), cells closest to the bead expressed *brachyury* (*xbra*). Cells in animal caps sandwiching a bead coated in 15 nM Activin ("strong" signaling bead) expressed *goosecoid* (*gsc*) closest to the bead and *xbra* beyond the *gsc*-expressing cells. When animal cap cells were first exposed to a weak bead for a set amount of time, and then a strong bead for an equivalent time frame, cells adopted an expression pattern seen with the high bead alone—*gsc* closest to the bead and *xbra* farther out (Gurdon et al., 1995). Thus, cells continuously assay the ligand concentration in their environment and change their response (in this example, their gene expression output) over time to reflect the highest level of morphogen that was detected. Cells are, apparently, unable to ratchet-down their response to a lower level once exposed to a higher level of signal – at least over the timeframe of the experiments that have been performed so far (Gurdon et al., 1995).

Experiments in which dissociated *Xenopus* animal cap or blastula cells were cultured with [^{35}S]-methionine and cysteine-labeled Activin showed that ligand concentration is determined by the number of occupied cell-surface receptors per cell, and that the absolute level of occupancy, not the ratio of unoccupied to occupied receptors, was most important when deciding cell fate outcome. For example, one hundred molecules of bound [^{35}S]Activin, occupying only 2% of the total receptors under wild-type conditions, was enough to activate expression of *Xbra*. Only a slight increase, to three hundred molecules of [^{35}S]Activin, or just 6% receptor occupation, was needed to change the expression output from *xbra* to *gsc*. Overexpression of cell-surface receptors did not change the number of activin molecules needed to activate the respective gene outputs. However, receptors bound ligands more quickly when there was a high ligand

concentration, and more slowly when the ligand concentration was low, indicating a dose-dependent on-rate (Dyson and Gurdon, 1998).

Type I and type II receptors do not have equal importance in determining the effect on cellular gene expression profile. Embryos overexpressing the type I receptor ALK4 did not display altered gene expression patterns compared to uninjected control embryos when incubated with increasing amounts of activin. However, overexpressing type II receptors changed gene expression in response to increasing activin concentrations, indicating that the type II receptor is the principal determinant in interpreting the level of the morphogen (Dyson and Gurdon, 1998).

Exposure of dissociated animal caps to activin for 10 minutes, followed by washes to remove excess unbound ligand, was enough time to activate gene expression, which still occurred three hours after ligand exposure, suggesting that cells "remember" the exposure and even the level of the activating signal (Bourillot et al., 2002; Jullien and Gurdon, 2005). Studies done in cell lines suggest that this memory comes from the ability to internalize the active type I/II receptor complexes. SARA, the anchor protein responsible for recruiting Smad2 to type I receptors for phosphorylation, also contains a FYVE domain, which is capable of associating with phospholipid-enriched EEA1 (early endosome antigen-1)-positive endosomes (Di Guglielmo et al., 2003). The type I/II receptor complex and SARA have been observed to be internalized from the plasma membrane in clathrin-coated endocytic vesicles both in vitro and in *Xenopus* embryonic cells (Di Guglielmo et al., 2003; Jullien and Gurdon, 2005).

The internalization of the receptors is thought to prolong signaling in at least two ways. First, it has been shown that receptors are capable of being internalized through a second pathway that is dependent on lipid-raft–caveolar internalization. These lipid rafts also contain Smad7 and the E3 ligase Smurf2, which mediate the ubiquitin-dependent degradation of the receptor complex (Di Guglielmo et al., 2003). Clathrin-dependent internalization is thought to sequester the activin receptors from the degradation pathway, and prolong their activity. Second, it has been shown that activin is internalized with SARA and the receptor complex in the endosomal compartments, and that impairment of ligand internalization inhibits gene induction in response to Activin signaling. Encapsulation of the ligand and receptor into endosomal compartments may also stabilize their interaction with each other, and prolong signaling within the cell, even when extracellular ligand levels have dropped below the threshold for active signaling (Jullien and Gurdon, 2005).

Signaling activity at the cell surface, or in ligand-receptor containing cytoplasmic vesicles, is proposed to be monitored by the nucleus through cytoplasmic shuttling of Smads (Inman et al., 2002). pSmad2 translocation to the nucleus occurs within twenty minutes of ligand binding to receptor complexes (Bourillot et al., 2002), and continuous receptor activity is required to maintain pSmad2 in the nucleus (Inman et al., 2002). Even when extracellular ligand levels decrease, pSmad2 nuclear levels are maintained at the highest level of signaling observed by the cell (Bourillot et al., 2002), because of the internalization of the ligand-receptor complex that continues to phosphorylate Smad2 (Jullien and Gurdon, 2005). In the nucleus, pSmad2 is dephosphorylated, leading to dissociation from Smad4. Both Smad4 and unphosphorylated R-Smads are then recycled back to the cytoplasm through independent processes. If receptors

are still active, Smad2 is again phosphorylated and trafficked to the nucleus, repeating another round of cytoplasmic-nuclear shuttling. If receptors are no longer active, Smad2 remains cytoplasmic and gene activation ceases. This process can last for hours, as receptors must signal for 3-4 hours – at least in cell culture – in order to achieve maximal gene expression (Inman et al., 2002).

Detection of active Nodal signaling

Current methods for analyzing Nodal-signaling dynamics (duration, intensity, location) *in vivo* primarily rely on detecting the expression of *Nodal* or its targets *Lefty2* and *Pitx2*. It is not fully understood, however, if the spatiotemporal dynamics of *Nodal* expression equate to the signaling dynamics of the Nodal ligand. Considering that Nodal is a morphogen, it would not be surprising if the spatial domain of the Nodal ligand exceeds the realm of its expression domain, or lasts and functions significantly longer than the expression detected by RNA *in situ* hybridization. In fact, experiments in *Xenopus* showed that Activin is capable of traveling up to 300 µm from its source (Gurdon et al., 1994), at a rate of 100 µm per hour (Gurdon and Bourillot, 2001). The Nodal ligand itself can travel from a Nodal producing graft positioned in the L LPM of *Xenopus*, reaching the far anterior end of the LPM and the notochord. In situations of tissue perturbation, Nodal takes additional routes into the endoderm and the R LPM (Marjoram and Wright, 2011). In mouse mutants that conditionally lack *Lefty2* in the LPM, *Pitx2* is unregulated in the R LPM leading to randomized *situs.* Importantly, because right-sided *Nodal* expression was not seen to occur in these mutants, the conclusion was made that the Nodal ligand travels beyond its expression domain to activate Nodal signaling in the R LPM

(Meno et al., 2001). The potential of the Nodal ligand to travel outside the *Nodal* expression domain is further suggested in normal developmental conditions during which Nodal downstream targets *Lefty1/2* are expressed in the midline where *Nodal* expression is not detected. These data reinforce the notion that RNA expression patterns do not fully reflect the dynamics (perdurance, tissue penetration, range) of the translated protein, and that alternative detection methods need to be investigated in order to reach a more complete understanding of how the level and duration of Nodal signaling pattern different developmental fates during embryogenesis. Clearly, sensitive reagents for detecting the endogenous Nodal ligand, and even differentiating its various forms within tissue (proprotein, cleaved active ligand, "old" inactive ligand in the process of clearance) would be useful tools.

Attempts to design antibodies that recognize Nodal or Lefty have been far from successful. The ligands are thought to be unstable and/or in low abundance. It has been calculated that morphogens are active at concentrations as low as 10^{-9} to 10^{-11} M (Gurdon and Bourillot, 2001). Also, in general, antibodies cannot discern between the Nodal proprotein and the cleaved ligand, adding uncertainty as to whether or not what is being recognized is the active ligand. Although observing tagged Nodal ligands has yielded useful information regarding ligand dynamics, as demonstrated in Marjoram and Wright (2011), the placement of tags is usually in the ligand domain therefore leading again to the problem of not distinguishing active ligand, proprotein, or inactive dead (and clearing) protein. In most of these experimental cases, tagged Nodal ligands were exogenously expressed, and not from the endogenous locus. Although there were somewhat convincing arguments that the ligands were not expressed at very supra-physiological levels, such analysis provides only a limited picture of what endogenous signaling

dynamics might look like across the embryo. Despite our success with tagged ligands, we and others have found that tagging Nodal without disrupting its function is quite challenging, and often not intuitive or logical. For these reasons, Nodal antibodies and tags leave open several distinct caveats regarding their ability to track ligand dynamics.

An alternative method for detecting active Nodal signaling has been to assay the localization pattern of pSmad2, the downstream intracellular signal transducer. Polyclonal antibodies against both pSmad2 and the BMP pathway signal transducer, pSmad1, have been generated by the lab of Peter ten Dijke and by commercial companies using his peptide design. The antibodies were generated in rabbits against the last four amino acids of pSmad2 (KKK-S[Sp]M[Sp]; [Sp] representing phosphorylated serine) and the last seven amino acids of pSmad1 (KKK-NPIS[Sp]V[Sp]) (Persson et al., 1998). The lysines (KKK) act as a spacer to move the haptenated epitope away from the carrier protein, increasing accessibility to the immune system during the immunization process. Decreased or increased R-Smad phosphorylation was detected by both antibodies in *Xenopus* embryos in which TGF-β or BMP signaling had been inhibited or activated, suggesting specificity of the pSmad1 and pSmad2 antibodies (Faure et al., 2000). However, the ability to replicate the endogenous staining patterns detected with the ten Dijke antibodies has been difficult. Also, when used on E5.5-7.5 mouse embryos, the ten Dijke pSmad2 antibody detected nuclear pSmad2 randomly throughout embryonic and extraembryonic tissues (Chuva de Sousa Lopes et al., 2003). During these stages, Nodal signaling is active in the primitive streak where it activates Nodal target genes (i.e. *Brachyury*, *Lefty2*) and patterns cells as they ingress the streak. Therefore, the expected restriction of pSmad2 to the streak was not seen, calling into question the specificity of this antibody *in vivo*.

Also hindering the wide use of currently available phospho-Smad antibodies is that the ten Dijke antibodies are very limited in supply (they had to be affinity purified). Commercial pSmad2 and pSmad1 antibodies suffer from high signal-to-noise and lack sensitivity, especially on embryonic tissue.

Generation of pSmad2 and pSmad1 antibodies

We proposed using pSmad2 localization as a read out for Nodal signaling in order to generate a spatiotemporal map of active Nodal signaling in the LPM during the various stages in which L-R patterning occurs, but the current reagents were not of high enough quality. We therefore decided to generate our own pSmad2 and pSmad1 antibodies. While our primary need was for a sensitive and reliable pSmad2 antibody, generating a pSmad1 antibody with the same novel design was expected to result in a higher quality antibody than currently available. For example, because right-sided BMP signaling counters *Nodal* autoregulatory expression in the R LPM of multiple species (Lenhart et al., 2011; Mine et al., 2008; Ramsdell and Yost, 1999), a pSmad1 antibody could help visualize areas where such BMP-induced inhibition occurs.

We contracted the production of the pSmad antibodies to "Abgent", a company specializing in the production of phospho-antibodies and claiming proprietary technology to improve antigen presentation to the immune system. To improve specificity, the length of the epitope for each R-Smad was increased to encompass the last nine amino acids of each protein, while preserving the native phosphoserine structure. Rabbits were inoculated with the following peptides: KKK-PSVRCS[Sp]M[Sp] for pSmad2 and CKKK-PHNPIS[Sp]V[Sp] for pSmad1. The commonly used cross-linker glutaraldehyde is very reactive with thiol moieties such as those in cysteine, making

it undesirable to use for coupling the pSmad2 epitope, with the internal cysteine, to keyhole limpet hemocyanin (KLH), a carrier protein that increases the size of the antigen for an effective immune response. To promote homogeneous coupling of the pSmad2 epitope through its N-terminus and not internal residues, special haptenization chemistry ("hydralink") was used for pSmad2. This special coupling was also used to help extend the pSmad2 epitope away from KLH to improve recognition by the immune system. pSmad1 had the additional N-terminal cysteine added for standard coupling with glutaraldehyde. Repeated inoculations of rabbits with these KLH-coupled peptides over several months led to a high titer of phospho-peptide antibodies. pSmad1 and pSmad2 antibodies were then peptide affinity-purified from the raw anti-sera by Abgent and provided to us for characterization.

The overall goal was that, if it were to be specific and sensitive enough, the new pSmad2 antibody could be used to generate spatiotemporal maps of active Nodal signaling during stages of L-R patterning in *Xenopus*. The resulting activity maps would then be overlaid with *Nodal* expression, derived from *in situ* hybridization analysis. From these mapping efforts, we hoped to gain insight into whether or not Smad2 activation was as transient as the *Nodal* posterior-to-anterior wave of expression, or longer lived, reflecting internalization of ligand-receptor complexes thought to maintain signaling. Furthermore, *Nodal* expression in the LPM is graded, with higher levels of expression seen dorsally, abutting the intermediate mesoderm, and at the leading anterior region of the expression domain. It is not known if the level of Nodal signaling mimics this gradient. The pSmad2 map could ascertain if signaling levels were uniform across the L LPM, or if there were regions in which cells experience higher ("hot spots") or lower ("cold spots") levels of signaling (Fig. 3.1). Because Nodal has been shown to travel far

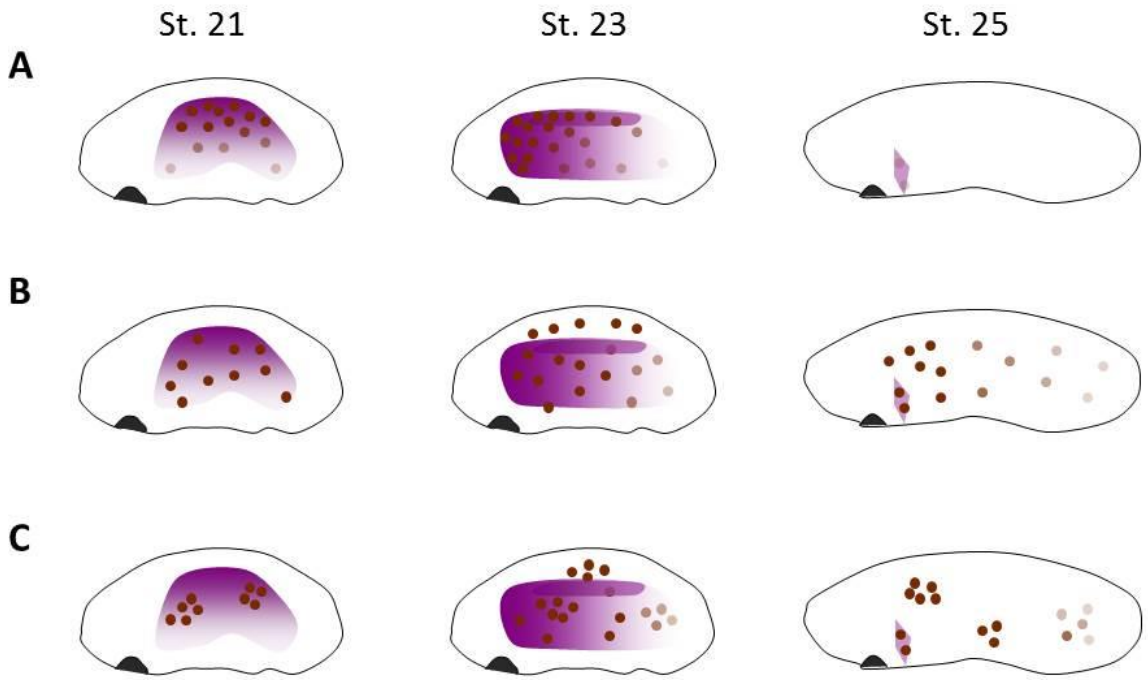

Fig. 3.1 pSmad2 spatiotemporal mapping as a read out of active Nodal signaling. pSmad2 localization (circles) overlaid on *Nodal* expression (purple) at various stages during asymmetric gene expression in the L LPM. (A) Smad2 activation may mimic the dynamics of *Nodal* expression, remaining localized with the *Nodal* expression domain and terminating with *Nodal* expression. (B) Or, Smad2 activation could be farther-reaching and longer-lasting than *Nodal* expression. (C) Smad2 activation may not be uniform across the L LPM. Instead there could be regions in which cells experience higher (circle clustering) or lower levels of Smad2 activation.

and activate downstream targets outside of its RNA expression domain, pSmad2 spatiotemporal maps would prove useful as to the ultimate range of influence of Nodal signaling, in the LPM and even beyond it. Mapping many embryos during the stages of asymmetric *Nodal* expression would determine the reproducibility of pSmad2 localization. These spatiotemporal maps could then be correlated to specific reproducible alterations in LPM morphology associated with establishing differential L-R anatomy (discussed in Chapter IV) to gain further insight into how Nodal signaling in the LPM influences the overall asymmetric morphology of the viscera.

Results

Antibody cross-reactivity and affinity purification

Much effort was put into characterizing the specificity of our newly generated pSmad1 and pSmad2 antibodies. A slot-blot assay determined the degree of undesirable cross-reaction with the C-terminal regions of other phosphorylated or unphosphorylated R-Smads (Fig. 3.2). Various amounts (0.25 ng to 100 ng) of peptides corresponding to the last 9 amino acids of pSmad2, pSmad1, Smad1, or Smad2 (the same peptides used to inoculate rabbits) were applied to supported nitrocellulose using a vacuum manifold. Membranes were then probed with either the pSmad1 or pSmad2 affinity-purified antibody. The pSmad1 antibody detected as little as 5 ng of pSmad1 peptide and chemiluminescence intensity varied with peptide amount. No specific signal was detected for any amount of Smad1, Smad2, or pSmad2 peptide, suggesting that our pSmad1 antibody was specific to pSmad1 and not likely to cross-react with

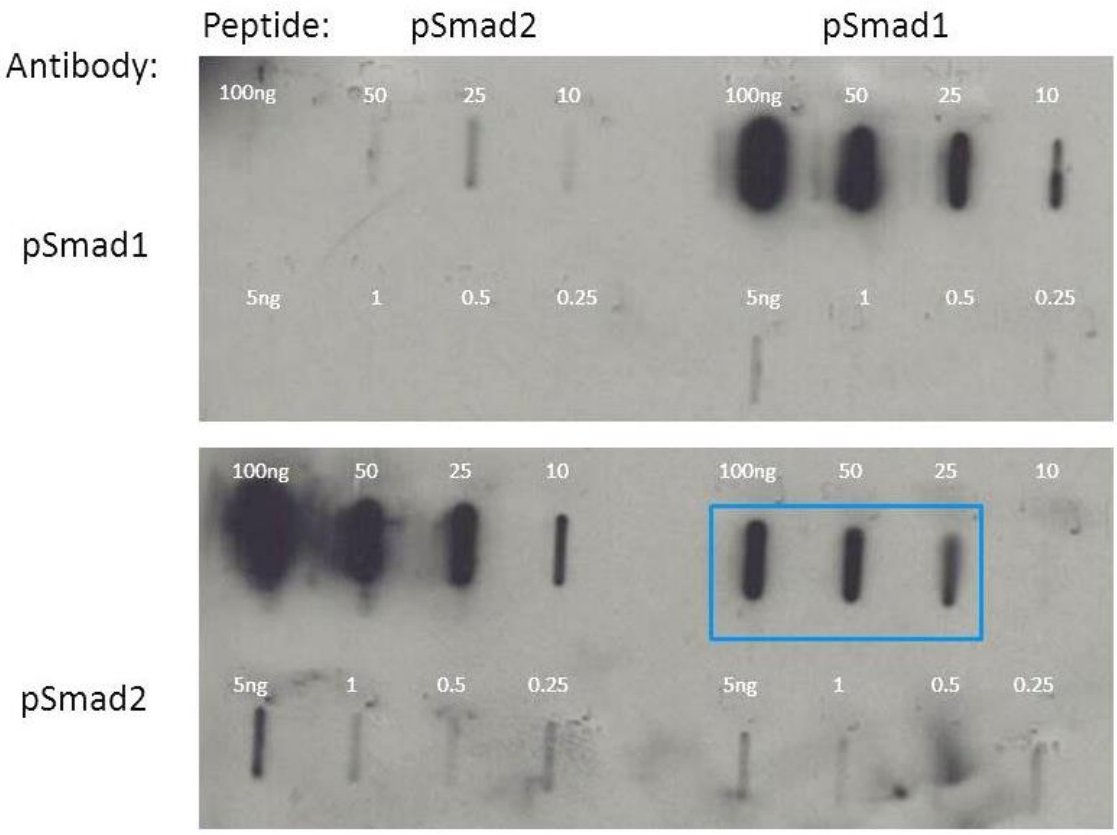

Fig. 3.2 Abgent pSmad2 antibody cross-reacts with pSmad1. Slot blot: pSmad1 and pSmad2 peptides on nitrocellulose, probed with pSmad1 (upper panel) or pSmad2 (lower panel) antibody. pSmad2 recognition of the pSmad1 peptide boxed in blue.

pSmad2 or unphosphorylated R-Smads *in vivo*. Similar to pSmad1, the pSmad2 antibody detected as little as 5 ng of pSmad2 peptide, with no unphosphorylated Smad1 or Smad2 detected. Unfortunately, cross-reactivity was seen with 25-100 ng of pSmad1 peptide (Fig. 3.2).

Recognition of the pSmad1 peptide by pSmad2 antibody could result from two possibilities: (1) the peptide-affinity-purified sample from Abgent contained a heterogeneous mixture of antibodies recognizing pSmad1 and those recognizing pSmad2, or (2) a homogeneous antibody population was capable of recognizing both pSmad1 and pSmad2. A peptide competition assay was used to discern between the two possibilities. The pSmad2 antibody was incubated with a 500-fold excess of soluble pSmad1 peptide, to bind any pSmad1-reactive antibody. A slot-blot assay as described above tested for improved specificity of the pSmad1-blocked antibody mixture, and detection of pSmad1 peptide on the membrane was now reduced or eliminated (Fig. 3.3). Detection of pSmad2 peptide was minimally diminished, suggesting that this improved-specificity, pSmad1-depleted antibody preparation could now be suitable for detecting pSmad2 within real tissue.

From this small-scale test, I showed that pSmad1 cross-reactivity could be removed to produce a pSmad2-specific antibody. Therefore, I decided to do a large-scale affinity purification of the pSmad2 antibody in house and deplete pSmad1 cross-reactivity from raw pSmad2 anti-serum (supplied by Abgent). Antiserum was incubated with pSmad2 matrix (pSmad2 peptide covalently immobilized on agarose beads; supplied by Abgent, who made the matrix as part of their standard affinity purification method for phospho-peptide antibodies) to select pSmad2 antibodies. After incubation, captured pSmad2 antibodies were eluted with a series of acidic

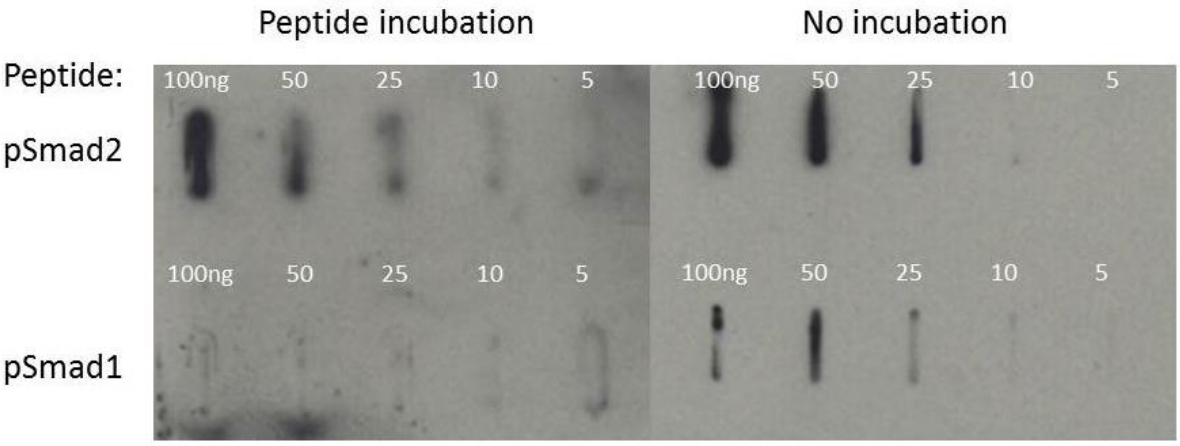

Fig. 3.3 pSmad2 cross-reactivity with pSmad1 can be removed. Anti-pSmad2 slot blot showing detection of various amounts of pSmad2 peptide (top row) or pSmad1 peptide (bottom row). Incubation of pSmad2 antibody with 500-fold excess of pSmad1 peptide prior to immunoblotting removes pSmad1 cross-reactivity.

and basic step-elutions. Acid and base fractions showing the highest reactivity with the pSmad2 peptide via slot blot were pooled (the acidic pool was kept separated from the basic pool), and dialyzed. To deplete pSmad1 cross-reactivity from the pSmad2 antibody, the dialyzed acidic and basic fractions were incubated with pSmad1 matrix (also obtained from Abgent). After incubation, the depleted antibody fractions were tested by slot-blot analysis to determine pSmad2 and pSmad1 reactivity. While the base-eluted pool showed slightly less reactivity with the pSmad2 peptide as compared to the acid-eluted pool, the acid-eluted pool showed an undesired reactivity with pSmad1, which was absent from the base-eluted pool. Therefore, only the affinity-purified base-eluted pooled fractions were used in the remaining assays, described below, to determine the quality and usefulness of this new pSmad2 antibody preparation. PLEASE NOTE: The "clean" base-eluted pool is henceforth referred to as "pSmad2 antibody", only for simplicity. Because the affinity-purified pSmad1 antibody as directly supplied by Abgent did not show cross-reaction on the slot blot assay, it was used "as is" in the remaining assays and was not subjected to our own in-house affinity purification.

Antibody specificity for western blotting

The usefulness of these new pSmad1 and pSmad2 antibodies for immunoblotting was first tested on lysates collected from unmanipulated gastrula-stage *Xenopus* embryos. On western blots, our pSmad2 antibody detected a doublet migrating between 55-60 kDa, the expected size of pSmad2 (Fig. 3.4A). pSmad2 is proposed to run as a doublet because of the two naturally present differentially spliced isoforms, with full-length pSmad2 being the upper band of the doublet, and pSmad2Δexon3 being the lower band (Faure et al, 2000). Our pSmad1 antibody

detected a single band also migrating between 55-60 kDa, although weakly (Fig. 3.4A). High-level activation of the Nodal pathway by co-injecting mRNAs encoding *Xnr1* and *Smad2* into 1-cell *Xenopus* embryos for analysis at gastrulation showed a consistent increase in pSmad2 over uninjected embryos. Similar results for the pSmad1 antibody were achieved by co-injecting *Bmp4* and *Smad1* (Fig. 3.4A). In the presence of the inhibitor Noggin (BMP pathway) or the ALK4/5/7 receptor-blocking drug SB505124 (Nodal pathway), both the pSmad1 and pSmad2 antibodies detected decreased or absent Smad1 and Smad2 phosphorylation, respectively (Fig. 3.4A). Pre-treatment of uninjected whole-embryo lysate samples with lambda phosphatase also resulted in the inability to detect Smad1 and Smad2 phosphorylation (Fig. 3.4B), further supporting the specificity of these antibodies.

Although the gain- and loss-of-function assays showed that the 55-60 kDa bands were specific to the R-Smads, both antibodies also detected proteins of very different relative molecular weights. This detection was variable and slightly dependent on lysate preparation (the type of homogenization buffer used), and the pSmad1 antibody detected more non-specific bands than the pSmad2 antibody. Some of these bands are thought to correspond to yolk proteins (phosvitin at 35 kDa, lipovitellin 2 at 31 kDa, and lipovitellin 1 at 115 kDa). Compared to commercially available antibodies (Cell Signaling, specifically), our pSmad2 antibody more cleanly detected pSmad2 on western blots, but our pSmad1 antibody did not, and in fact would not be preferred over commercially available antibodies for immunoblotting. Also of note, it appeared that the ability of the pSmad1 antibody to detect pSmad1 via immunoblotting declined with the age of the antibody. It worked well and cleanly when first received from

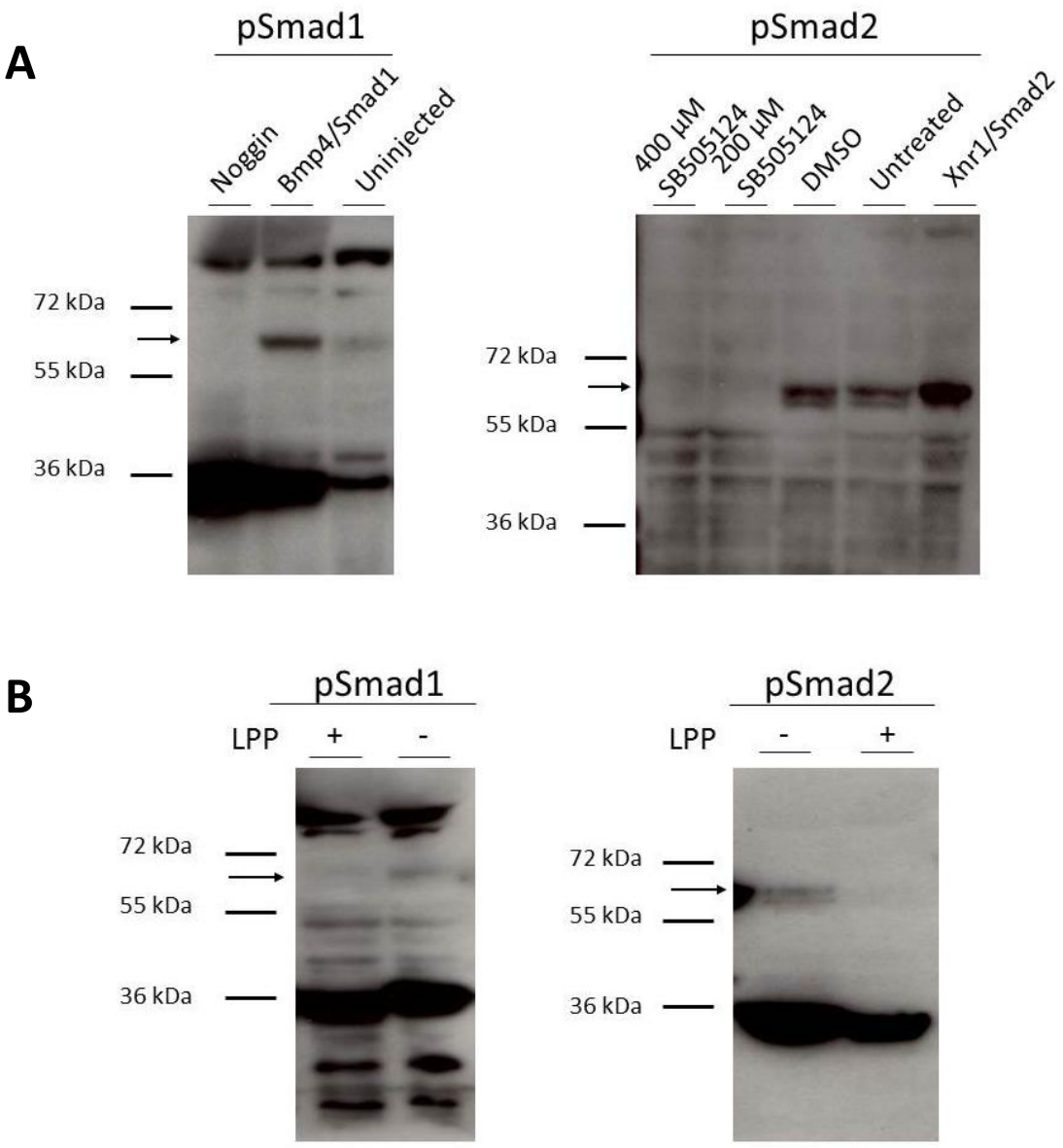

Fig. 3.4 Antibodies recognize phosphorylation motifs of pSmad1 and pSmad2 on western blots. (A) Gain- and loss-of-function assays confirm that the 60 kDa band (arrow) detected by the pSmad1 and pSmad2 antibodies are specific to pSmad1 and pSmad2, respectively. (B) Addition of lambda phosphatase (LPP) to *Xenopus* lysates prevents detection of the 60 kDa band by the pSmad1 and pSmad2 antibodies, confirming that the antibodies recognize the C-terminal phosphorylation motif of Smad1 and Smad2. The bank running at approximately 36 kDa is the yolk protein phosvitin.

Abgent, but declined with later use, even with aliquoted storage at -80°C and limited freeze-thaw cycling.

Antibody specificity for immunohistochemistry

Previously published immunolocalization patterns for pSmad2 show a gradient of pSmad2 across the marginal and vegetal cells of a bisected stage 9 *Xenopus* embryo, with greater pSmad2 localization dorsally and little to no localization in the animal cap and ventral half. By stage 10.5, in the middle of the gastrulation process, pSmad2 localization is reported as more symmetric across the dorsal-ventral axis. pSmad1 exhibits the opposite pattern, starting out symmetric across the dorsal-ventral axis in the marginal and vegetal cells, then becoming localized in a ventral-to-dorsal gradient as gastrulation begins. Unlike pSmad2, pSmad1 was also detected in animal cap cells (Faure et al, 2000; Schohl and Fagotto, 2002). With our phospho-Smad antibodies, pSmad1 and pSmad2 were detected symmetrically across the dorsal-ventral axis in both blastula- and gastrula-stage embryos (Fig. 3.5A-C). Also, pSmad2 was detected in the animal cap cells at these stages (Fig 3.5A-C). The more widespread detection of pSmad localization by our antibodies, if specific, could imply that these new reagents are more sensitive and capable of detecting low-level phosphorylation that has been missed by the currently available commercial reagents.

Gain- and loss-of-function experiments were performed on *Xenopus* embryos to determine if the immunolocalization with our pSmad2 antibody was indeed specific to pSmad2. One-cell *Xenopus* embryos were injected with mRNA encoding a dominant-negative (kinase-deficient)

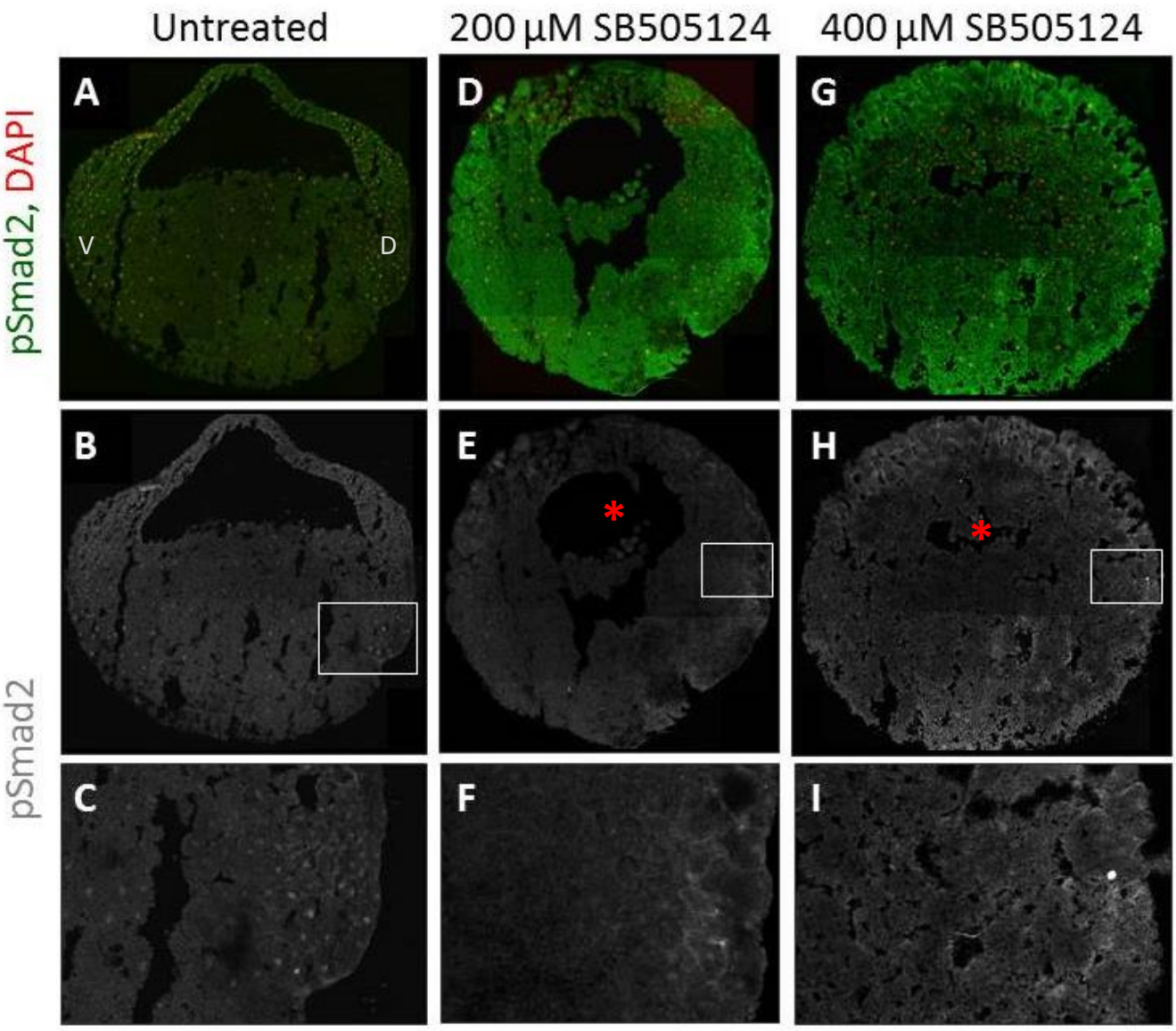

Fig. 3.5 pSmad2 antibody reactivity lost when Nodal signaling inhibited in gastrulas. (A-C) pSmad2 immunodetection on cryosections of unmanipulated stage 10.5 embryos, showing widespread pSmad2 localization. (D-I) pSmad2 immunodetection on SB505124-treated embryos lacking Nodal signaling. Boxed regions in (B,E,H) are shown in (C,F,I). Asterisks in (E,H) mark decreased or absent blastocoel cavity. D, dorsal; V, ventral.

ALK4 that is incapable of phosphorylating Smad2, and were allowed to develop until the dorsal lip became visible (approximately stage 10.5). Analysis of pSmad2 localization by immunofluorescence on 14 µm thick cryosections showed that the localization pattern was unchanged in injected embryos compared to uninjected control embryos. When overexpressed at high enough concentrations, dominant-negative *ALK4* can block all TGF-β signaling, as indicated by the lack of *xbra* expression in injected embryos (Cha et al., 2006), possibly by outcompeting other type I receptors for the type II receptors. Therefore, this result suggested that the pSmad2 antibody may not be specific on tissue. Additional Nodal-signaling loss-of-function experiments were performed with SB505124 to further test antibody specificity. Embryos were incubated in 200 µM or 400 µM SB505124 from the 4-cell stage to early gastrulation, at which point embryos were collected and processed as in the ALK4 experiment. At these concentrations, recognition of pSmad2 by the antibody was greatly reduced or absent in drug-treated embryos (Fig. 3.5D-I). However, the embryos did not appear healthy (failing cell divisions were apparent, a much smaller blastocoel cavity), calling into question whether the lack of antibody reactivity was related to the impending death of the embryo. Also, Nodal pathway activation by injecting mRNA encoding *Xnr1* and *Smad2* did not cause a reproducible or detectable increase in pSmad2 immunolocalization compared to controls.

Because the primary purpose of making these antibodies was to map active Nodal signaling during stages of L-R patterning, specificity of the antibody was also characterized on early tailbud-stage embryos (stages 18-27) when *Xnr1* and *Lefty2* are expressed in the L LPM. A nuclear immunodetection signal was detected broadly within all tissue types – mesoderm, endoderm, and ectoderm – with no obvious difference in pSmad2 localization or signal intensity

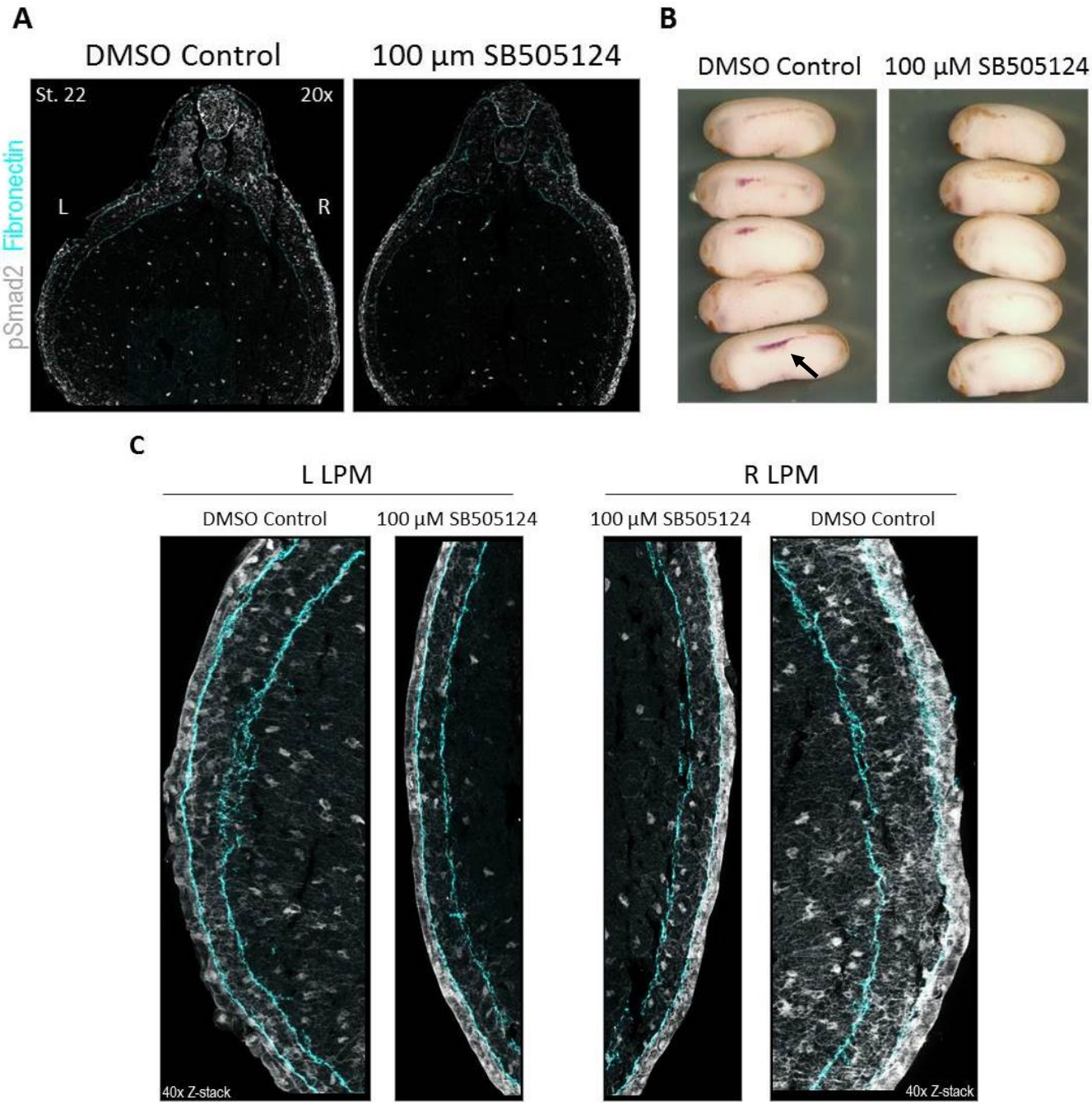

Fig. 3.6 pSmad2 antibody is not specific for pSmad2 in *Xenopus* tailbuds. (A,C) pSmad2 immunolabeling on cryosections of stage 22 *Xenopus* embryos. Fibronectin demarcates the LPM. Signal is detected widely throughout the LPM and endoderm of DMSO control embryos. Localization of this signal is unchanged in SB505124-treated embryos. (C) Higher magnification images of the LPM. No differences in signal localization are seen between the L and R LPM. (B) *Xnr1* (*Xenopus Nodal* homolog) *in situ* hybridization analysis on control and treated embryos confirming that Nodal signaling in blocked by SB505124 treatment. Arrow points to *Xnr1* expression in L LPM of controls. L, left; R, right.

between L and R LPM (Fig. 3.6A,C). Previously published reports are consistent with my observation, describing the presence of pSmad2 in multiple tissues outside of the LPM (somites, most likely caused by signaling from TGF-β ligands) (Schohl and Fagotto, 2002). However, in embryos in which Nodal signaling was inhibited—either by SB505124 drug treatment, or by cropping neurula-stage embryos to remove the posterior bilateral *Xnr1* expression domain, preventing initiation of asymmetric L LPM *Xnr1* expression (Ohi and Wright, 2007)—the pattern of pSmad2 immunodetection in the L LPM remained indistinguishable from unmanipulated embryos (Fig. 3.6A,C). No differences between the L and R LPM were observed in manipulated or control embryos (Fig. 3.6C). *In situ* RNA hybridization analysis confirmed the absence of *Xnr1* expression in the L LPM of manipulated embryos, indicating that the drug treatment and posterior-cropping had each effectively abolished Nodal signaling (Fig. 3.6B).

Similar loss- and gain-of-function analyses were done for the pSmad1 antibody with gastrula-stage embryos. Loss-of-function experiments to test for specificity of the immunodetection signal by injecting *Noggin* mRNA failed to cause a reduction or loss of pSmad1 nuclear immunofluorescence in treated embryos. Embryos were also treated with 0.5 µM or 10 µM concentrations of the BMP-specific small molecule inhibitor DMH1 (a gift courtesy of Dr. Charles Hong, Vanderbilt). At these concentrations, embryos exhibited a typical and expected dorsalized phenotype, with a bent axis and posterior truncation. Although this morphology would suggest that DMH1 had a developmental and specific effect on BMP signaling, the pSmad1 immunolocalization signal was unchanged. For comparison, we requested and obtained pSmad1 antibodies (one from rabbit, another from guinea pig) generated by Drs. Ed Laufer and Tom Jessell (Columbia University). Both antibodies detected a ventral-to-dorsal

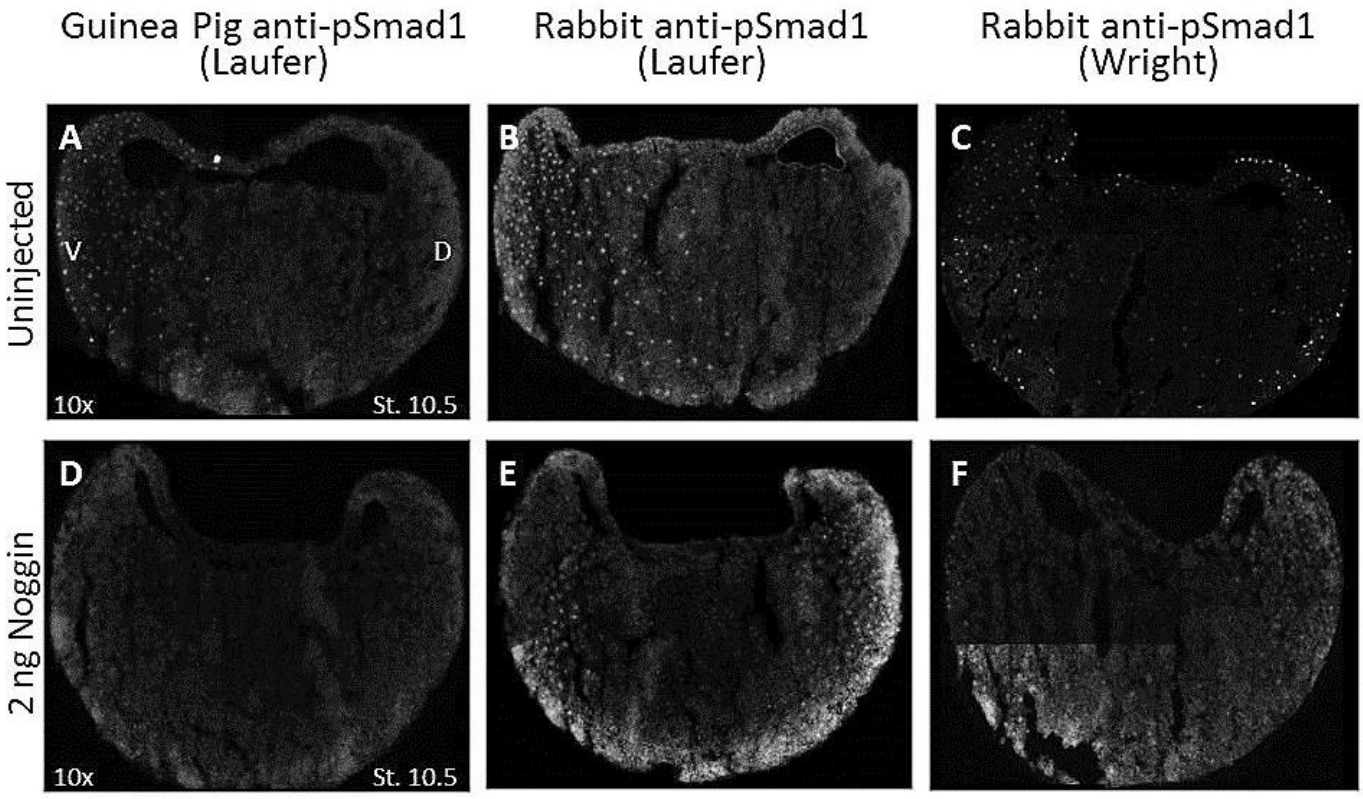

Fig. 3.7 pSmad2 antibody is not specific for pSmad1. pSmad1 immunolabeling on cryosections of stage 10.5 embryos that were (A-C) uninjected or (D-F) injected with 2 ng RNA encoding *Noggin* to block BMP signaling. (A,B) Laufer pSmad1 antibodies show expected ventral-dorsal gradient localization. (C) Our antibody symmetric signal. (D,E) pSmad1 immunodetection with Laufer pSmad1 antibodies is lost or greatly reduced in injected embryos, (F) while our antibody still shows symmetric signal.

gradient of pSmad1 across the marginal and vegetal cells of cryosectioned gastrula-stage embryos (Fig. 3.7A,B). Pathway inactivation by the expression of mRNA encoding *Noggin* (2 ng) was confirmed by the loss of pSmad1 detection, with a cleaner inhibition detected by the guinea pig antibody compared to the rabbit antibody (Fig. 3.7D,E). However, on nearby serial cryosections from the exact same *Noggin*-injected embryo, the immunofluorescence signal with our pSmad1 antibody was equivalent to uninjected controls (Fig. 3.7F). From these analyses, we concluded that our pSmad1 antibody was, for unknown reasons, detecting epitopes unrelated to BMP signaling, and we decided not to proceed with further characterization of the antibody using tailbud-stage embryos.

Discussion

The goal of chapter was to generate a spatiotemporal map of Nodal signaling dynamics in *Xenopus* during stages of L-R patterning, which occurs between stages 18-27, in order to better understand how the *Xnr1* expression wave could be functionally registered by the L LPM – as a link to the future asymmetric tissue reorganizations that result in the final differential L-R anatomy. In other words, we would have liked to combine this map with the studies being performed in Chapter IV ("*Identifying and characterizing tissue architecture asymmetries in the L vs. R LPM prior to and during organ looping"*), which look to identify the initiating tissue architecture asymmetries in the L and R LPM that underlie the larger and more coordinated movements of asymmetric morphogenesis. For example, if reproducible "hot" or "cold" spots for pSmad2 localization existed within the LPM, which could be reproducibly mapped, then future experiments could involve their potential tracing, for example either by injection of a

vital dye or fluorescent dextran, to see if these regions correspond to regions that initiate asymmetric and perhaps focal alterations in tissue architecture at later stages. Such analysis would help us better understand the instructive role that Nodal signaling plays in dictating the chirality of the visceral organs. Unfortunately, we concluded from the characterization of the pSmad2 antibody described above, that this new antibody was not specific or sensitive enough for this endeavor. Although the goal of this project is still considered valuable and worth pursuing, the project was reprioritized in order to focus on the other studies discussed in Chapters IV and V.

Reasons for lack of pSmad1 and pSmad2 antibody specificity

It is difficult to determine why either antibody was not specific. The epitope(s) detected by our pSmad1 and pSmad2 antibodies seemed clearly nuclear, as expected for active pSmad1 or pSmad2. It is unlikely that these antibodies are exceptionally sensitive and capable of detecting a basal level of Smad phosphorylation that occurs in every cell, as this would still be expected to be eliminated by pathway inhibition using drugs or other loss-of-function manipulations. Also, if the antibody was specific enough to discriminate between low, basal levels of phosphorylation and increased phosphorylation as a response to active signaling, it would be expected that staining intensity in the nuclei would be variable, but it was not. The presence of immunodetection signal in tissues where Nodal signaling is thought not to occur, such as in animal cap cells and throughout the embryo (epidermis, endoderm, somites) at tailbud stages, also suggests a lack of specificity in our pSmad2 antibody. Even though some TGF-β ligands are present in the notochord and somites, the sheer expanse of “pSmad2” localization detected

with this antibody, and the inability to alter the localization pattern in response to inactivating not just Nodal signaling, but the entire arm of the TGF-β/Activin/Nodal pathway, suggests that this staining is not reflective of TGF-β signaling.

The pSmad2/Smad4 complex is thought to be partially stabilized by an interaction between the C-terminal phosphorylation motif of pSmad2 and a phosphoserine-binding region in the MH2 domain of both pSmad2 and Smad4 (Wu et al., 2001; Wrana, 2002). Formation of the pSmad2/Smad4 complex may therefore hinder detection of the phospho-motif by burying the C-terminus of pSmad2 within another Smad. This could be one explanation as to why current antibodies detect pSmad2 on western blots, when proteins are denatured before immunoblotting, but detect it inconsistently on tissue. Our antibodies may have also been nonspecific due to some inherent flaw in the design of the epitope that we are unaware of, or certain species (rabbit vs. guinea pig) may have a better immune response to the pSmad epitopes.

Alternative methods

Bimolecular fluorescence complementation (BiFC) has been used to visualize nuclear accumulation of the Smad complex in frog, and the Nodal gradient during mesendoderm induction in fish (Saka et al., 2007; Harvey and Smith, 2009). BiFC involves fusing an N-terminal fragment of VENUS, a variant of enhanced yellow fluorescent protein (EYFP), to the N-terminus of Smad4 and a C-terminal fragment of VENUS to the N-terminus of Smad2. These VENUS portions reassemble and fluoresce when pSmad2 and Smad4 bind each other (Harvey and Smith, 2009). The use of a fluorescent reporter can be problematic in *Xenopus* embryos, as the

cells are packed with yolk platelets that have broad-spectrum autofluorescence and interfere with detection of a fluorescent reporter signal. Although it may not be impossible to fully eliminate fluorescence from yolk platelets, there are regions within the UV spectrum where yolk autofluorescence is less strong, and using reporters that emit at these wavelengths could overcome or minimize the interference from yolk. One concern with this idea is that VENUS fluorescence may not be as long-lived as the pSmad2/Smad4 complex, preventing us from accurately depicting the duration of Nodal signaling. Another major caveat to this technique is that the Smad-VENUS constructs are usually expressed exogenously in the embryo. Exogenously introduced Smad2 must compete with endogenous Smad2 for phosphorylation and it could superactivate the Nodal pathway just by its very presence.

To gain a more accurate picture of endogenous Nodal signaling, it may be possible to express the Smad-VENUS constructs from the native *Smad* loci in *Xenopus*. In recent years, the use of transgenic frogs has increased in the community, as well as the techniques that support the generation and use of these animals. Genome editing techniques such as CRISPr/Cas (clustered regularly interspaced short palindromic repeats-associated/CRISPr associated), TALENs (transcription activator-like effector nucleases), and zinc-finger endonucleases have all been used to generate transgenic frogs (Blitz et al., 2013; Lei et al., 2012; Nakayama et al., 2013; Young and Harland, 2012). In the future it may be worth pursuing the generation of frogs that express the Smad-VENUS fusion proteins from the endogenous Smad loci using *Xenopus tropicalis*, which has the distinct advantages of being diploid and having a shorter generation time (4 months compared to 1-2 years in *laevis*).

CHAPTER IV

IDENTIFYING AND CHARACTERIZING TISSUE ARCHITECTURE ASYMMETRIES IN L VS. R LPM PRIOR TO GUT LOOPING

Introduction

During stages of asymmetric gene expression, Nodal signals within the lateral plate mesoderm (LPM), which eventually gives rise to tissues of the heart, and the smooth muscle and mesenchyme that help pattern the overlying endoderm of the gut (Chalmers and Slack, 1998; Deimling and Drysdale, 2011; Mclin et al., 2009). High-resolution studies of *Xenopus* LPM architecture performed by a former graduate student in the lab, Lindsay Marjoram, showed that the LPM consists of two, closely apposed, cell layers that give rise to the future somatic (boarders epidermis) and splanchnic (boarders endoderm) epithelial layers, both of which are one cell-layer thick (Marjoram and Wright, 2011). Later in development, when the coelom begins to form, the somatic and splanchnic layers separate, with the splanchnic layer giving rise to the visceral mesoderm that encompasses the gut endoderm (Mclin et al., 2009). During the peak period of L-sided *Nodal* expression (stage 23), the cells within the LPM undergo differential shape changes, with somatic cells becoming more squamous and splanchnic cells more columnar. These cell-shape differences occur in both the L and R LPM and persist into organ-looping stages. After asymmetric *Nodal* expression ceases (stage 25), the LPM undergoes a symmetrical A-to-P epithelialization event lasting through stage 34 (the latest stage analyzed), which is just prior to the start of gut looping (Marjoram and Wright, 2011).

During gut looping, the L and R LPM contribute equally to the gut, but distinctly localize to different regions within the first two loops formed. L LPM cells localize to concave surfaces (normally on the left) of loops and R LPM cells localize to the convex surfaces (normally on the right). R-sided misexpression of *Pitx2* causes ectopic concavities to form in the gut (Muller et al., 2003). This study and many others suggest that Nodal signaling in the LPM acts as a morphogenetic cue that somehow triggers asymmetric architectural changes in the LPM that are essential for establishing proper laterality and morphology of the visceral organs. What these architectural changes are, how they become initiated, and how they guide asymmetric organogenesis are open-ended questions in the field. While both the heart and gut undergo asymmetric looping that is dependent upon Nodal signaling, development of the vertebrate heart is well documented and will not be discussed here. The processes driving chiral gut looping (which is also linked to the positioning of the liver and pancreas that bud off the gut), on the other hand, are only just beginning to be understood and are the focus of this chapter.

Pitx2 as an effector of Nodal signaling

In the frog, approximately 24 hours elapse between the end of asymmetric *Xnr1* expression (stage 25) and the start of asymmetric gut morphogenesis (stage 38). Little is known about what happens during this time period in terms of the initial architectural changes occurring within the LPM and how Nodal signaling influences these early changes. During this 24-hour time window, *Pitx2*, which encodes a transcription factor that is the only primary effector of Nodal signaling identified to date, continues to be expressed after the termination of *Nodal* and *Lefty2* expression, and is present in the tubular heart and gut. Furthermore, *Pitx2* localizes to

areas of tissue displacement such as the greater curvature (left side) of the stomach and the left sides of loops in the gut (Campione et al., 1999). The association of *Pitx2* expression with areas of tissue displacement suggests that Pitx2 may help elicit the cellular changes needed for tissue morphogenesis.

Misexpression studies demonstrated the ability of ectopic *Pitx2* to alter organ situs, and suggested that Pitx2 serves as a mediator between L-R signaling and asymmetric morphogenesis (Campione et al., 1999; Logan et al., 1998; Ryan et al., 1998). Not only is there a general dependency of correct visceral organ *situs* on *Pitx2* expression, but each organ appears to have a differential requirement for Pitx2 as proven by genetic dosage experiments in the mouse. Mice heterozygous for *Pitx2* (which express approximately half the level of *Pitx2* compared to wild-type mice) display a less severe phenotype than mice carrying a hypomorphic *Pitx2* allele (over *Pitx2* null allele) that expresses 37% of the level of *Pitx2* found in wild-type mice. Pulmonary right isomerism was seen in all *Pitx2* mutants regardless of the level of *Pitx2*. In contrast, the severity of heart and gut defects varied according to the level of *Pitx2*. The duodenum failed to loop at all in approximately 15% of hypomorphic embryos, and an additional third had reversed rotation. By comparison, three-fourths of *Pitx2* null embryos showed complete lack of duodenal looping. Duodenal looping was restored in *Pitx2* heterozygotes, but the direction of rotation remained affected and at least 80% of the embryos displaying reversed gut rotation. Similar dosage effects were seen on atrial development. *Pitx2* nulls had septal and valve defects, and a single atrium. While the septal and valve defects persisted in *Pitx2* heterozygotes and hypomorphs, the atria seemed to develop normally (Gage et al., 1999; Liu et al., 2001). Although these studies cemented Pitx2 as a major regulator of

asymmetric organ situs, they did not address how Pitx2 may be regulating tissue morphogenesis.

Potential mechanisms driving LPM architecture changes

Insight into how Pitx2 might drive changes in architecture of the LPM tissue was first gleaned from HeLa cell culture studies with *Pitx2a:* one of 3 transcripts from the locus, which is non-asymmetrically expressed, but encodes a bicoid-type homeodomain transcription factor similar to Pitx2c (the asymmetrically localized Nodal effector; PItx2 isoforms only have last two exons in common) (Schweickert et al., 2000). Pitx2a strengthened homotypic cell-cell adhesions, with increased N-cadherin and β-catenin. Rho GTPases Rac1 and RhoA were also activated, causing substantial induction of actin reorganization and cells to adopt a spread morphology (Wei and Adelstein, 2002). Ectopic expression of *Pitx2a* in the R LPM of chick embryos was able to randomize heart looping, the same activity seen with ectopic expression of *Pitx2c*. Both *Pitx2*c and *a* isoforms have identical C-terminal regions, where the transactivation domain is located, and plausibly Pitx2c and Pitx2a function similarly in instructing altered cell architecture (Yu et al., 2001).

Studies in chick and frog correlate the spatiotemporal pattern of *Pitx2* expression with distinct physical and molecular asymmetries between the L and R LPM, further strengthening the case for Pitx2 as an effector of cell and tissue architecture. In frog, *Pitx2* expression is associated with concave surfaces of the gastroduodenal loop (the first loop formed) and the midgut loop (the second loop to form) (Muller et al., 2003). Gut asymmetry has been focused on in seminal studies of the asymmetric movement of the midgut in the chicken embryo (Davis et al., 2008;

Kurpios et al., 2008). In this region, cells of the left of the midgut dorsal mesentery (DM) differ in numerous ways from those on the right, resulting in the relatively rapid development of an overall leftward tilt of the gut. Cells of the coloemic epithelium are columnar on the left but cuboidal on the right, *N-cadherin* is asymmetrically expressed preferentially in left DM cells, and mesenchymal cells are packed together in a more condensed fashion on the left.

These differences are linked to L-R asymmetry in ECM composition and cell-cell adhesion. For example, hyaluronic acid, a large space-filling component of the ECM that often surrounds cells and disrupts close cell-cell adhesions, is found more in the loosely packed R-side DM. Introducing ectopic *Pitx2* or *N-cadherin* on the right side reduces HA production, leading to a relative compaction (compared to normal) of the right-side mesenchyme (Davis et al., 2008; Kurpios et al., 2008). Furthermore, scanning electron microscopy showed that closely abutted left-side mesenchymal cells have relatively tight membrane connections, while the looser-packed right-sided cells have filopodial connections. In addition to increased N-cadherin on the left-side DM, α-catenin, important for formation and stabilization of adherens junctions, is also at higher levels on the left (Welsh et al., 2013).

The use of laser capture on the L and R DM of chicken embryos during gut tilting revealed differential expression of Wnt pathway regulators. Genes encoding inhibitors of Wnt signaling such as *Sfrp1* and Sfrp2 (Secreted frizzled-related protein 1 and 2, which prevent Wnt ligands from interacting with Frizzled receptors) were elevated in the right DM, while complementary upregulation of positive regulators of Wnt signaling, such as *Frizzled4* and *Daam2*, was detected in the left DM. *Daam2* encodes a formin that regulates actin dynamics and the formation of

adherens junctions through partnerships with N-cadherin and α-catenin. Predicted Pitx2 binding sites were found in the *cis*-regulatory regions of *Fzd4* and *Daam2*. Ectopic R-sided expression of *Pitx2* resulted in symmetric expression of *Daam2* across the DM. These findings suggest that regulators of Wnt signaling, such as *Daam2*, are targets of Pitx2. Importantly, nuclear β-catenin did not localize to either side of the DM, strongly indicating that Pitx2 activates non-canonical Wnt signaling on the left side of the DM to effect tissue architectural changes (Welsh et al., 2013).

These studies also suggest that *N-cadherin* is a potential target of Pitx2 that is capable of effecting change on the LPM tissue architecture. N-cadherin has been linked to remodeling of the actin cytoskeleton to drive morphogenesis in other systems. In *Xenopus,* N- and E-cadherins play actin-assembly roles in neural and non-neural ectoderm, respectively (Nandadasa et al., 2009). In chick lens-fiber cells, the maturation of N-cadherin junctions precedes organization of the cortical actin cytoskeleton. Blockage of N-cadherin junctions in this system led to decreased association of α-catenin with N-cadherin, blocked organization of actin, and prevented cell elongation (Leonard et al., 2011), which reflects cellular behavior seen on the (N-cadherin non-expressing) R-side of the chick DM (Davis et al., 2008; Kurpios et al., 2008; Welsh et al., 2013). In the mouse, N-cadherin, in cooperation with the cytoskeletal protein Shroom3, has been shown to regulate cell shape asymmetry in the DM – as in the chicken, the mouse DM shows a L-sided columnar, and R-sided cuboidal epithelium – by increasing apical F-actin and Myosin II in the left DM (Plageman Jr. et al., 2011). Myosin II has also been implicated in the L-R asymmetric development of the anterior midgut in the fruit fly

D. melanogaster, a species that has no *Nodal* homolog, and this gut morphogenesis process is also tightly dependent upon the actin cytoskeleton (Okumura et al., 2010).

Characterizing LPM tissue architecture before gut looping

The studies described above begin to address the general mechanisms of asymmetric organogenesis by identifying molecular and architectural asymmetries within the looping gut, and hint towards a role for Nodal signaling – largely acting through Pitx2 – in this process. However, those studies have a narrow focus, analyzing after the start of asymmetric morphogenesis, and are only directed at a limited region of the gut – the midgut. Also, The degree to which this DM of the chicken midgut is a model for gut looping in other organisms that have differing gut architecture is not known.

We wanted to expand upon these studies by characterizing the cell shape, ECM, and cytoskeletal characteristics for the entire length of the R and L LPM that flanks the gut endoderm, and focused on the period prior to the actual initiation of gut looping in *Xenopus*. By analyzing the changes in LPM tissue architecture between stages 25 (when *Nodal* is last seen) and 38, we were hoping to gain insight into how small alterations in L and R LPM architecture, which form before the large-scale movement of the actual tissue, potentially complement each other to synergistically guide looping of the gut.

Because most of the factors identified as asymmetrically localized in regions of gut bending act either indirectly or directly on the actin cytoskeleton, a previous graduate student initiated this project by first characterizing actin cytoskeleton dynamics in the L and R LPM by labeling the cytoskeletal component F-actin with phalloidin. Increased F-actin labeling in the R LPM

compared to the L LPM was detected starting at stage 35 and persisting through at least stage 43. Interestingly, the preference in phalloidin-labeling was not uniform along the A-P axis of the R LPM, but appeared focally more concentrated in specific locations. Further analysis at higher magnification suggested that the increased relative labeling with phalloidin was associated with increased bundling of actin filaments on the right side. The thickening of actin filaments implies that cells in the R LPM are undergoing active constriction, and therefore that the F-actin foci may be one potential mark of future sites of tissue morphogenesis. The R-sided increases in F-actin labeling intensity became symmetrical or reversed in manipulations that dominantly altered L-R asymmetry by ectopic R-sided *Nodal* expression, indicating a potential instructive link between Nodal signaling and actin cytoarchitecture (Marjoram and Wright, unpublished).

My goal when I inherited this project was to confirm these initial findings on F-actin and to expand the study by determining the cell shape and additional cytoskeletal characteristics of the L and R LPM. Specifically, I wanted to identify alterations that pre-empted tissue movements of the gut and that were asymmetric between the L and R LPM, with the idea that such alterations are instrumental in guiding directional looping of the gut. Any identified variation in tissue architecture between the L and R LPM would be quantified and mapped along the A-P and D-V axes. Using fate mapping, cells that compose these architectural points of interest would then be labeled and followed through stages of gut looping to investigate where they localize within the looping gut (i.e. concave, convex, linear regions). This analysis would provide insight into how architectural changes in the LPM influence tissue morphogenesis in the underlying gut endoderm. Identification of tissue architecture

asymmetries between the L and R LPM would lead to additional studies in which *Nodal* is inhibited or ectopically expressed in the R LPM to determine if these differences result from asymmetric Nodal signaling. In this chapter, I describe also my development of a Technovit resin embedding technique that excellently preserves tissue architecture, thus increasing the resolution at which we can study LPM architecture. This chapter is considered a 'work in progress' report, as the studies had to be terminated/truncated in favor of the Foxh1 study described in Chapter V. However, it can be preliminarily concluded that architectural asymmetries do exist between the L and R LPM, and that these asymmetries are potentially linked to Nodal signaling.

Results

F-actin and β-1 integrin have increased localization in R LPM

To confirm the increased bundling of F-actin in the R LPM, cryosections of *Xenopus* embryos stage 35-41 were labeled with phalloidin and imaged via confocal microscopy (Fig. 4.1). Fluorescent intensity of phalloidin labeling within the boundaries of the LPM was calculated using ImageJ and presented as a quotient of the percentage of R LPM area labeled by phalloidin over the percentage of labeled L LPM area. A quotient of one indicates that the tissue area containing phalloidin-labeled F-actin is equivalent between L and R LPM, and a value greater or less than one reflects it being greater in the R LPM or L LPM, respectively. Sections, 10 µm thick, containing LPM were analyzed every 80-100 µM along the A-P axis of the embryo (approximately 8-10 sections/embryo). Eleven out of 14 embryos analyzed at various stages

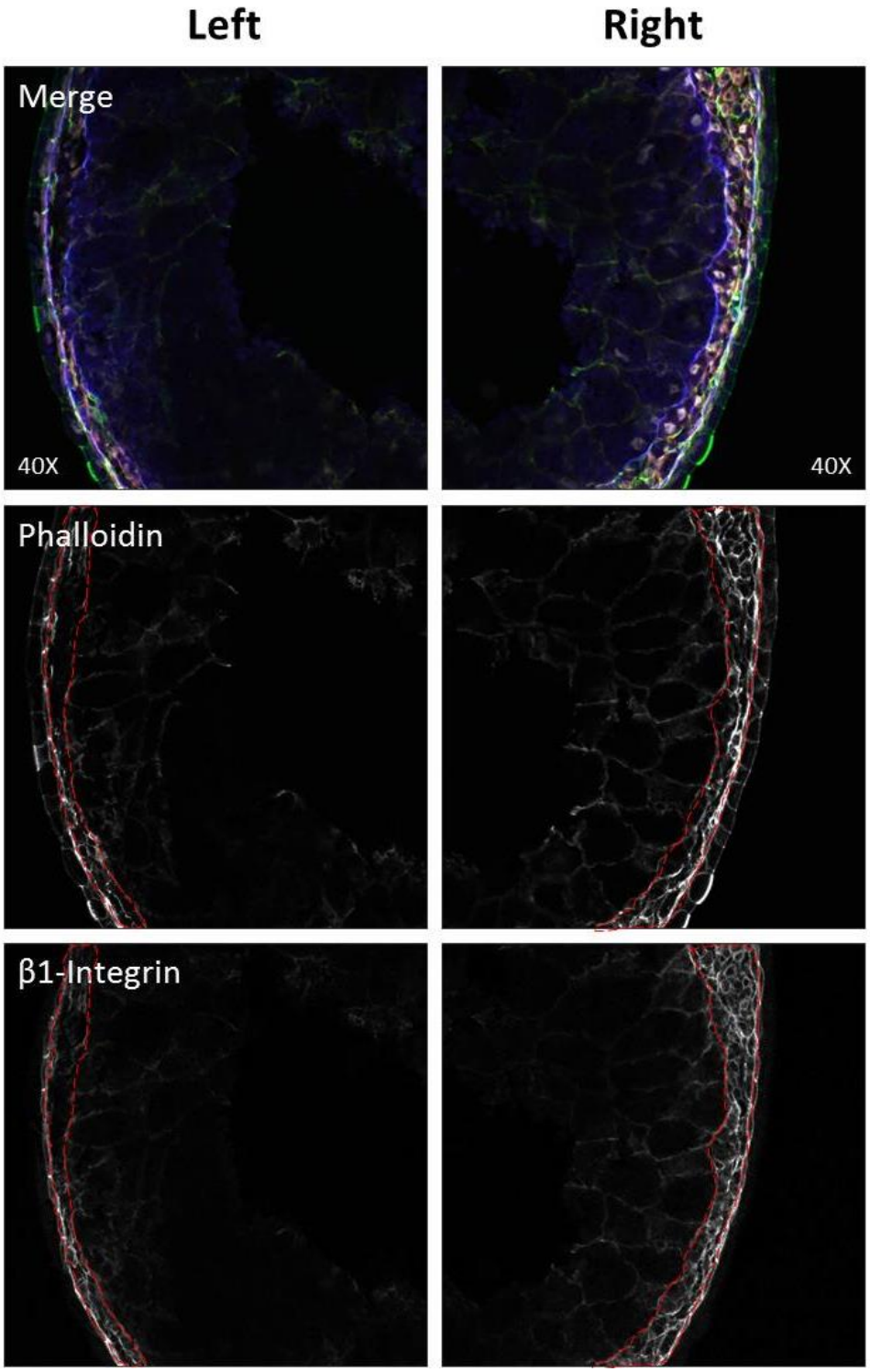

Fig. 4.1 F-actin and β-1 integrin have increased localization in R LPM. Cryosections of a stage 39 *Xenopus* embryo labeled for F-actin (phalloidin; green), β-1 integrin (red), laminin (blue), and DAPI (DNA; white). LPM is demarcated by laminin in the "Merge" and by the dashed red lines in the phalloidin and β-integrin single channels.

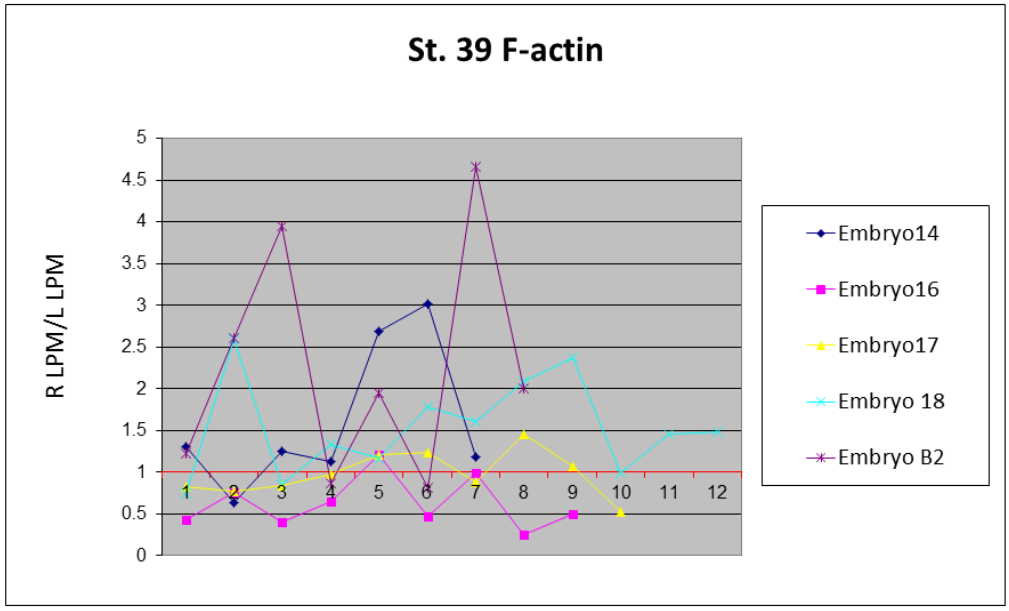

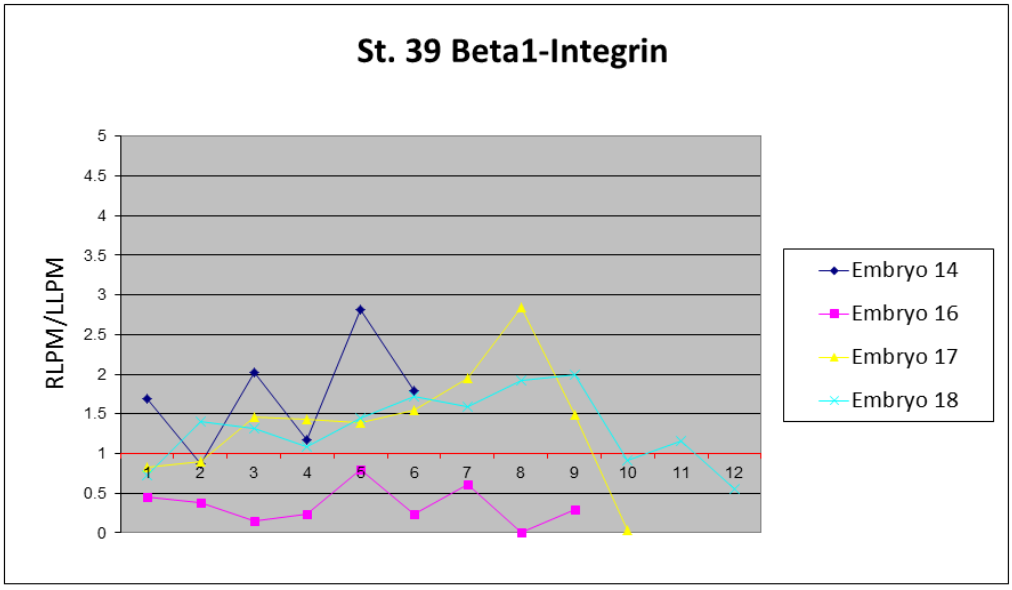

Fig. 4.2 F-actin and β-1 integrin staining intensity ratios. Plots of the percentage of R LPM area labeled for F-actin or β-1 integrin over the percentage of the L LPM area labeled in stage 39 embryos. Values greater than 1 indicate that the R LPM had more labeling and values less than 1 indicate that the L LPM had more label. X-axis represents distance along the A-P axis ("1" more anterior and "12" more posterior. The majority of values plotted were greater than 1.

showed greater F-actin labeling intensity in the R LPM, confirming the preliminary results (Fig. 4.2). The nature of F-actin localization in this assay, for example if it was focal or diffuse, was not investigated. A similar analysis was performed for β-1 integrin, a transmembrane protein that mediates cell adhesion to the ECM and other cells. Preliminary results showed that 10/13 embryos, at various stages, generally had greater β-1 integrin localization within the R LPM compared to the L LPM (Fig. 4.1; Fig. 4.2). Further analysis would be needed to determine if this increase was uniform along the A-P axis of the LPM or if, like F-actin, the increases were focal.

Whole-mount immunolabeling and Technovit 7100 embedding protocol

During these analyses it became apparent that cryosectioning of embryos did not fully preserve tissue architecture and that valuable information on the exact cell shape, localization of cytoskeletal/ECM components—important in this case because of the potential for small differences between the L and R sides having an instructive effect—was potentially being lost or distorted. Across all of the embryonic stages that I was analyzing, cells are filled with yolk platelets, which become crystalline and brittle under the processing for cryosectioning. This makes *Xenopus* tissue prone to tearing during sectioning, distorting cell boundaries or even resulting in substantial loss of tissue (Fig. 4.3A). To circumvent this issue, I began to optimize a recently published protocol (Kurth et al., 2012), never before used in the Wright lab, for the whole-mount immunofluorescent labeling and then embedding and sectioning of *Xenopus* embryos using Technovit 7100. Technovit 7100 is a plastic-like resin that hardens at room

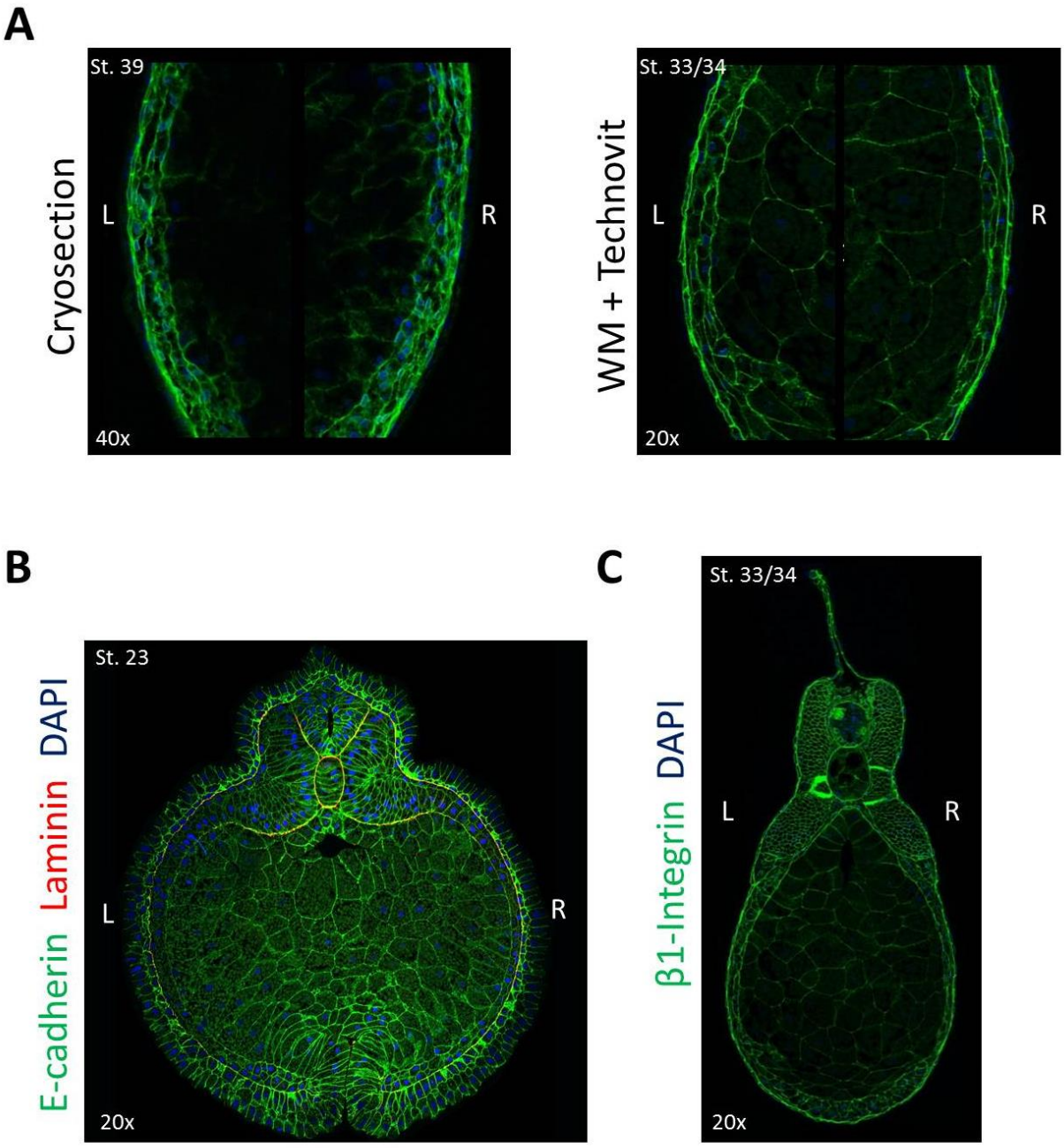

Fig. 4.3 Tissue architecture preservation with Technovit embedding. (A) Comparison of tissue architecture between an immunolabeled cryosection and a whole-mount immunolabeled embryo embedded and sectioned in Technovit. (B,C) Examples of tissue preservation with Technovit sections. (B) Stage 23 embryo whole-mount immunolabeled for E-cadherin (green) and laminin (red), and stained for DNA (DAPI; blue). (C) Stage 33/34 embryos whole-mount immunolabeled for β-1 integrin (green) and stained for DNA.

temperature and therefore avoids any freezing of the embryos. Unlike cryosectioning, Technovit 7100 immaculately preserves tissue architecture with little or no ripping of the section (Fig. 4.3). Whole-mount immunostaining prior to embedding is required with Technovit 7100 as the densely infiltrated resin can mask antigens, preventing their recognition by antibodies (note, however, that DNA can still be detected on Technovit 7100 sections using prepared mounting medium containing DAPI). I optimized the published protocol for maximum antibody penetration and for use with a microtome equipped with the standard metal blade instead of the recommended glass knife. Detailed protocols for whole-mount immunofluorescent labeling and embedding of *Xenopus* embryos in Technovit 7100 can be found in Chapter II – *Materials and Methods*.

Antibodies compatible with whole-mount immunolabeling and Technovit 7100 embedding include those against β-1 integrin, β-catenin, E-cadherin, chondroitin sulfate proteoglycan (CSPG), fibronectin, laminin and to a lesser extent C-cadherin (Fig. 4.3B,C). No signal was detected with phalloidin, as a detector of F-actin, possibly because of the use of the methanol-based Dent's fixative prior to staining. Because methanol disrupts actin, it is not recommended for the detection of F-actin. A caveat to embedding in Technovit 7100 is the almost perfect preservation of yolk platelets, which autofluoresce and can sometimes interfere with signal emitted by fluorescently tagged antibodies. At lower magnifications (10x, 20x), this autofluorescence minimally interferes with the signal of interest, but at higher magnifications, such as 40x and beyond, yolk autofluorescence sometimes overpowers the real signal. This problem is somewhat offset by the increased cellular resolution afforded by Technovit 7100 sections, so that enlargement of images taken at a lower magnification might still result in

significant gains and more accurate estimations of cell shape or other parameters compared to other methods.

Imaging Xenopus embryos in whole mount

The observation that the increase in F-actin within the R LPM was focal along the A-P axis led to the hypothesis that the F-actin foci might function as "pioneer centers" for the local initiation of progressive alterations in regional tissue architecture. The general idea was that determining if the location of these foci was reproducible along the A-P and D-V axes, comparing multiple embryos of the same stage, could signify an importance in tissue morphogenesis, such as marking future points of initiating looping or bending one way or the other. Because it is extremely difficult to register multiple sections against each other, and reconstruct such three-dimensional information, I pursued immunolabeling and imaging embryos in whole mount.

Because phalloidin-based F-actin detection is not compatible with the whole-mount immunolabeling protocol for Technovit 7100, I worked to devise a different method. Embryos were fixed in the formaldehyde-based fixative MEMFA, and bisected along the ventral midline. The epidermis was carefully peeled away as an attempt to expose the LPM, with the aim of improving antibody access to these interior tissue layers. The outer, pigmented layer of epidermis peeled away quite easily and cleanly, but it was uncertain if the newly exposed surface was the inner epidermal layer or the true outside of the LPM. Embryo halves were then incubated with fluorescently tagged phalloidin, cleared in BABB (1:2 benzyl alcohol:benzyl benzoate), mounted on a depression slide, and imaged using an Axio CamMRm-fitted ApoTome Zeiss microscope.

While I was able to detect the F-actin in whole mount using this method (Fig. 4.4), several problems were encountered. First, the LPM is a curved tissue layer, and it cannot be flattened into a single plane for quantitative analysis of the entire LPM layer. A way of flattening the LPM without breaking the tissue would lead to an easier investigation of the LPM architecture, but even then, there are concerns over the undesired stretching or compression of specific cellular shapes. Second, I was unable to determine how deep the fluorescent phalloidin penetrated into the tissue with this rather crude labeling method. Little to no permeabilization of the tissue was done, and I could not determine from the whole-mount analysis which tissue layers (epidermis, somatic or splanchnic LPM, endoderm) were in fact being labeled. Also, identifying the epidermal-LPM and LPM-endodermal boundaries in whole mount is difficult compared to transverse sections. In the future, labeling of laminin or fibronectin in the same whole mount while carrying out the F-actin analysis might demarcate the LPM boundaries and aid in setting limits for confocal z-stack analysis and three-dimensional (3-D) reconstruction using, for example, the Imaris or Volocity image-rendering applications. Regardless of these problems, points of intense F-actin labeling were identified (Fig. 4.5B), suggesting that some future refinement of the protocol could lead to an accurate mapping of cells with enriched F-actin foci through the LPM.

Another possibility is that 3-D reconstructions of thick transverse sections could be used to map F-actin foci and other characteristics such as cell shape and volume. Unfortunately, 3-D reconstructions of Technovit sections are not very useful as the thickest section obtained is approximately 20 μm, and would provide little information about cell volume as very few cells would be included in the Z-plane. Experimenting with different embedding materials, I found

A

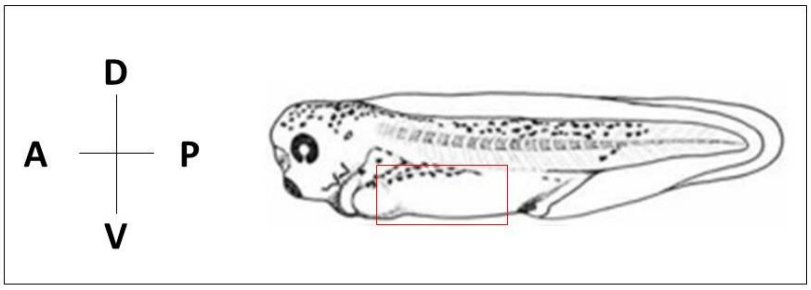

B

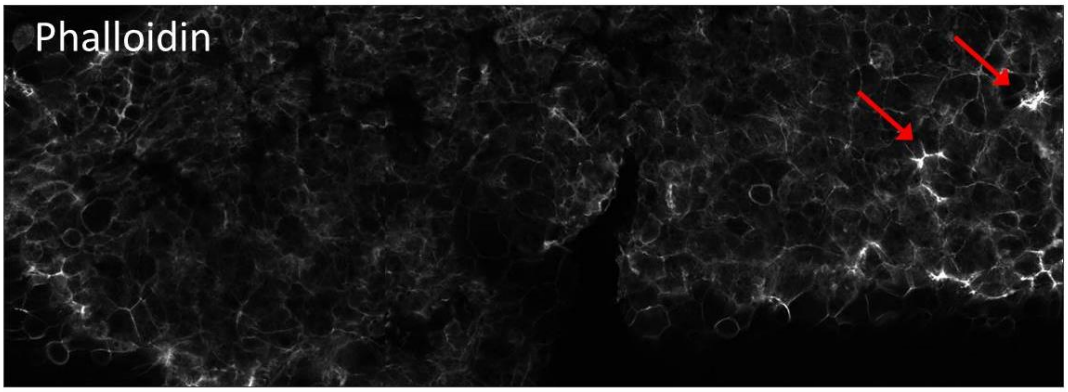

Fig. 4.4 Whole-mount labeling of F-actin with phalloidin. (A) Schematic showing the orientation and location of the tissue in (B) within the embryo. (B) Labeling of F-actin in what is presumed to be L LPM. Arrows point to areas of increased labeling, possibly representing F-actin contraction or bundling.

that embedding embryos in 15% fish gelatin led to a much better preserved tissue architecture compared to bacto agar (agar being originally used for embedding embryos for cryosectioning), and cryosections of at least 60 µm could be collected. These thicker sections could permit collection of accurately registered z-stacks and final 3-D rendering of the LPM. One drawback with imaging thicker *Xenopus* tissue is the amount of yolk autofluorescence under confocal illumination, which reduced the clarity of the desired signal and limited the depth of the z-stacks, so that I was only able to collect total z-stack thicknesses of 12–17 µm. To increase the depth of focus, the use of two-photon microscopy was considered, but this was not aggressively pursued. In very preliminary use, I decided that it did not seem to result in a dramatically increased depth of field.

Discussion

The goal of this chapter was to identify and characterize any tissue architectural asymmetries between the L and R LPM, with the hope of better understanding how Nodal signaling is translated into the specific morphogenetic cues that drive asymmetric organogenesis. The initial characterization of LPM architecture prior to, during, and immediately following the asymmetric expression of *Nodal* was done by a previous graduate student. Through thorough analysis, she was able to identify the timing of LPM apicobasal polarization and the first appearance of cell-shape differences between the somatic and splanchnic layers, which were described in the Introduction to this chapter. She also identified potential L-R differences in the organization of the actin cytoskeleton that preceded gut looping.

I began by confirming the R-sided increase in F-actin labeling intensity. I also preliminarily found that β-1 integrin, like F-actin, appeared enriched in the R LPM over the L LPM. Integrins

are important for cell-cell and cell-ECM interactions; therefore, seeing an increase in β-1 integrin is not all too surprising as this supports the theory that cells in the R LPM may be in the process of contracting to become smaller, leading to the introduction of concavities in the gut. In order to make accurate interpretations about LPM tissue architecture, we needed high-quality and high-resolution images. My major contribution to this project was the establishment of a whole-mount immunolabeling and Technovit embedding protocol that immaculately preserved embryonic tissue architecture. This protocol will be useful in further characterizing LPM architecture and in addressing the points discussed below, which because of time constraints and my drastically shifted focus to the mouse Foxh1 project, I could not pursue further.

R-sided cellular contractility differs from other vertebrates

Because F-actin characteristics are altered in the R LPM, it might be expected that adherens junctions, which connect to the actin cytoskeleton, and the cell-adhesion proteins (cadherins, catenins) associated with these junctions, would also show (focal) unilateral enrichment in the R LPM. High-resolution (100x) confocal images of the R LPM suggested that the increase in F-actin labeling represented a thickening or contraction of actin filaments. Based on these data, we would predict R LPM cells with contracting F-actin might start to become more compact in shape and volume, with their direct counterpart cells that lie in the L LPM being more spread and loosely packed. Within a restricted A-P domain, a complementary pattern of right-sided contracting actin bundles and tightly abutted cells and left-sided cells that are more disperse with thinner, diffuse actin filaments might produce an overall push-pull influence, across the

nascent gut tube, beginning to direct asymmetric gut coiling. In this context, regions with distinct L-R differences in cell shape or other architectural features could be the active driver of gut looping/bending, and areas without any L-R distinction would be relatively passive, either forming linear tube regions, or being pulled mechanically by the actively moving regions of the gut tube.

It was surprising that the thickened F-actin bundles and increased β-1 integrin were found in the right, not left, LPM. This observation opposes previous findings in chicken and mouse in which *Pitx2* expression on the left was correlated with increased cell-cell contact, cell condensation, and increased deposition of ECM components in left DM cells. Given the different architecture of mammalian and avian guts compared to that of *Xenopus*—in the later endoderm is flanked by LPM, which provides a rigid support encircling the gut endoderm, while the former the DM "hangs" the gut tube from the dorsal side of the body—it is possible that different mechanisms have evolved to direct looping.

This species-variance idea is exemplified in zebrafish, which has an LPM structure yet again different from that of the mouse, chicken, or frog, in which the asymmetric migration of the LPM has been proposed to drive chiral gut looping. The LPM of fish forms a U-like structure on either side of the gut, and the L LPM becomes positioned slightly more dorsal to the endoderm and the R LPM slightly more ventrolateral. This asymmetry in "vertical LPM positioning" only exists in regions where looping occurs. In straight regions, both L and R LPM are positioned equivalently dorsal to the endoderm. As the LPM grows toward the endoderm, the

asymmetrical localization forces directional movement of the gut tube (Horne-Badovinac et al., 2003).

The role of endoderm in shaping the gut

It has been suggested that one mechanism for introducing concavities in the developing *Xenopus* gut is left vs. right differential elongation of the LPM. While both the L and R LPM elongate during the beginning stages of gut looping, the R LPM does slightly faster, reaching a length almost twice that of the L LPM by stage 43 (approximately 24 hours after gut looping is first visible) (Muller et al., 2003). Differences in cell proliferation and death are not detected between the L and R LPM. Instead, this elongation is in part thought to be due to radial intercalation of endoderm cells during the formation of the gut lumen (stages 40-45) (Chalmers and Slack, 2000). Muller et al. noted left-right differences in endodermal thickness during gut looping. In Technovit sections of stage 35/36 (just prior to gut looping initiation) embryos, I also observed asymmetries in endoderm thickness, with the left-side endoderm being thicker than the right (Fig. 4.5). The increased thickness on the left may translate into decreased surface area on the left, and a thinner endoderm layer on the right may translate into increased surface area. Therefore, cells in the R LPM would have to become more spread in order t0 maintain coverage of the increasing endodermal surface area, leading to an increased elongation rate in the R LPM compared to the L LPM. It remains to be seen if differential elongation of the left vs. right LPM is linked to asymmetric Nodal signaling. In *Xenopus*, strong expression of *Lefty2,* a downstream target of Nodal signaling, is seen within the left dorsal anterior endoderm, suggesting that the endoderm can respond to Nodal signaling (Cheng et al.,

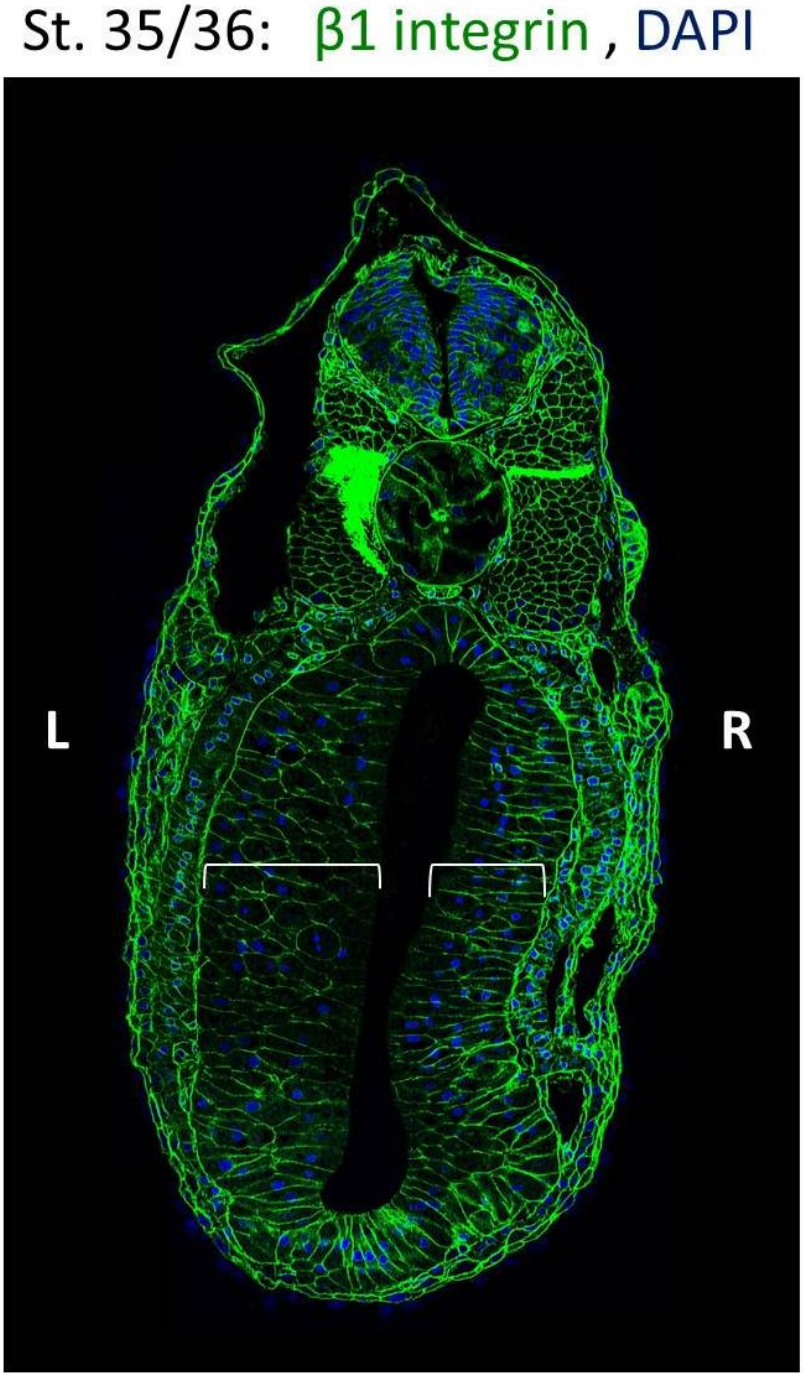

Fig. 4.5 L-R asymmetries in endoderm thickness. Technovit section of a stage 35/36 embryo whole-mount immunolabeled for β-1 integrin (green). DNA is labeled with DAPI (blue). Left endodermis thicker than right endoderm, as denoted by the brackets. L, left; R, right.

2000). So far, a possible instructive role for Nodal signaling in gut looping has only been studied in the very first loops to form, which are located in the anterior region of the gut (Davis et al., 2008; Liu et al., 2001; Muller et al., 2003). Nodal signaling in the anterior endoderm at early stages may be occurring, and thus imparting asymmetric morphogenetic cues, in the endodermal regions that make up these loops in later development. It will be interesting to see if mechanisms driving tissue morphogenesis in the LPM, like those seen in the chicken, are linked to mechanisms controlling the structural differences in the endoderm, or if there are parallel pathways in the LPM and endoderm that both control gut tube chirality. It will also be interesting to investigate if Nodal signaling is only required for directing tissue morphogenesis in the most anterior loops, with subsequent loops forming via other mechanisms, or if Nodal signaling can alter tissue architecture in all loops. Possible ways to address these questions will be discussed in Chapter VI – *Summary and Future Directions*.

CHAPTER V

DISRUPTING FOXH1-GROUCHO INTERACTION REVEALS ROBUSTNESS OF NODAL-BASED EMBRYONIC PATTERNING

Introduction

Foxh1 is essential to the initiation and maintenance of the Nodal autoregulatory circuit by which Nodal signaling initiates the expression of *Nodal* itself, its feedback inhibitor *Lefty2*, and the homeodomain transcription factor *Pitx2*, an important effector of Nodal signaling (Norris et al., 2002; Saijoh et al., 2000; Shiratori et al., 2001). As noted in the Introduction of the dissertation, Foxh1 binds conserved sequences in the asymmetric enhancer (ASE; named for its ability to drive expression on the left but not right side of the embryo), which is present in all three Nodal autoregulatory circuit genes (*Nodal*, *Lefty2*, *Pitx2*) (Meno et al., 2001; Saijoh et al., 1999; Saijoh et al., 2000; Shiratori et al., 2001). The ASE, along with another enhancer, drives *Nodal* expression during early patterning events and then initiates the expression of *Nodal*, *Lefty2*, and *Pitx2* solely within the left lateral plate mesoderm (L LPM) during L-R patterning (Adachi et al., 1999; Norris and Robertson, 1999; Saijoh et al., 1999; Shiratori et al., 2001). Deletion of the Foxh1 binding-sites, or deletion of the ASE as a whole in mouse, leads to decreased *Nodal* expression in the epiblast and complete loss of *Nodal*, *Lefty2*, and *Pitx2* expression in the L LPM (Adachi et al., 1999; Norris and Robertson, 1999; Norris et al., 2002; Saijoh et al., 2000; Shiratori et al., 2001). Foxh1 binding sites play a conserved role in the ASE as deletion of these sites also attenuated Nodal signaling in other species (Osada et al., 2000). Furthermore, the majority of embryos with a global deletion of *Foxh1* fail to orient the A-P axis

appropriately, elongate the primitive streak, or form a node; together these defects cause embryonic lethality (Hoodless et al., 2001; Yamamoto et al., 2001). Embryos in which *Foxh1* was conditionally inactivated within the L LPM failed to express *Nodal*, *Lefty2*, and *Pitx2* in that tissue and exhibited right isomerism (Yamamoto et al., 2003).

The ability of Foxh1 to promote transcription of *Nodal*, *Lefty2*, and *Pitx2* arises from its interaction with the pSmad2/Smad4 complex, which binds the Smad interaction domain (SID) on the C-terminus of Foxh1 (Chen et al., 1997; Weisberg et al., 1998). In addition to the SID, Foxh1 contains another more N-terminally located co-factor interaction motif called the Engrailed homology-1 (EH1) motif, which is an 8 amino-acid sequence recognized and bound by the Groucho/Groucho-related-gene/Transducin-like enhancer of split (Gro/Grg/TLE) family of co-repressors (Yaklichkin et al., 2007a). The Gro/Grg/TLE protein family comprises four full-length members (TLE1-4 in human and originally termed Grg1-4 in mouse, which is the nomenclature used henceforth), each containing a conserved C-terminal WD-repeat domain (Fig. 5.3B) that mediates interactions with transcription factors by recognizing two classes of motifs: the full EH1 or a smaller tetrapeptide (WRPW). It is currently unclear as to the direct mode by which Grg proteins repress transcription, but likely multiple mechanisms are used, and dependent on biological context. One reported mechanism is the recruitment of histone deacetylases (HDACs) to Groucho-bound loci, to promote a closed chromatin conformation (Jennings and Ish-Horowicz, 2008).

The presence of both the EH1 motif and SID suggests that Foxh1 acts as a transcriptional switch, toggling between active and repressive states of transcription by switching between

pSmad2/Smad4 and Grg (Fig. 5.1). This is an attractive mechanism for rapid and precise transcriptional control of Nodal signaling, which underlies the dynamic expression of *Nodal* in both the epiblast and L LPM (described in detail in the Introduction). During stages of L-R patterning in mouse, *Foxh1*, as well as *Grg3* and *Grg4*, are expressed bilaterally in the LPM (Koop et al., 1996; Leon and Lobe, 1997; Weisberg et al., 1998). Colocalization of the proposed switch components in the R LPM, which does not express *Nodal* but is competent to respond to Nodal signaling (Ohi and Wright, 2007; Yamamoto et al., 2003), as well as in the L LPM which expresses *Nodal* under fast spatiotemporal control, further supports the idea that Foxh1 may be a transcriptional switch and thus participates in repressing *Nodal* transcription. The bifunctionality of Foxh1, conveyed by interchangeable binding of pSmad2 and Grg, may facilitate rapid and precise tailoring of transcript levels to varying thresholds of external instructive signals, as compared to regulatory mechanisms that use distinct transcriptional activation and repression complexes (Cinnamon and Paroush, 2008).

Recent work in *Xenopus* fits the proposal that FoxH1 is a transcriptional switch with respect to regulating *Nodal* expression, and with pSmad2 and Grg4, respectively, acting as co-activator and co-repressor. Overexpression of Grg4 in *Xenopus* embryos strongly reduced Nodal-dependent transcriptional activation, and chromatin-immunoprecipitation (ChIP) showed Grg4 occupancy at the *Nodal* ASE that was dependent on the EH1 motif of FoxH1. ASE occupancy by Grg4 was greatly decreased with *Nodal* or *Smad2* overexpression (D. S. Kessler, personal communication). These results suggest that pSmad2 displaces Grg4 in response to Nodal signaling, with complementary Grg4 displacement of pSmad2 causing transcriptional repression.

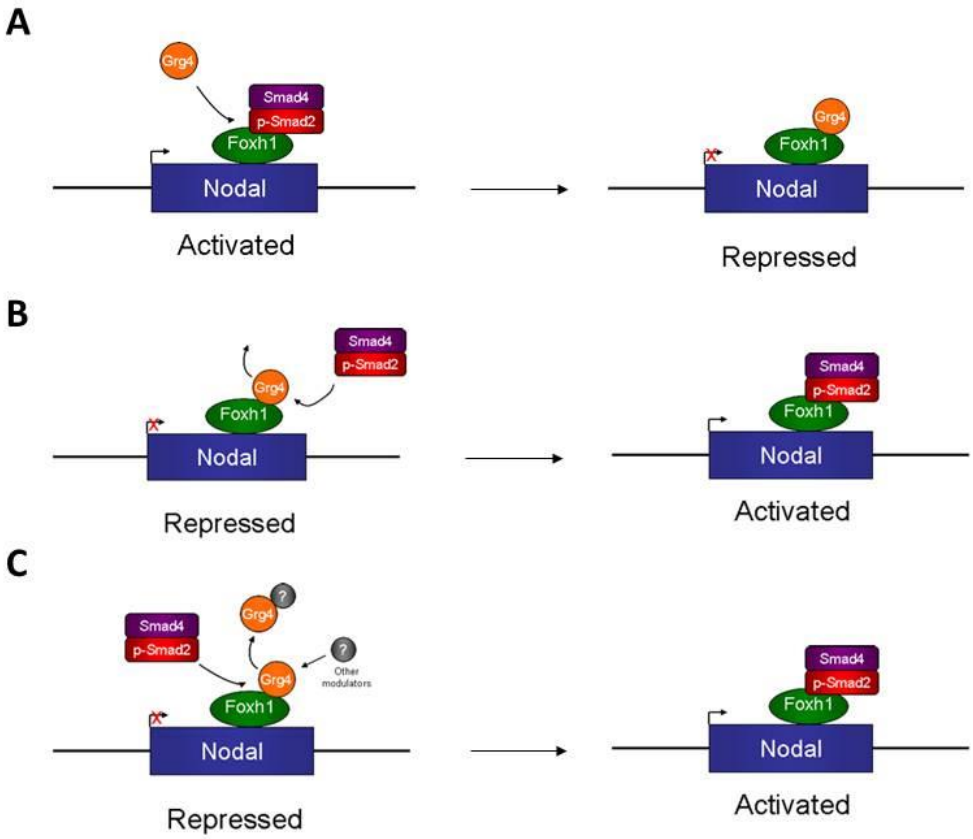

Fig. 5.1 Model of Foxh1 transcriptional switching. (A) Foxh1 activates transcription of *Nodal,* and potentially other ASE-containing genes, through interactions with the co-activator pSmad2/Smad4 complex (red and purple rectangles). Foxh1 becomes a repressor of transcription by binding members of the Groucho co-repressor family, represented here by Grg4 (orange circle). (B) Co-factor switching may occur through direct-competitive interaction for binding space on Foxh1. (C) Or, other unidentified modulators (gray circle) may remove the Foxh1-bound co-factor, opening up binding space on Foxh1 for the incoming co-factor.

Transcriptional switching has been documented to control target gene transcription for other developmental signaling pathways such as Notch and Wnt (Bray and Furriols, 2001; Daniels and Weis, 2005). For Wnt signaling, β-catenin and Grg co-repressors have overlapping binding domains on Tcf/Lef and compete with each other for occupancy at the locus (Daniels and Weis, 2005). The EH1 motif and SID do not overlap in Foxh1 and it is not known if pSmad2 and Grg show direct steric competition in the complete transcriptional complex. Alternatively, unknown components of the transcriptional complex might promote removal of pSmad2/Smad4 and/or Grg, leading to a mutual interference model that is highly dependent upon levels of the activator or the repressor (Fig. 5.1).

Knowledge about mechanisms regulating transcriptional repression of *Nodal* expression is greatly lacking. To determine if Foxh1 is conserved as a transcriptional switch and to identify the developmental consequences of removing the Foxh1-Grg repression arm of this switch, we developed a novel mouse model (*Foxh1*^{mEH1}) in which the interaction between Foxh1 and Grg is greatly perturbed. Manipulations made to the *Foxh1*^{mEH1} locus were carefully controlled for, by deriving a control line carrying identical insertions while maintaining a wild-type EH1 motif. This study is the first in mouse to address the role of Foxh1 as a transcriptional repressor of *Nodal* expression. Our findings support the idea that the embryo has evolved a robust and potentially diverse set of mechanisms to control Nodal signaling levels and ensure successful germ-layer development and embryonic patterning.

Results

Construction of Foxh1^{LCA}

BAC recombineering and gene targeting were used to generate a loxed cassette acceptor (LCA) allele of the *Foxh1* locus in ES cells (Fig. 5.2). The *Foxh1^{LCA}* allele easily allows for the insertion of Foxh1 variant alleles into the endogenous *Foxh1* locus through the highly efficient method of recombinase-mediated cassette exchange (RMCE). Using the LCA and RMCE, multiple mouse lines carrying different modifications to the *Foxh1* locus can be derived without BAC recombineering, which can be time consuming and inefficient. Analysis of *Foxh1* genomic organization across multiple species helped to avoid areas of conservation and locate the least disruptive points for inserting variant lox sites into the *Foxh1* locus. *Foxh1* and its neighboring gene *Kifc2*, a kinesin superfamily member expressed exclusively in neural tissue, are reported to share an overlapping 3' untranslated region (UTR) (Liu et al., 1999) (Fig. 5.2). *Kifc2$^{-/-}$* mice have no apparent phenotype, suggesting that Kifc2 is dispensable for normal development and behavior in the mouse (Yang et al., 2001). Because Kifc2 is dispensable, a Lox2272 site was placed within its 3' UTR.

Injection of the *Foxh1* targeting vector into ESCs was performed by the Vanderbilt Transgenic Mouse/ESC Shared Resource (TMESCSR). Correct targeting of the *Foxh1* locus was verified by Southern blot analysis of *Bam*HI-digested genomic DNA with two probes, a 3' probe external to the 3' homology arm and a 5' probe that had to be derived from within the 5' homology arm because of a repetitive short interspersed nuclear element (SINE) just outside the homology arm (Fig. 5.2, Fig. 5.3C). Out of the 317 colonies screened, five clones were identified for having

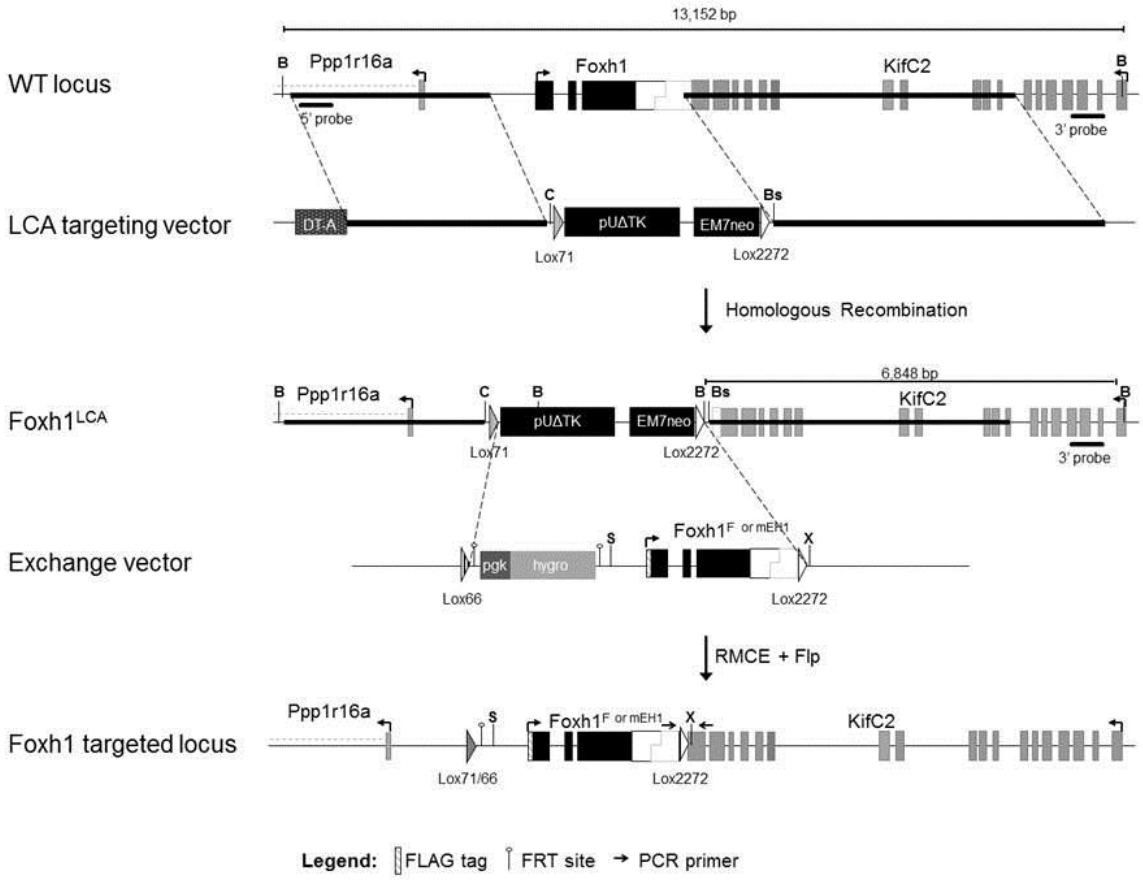

Fig. 5.2 Strategy for *Foxh1* engineering. A *Foxh1* lox cassette acceptor (LCA) allele (*Foxh1*^{LCA}) was generated by homologous recombination. After testing for germline competence, the *Foxh1*^{mEH1} allele was exchanged into the *Foxh1*^{LCA} using recombinase-mediated cassette exchange (RMCE). Chimeras were then derived by blastocyst injection of ES cells undergoing precise exchange, and the residual hygromycin-resistance cassette was excised by crossing the *Foxh1*^{mEH1} chimeras with mice carrying *Flpase* under direction of human *ACTB* promoter. The *Foxh1*^{F} control line was generated similarly, using an identical exchange vector, except that the EH1 motif was not mutated (not shown).

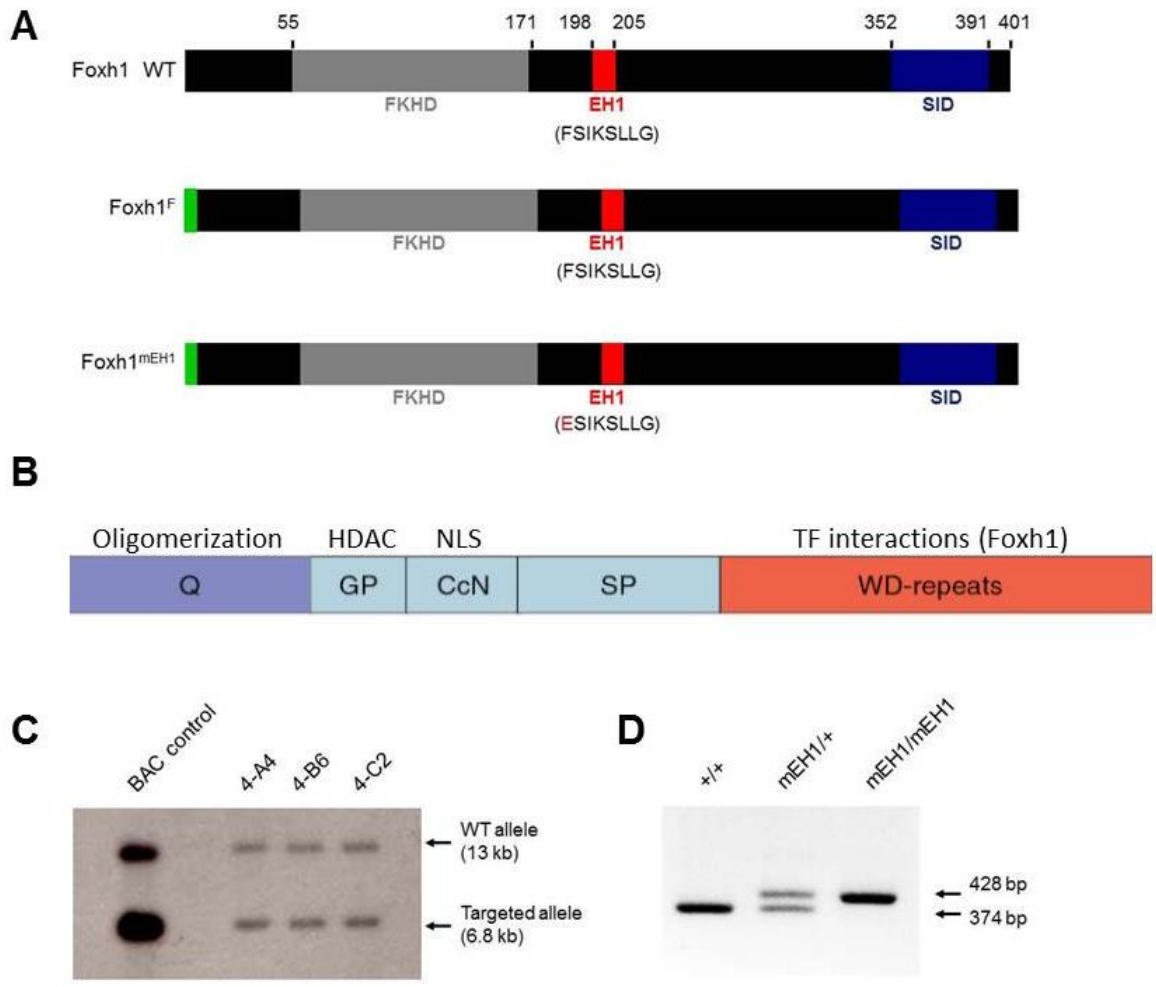

Fig. 5.3 Gene targeting and manipulation of Foxh1 EH1 domain. (A) The locations of FLAG tag (green), forkhead DNA-binding domain (gray), EH1 motif (red), and Smad-interacting domain (blue) in wild-type and variant Foxh1 proteins. Numbers denote amino acid position. Altered EH1 amino acids in Foxh1^{mEH1} are in red. (B) Schematic showing the five domains comprising long Groucho proteins. Adapted from Jennings and Ish-Horowicz, 2008. (C) Southern blot analysis showing correct targeting of *Foxh1* locus in three independent mESC clonal cell lines heterozygous for *Foxh1*^{LCA} allele. (D) PCR analysis of offspring derived from *Foxh1*^{mEH1} chimeras detects two bands, 428 bp and 374 bp, for the *Foxh1*^{mEH1} and wild-type *Foxh1* alleles, respectively.

correctly targeted the *Foxh1* locus. Three of these clones were expanded and karyotyped. Two clones showing strongest evidence of being normal (most spreads with 40 chromosomes: clone 4B6, 80% and clone 4A4, 47.62% normal) were injected into C57BL/6-derived blastocysts in order to generate chimeric mice. The injections resulted in eight chimeras, all from clone 4B6. Five were females estimated as 80% or less chimeric (based on coat color) and three were males estimated to be 100% chimeric. One male died before being released from TMESCR. Southern blotting and PCR analysis confirmed *Foxh1*^{LCA} germline transmission from the two surviving male chimeras that were crossed with Black Swiss females (Fig. 5.3D). Embryos homozygous for the *Foxh1*^{LCA} allele resembled *Foxh1*$^{-/-}$ embryos (data not shown), further verifying that wild-type *Foxh1* was correctly targeted and replaced.

Derivation of Foxh1$^{mEH1/mEH1}$ *mice*

In an effort to disrupt binding between Foxh1 and Grg co-repressors, we mutated the Foxh1 EH1 motif, FSIKSLLG. Before mutating the motif in mouse, three different EH1 mutations (eight amino-acid deletion [ΔEH1], AAAAAALG [6xAla], or **E**SIKSLLG [F>E]) were tested for their effect on the production and stability of Foxh1. Western blot analyses on lysates collected from *Xenopus* embryos injected with RNA encoding the Foxh1 variants confirmed that the EH1 mutations did not destabilize or over stabilize Foxh1 (Fig. 5.4A). I also assayed the mesendoderm-inducing and Grg-binding potential of each Foxh1 variant to confirm that the EH1 mutation prevented binding to Grg co-repressors, but did not alter the activator function of Foxh1. RNA encoding Foxh1$^{\Delta EH1}$, Foxh1^{6xAla}, Foxh1$^{F>E}$, or wild-type Foxh1 was injected into the animal region of 1-cell *Xenopus* embryos. The injected embryos were cultured until the start of

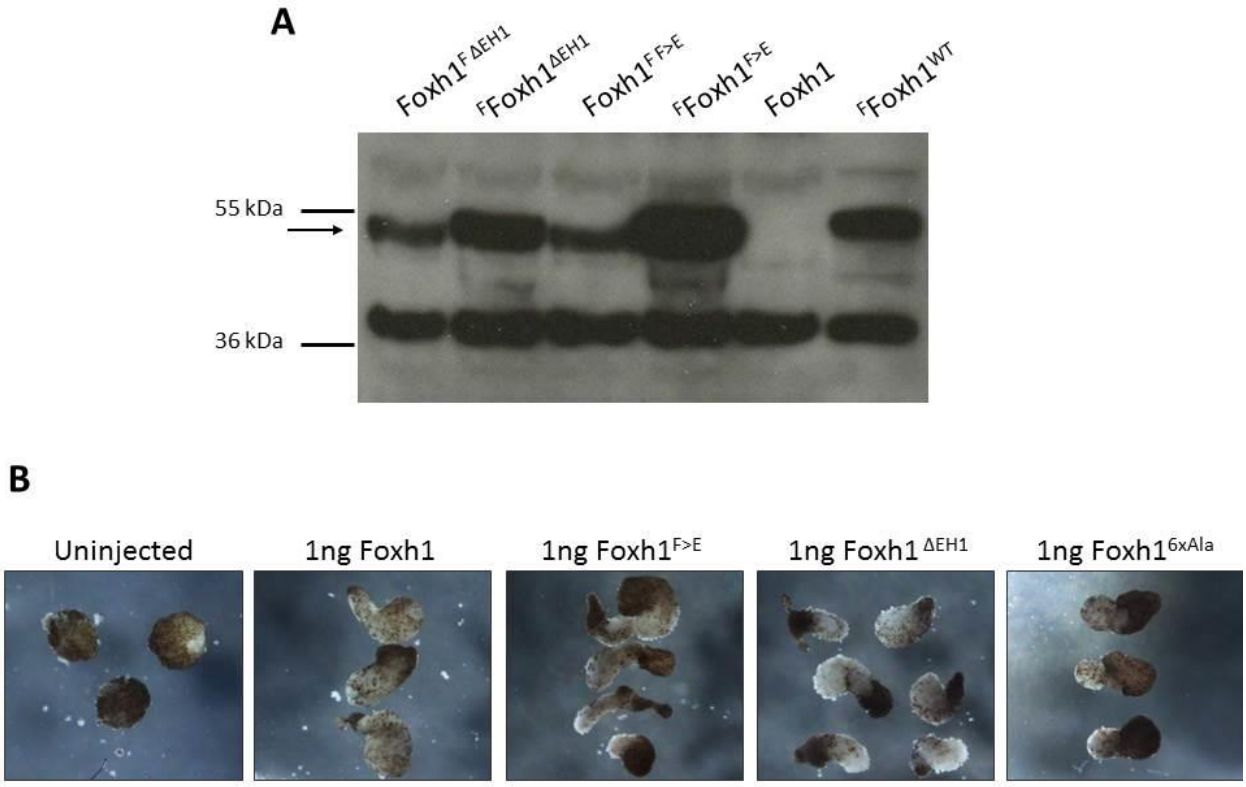

Fig. 5.4 Characterization of Foxh1 FLAG-tagged and EH1 variants. (A) Foxh1 EH1 variants with a C-terminal FLAG tag (denoted by superscript "F") show decreased protein stability over variants with a N-terminal FLAG tag as seen on an anti-FLAG western blot of lysates from *Xenopus* embryos injected with equivalent amounts of RNA encoding the Foxh1 variants or wild-type (no tag, no EH1 mutation) Foxh1. The EH1 mutations do not greatly alter Foxh1 protein stability. (B) The EH1 mutations do not inhibit the mesoderm inducing function of Foxh1 as assayed by elongation of animal caps cut from *Xenopus* embryos injected with 1 ng RNA encoding the Foxh1 EH1 variants. However, the 6xAla mutation did not induce animal cap elongation as effectively or reproducibly as the F>E and ΔEH1 mutation.

gastrulation, when animal caps were cut, cultured overnight, and assessed next day for their elongation, as a measure of the induction of mesendoderm and other tissues that undergo convergent extension. Compared to caps from uninjected embryos that rounded up and became atypical epidermis, caps from all injection conditions had elongated (Fig. 5.4B), indicating activation of mesendoderm-inducing pathways, which are currently held to be initiated by threshold-dependent Nodal signaling (see, for example, Jones et al., 1995). Although, Foxh1^{6xAla} animal caps elongated, they did so less reproducibly than the other two Foxh1 EH1 variant-expressing caps. Therefore, only Foxh1$^{F>E}$ and Foxh1$^{\Delta EH1}$ were further characterized. Quantitative real-time PCR (qRT-PCR) analysis of the Foxh1$^{\Delta EH1}$, Foxh1$^{F>E}$, and wild-type Foxh1 "induced" animal caps showed increased relative expression levels of the mesendodermal markers *Brachyury* (*xbra*) and *Goosecoid* (*gsc*), as well as the mesodermal derivative *Muscle actin*, compared to control caps from uninjected embryos. Conversely, these animal caps had decreased relative expression of the ectodermal marker *Epidermal keratin* compared to uninjected controls (Fig. 5.5). Results of the animal cap and qRT-PCR assays concluded that the EH1 mutations did not compromise the ability of Foxh1 to facilitate mesendoderm induction.

To verify that the EH1 mutations disrupted Foxh1-Grg binding, co-immunoprecipitation (co-IP) assays were performed with homogenized *Xenopus* gastrula embryos that had been injected at the 1-cell stage with RNA encoding the Foxh1 variants alone, or in combination with Myc-tagged *Xenopus* Grg4 (^{Myc}Grg4). *Xenopus* Grg4 is highly homologous to mouse Grg4 (100% homology over domain known to bind EH1), eliminating concerns that the *Xenopus* (Grg4) and mouse (Foxh1 variants) proteins would not interact because they are from different species.

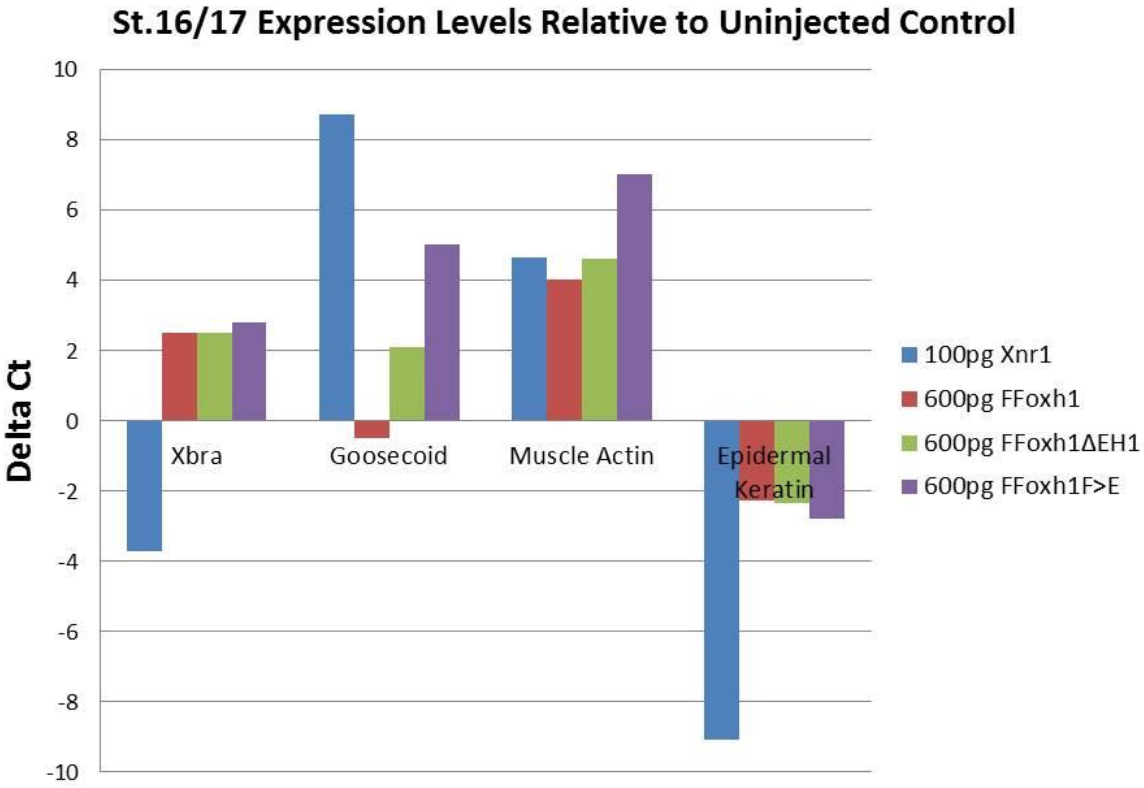

Fig. 5.5 EH1 mutations do not impair Foxh1-facilitated mesendoderm induction. Results of qRT-PCR analysis performed on stage 16/17-equivalent animal caps cut from *Xenopus* embryos injected with RNA encoding the frog *Nodal* homolog *Xnr1* (positive control) or *Foxh1* N-terminally FLAG-tagged EH1 variants. The EH1 mutations do not disrupt the ability of Foxh1 to facilitate mesendoderm induction as seen by the increase in mesendodermal markers *xbra* and *gsc*, and the mesoderm derivative *muscle actin*. The ectodermal marker *epidermal keratin* was decreased in these animal caps. All expression levels are relative to animal caps cut from uninjected control embryos (n = one biological replicate).

Optimization of the co-IP conditions was complicated by non-specific adherence of ^{Myc}Grg4 to the protein A/G agarose-based beads (to which a FLAG antibody was conjugated) originally used for the IP. This caused significant amounts of ^{Myc}Grg4 to immunoprecipitate in the absence of Foxh1 or an IP antibody. Switching from agarose-based beads to magnetic beads abolished the non-specific binding.

I also encountered a problem where the IP antibody heavy chain (~50 kDa) would mask Foxh1 (~45 kDa) on a western blot if both the IP and the primary immunoblotting antibodies were raised in the same species. I eventually found a combination of antibodies that could be used together when immunoprecipitating Foxh1 and blotting for ^{Myc}Grg4. Unfortunately, Foxh1 still became masked by the IP antibody heavy chain when immunoprecipitating ^{Myc}Grg4 and blotting for Foxh1. Therefore, co-IPs could only be performed in one "direction." Because optimizing co-IP conditions took longer than anticipated, we decided to proceed with RMCE without the interaction data.

We chose to submit the Foxh1$^{F>E}$ variant (referred to as Foxh1^{mEH1} henceforth) for RMCE because it altered only one residue and seemed less likely to cause a local or global disruption of protein conformation or stability compared to deleting 8 residues in the ΔEH1 variant. This minimal mutation has been shown to fully disrupt interactions between EH1-motif-containing proteins and Grg co-repressors in numerous species (Jennings et al., 2006; Jiménez et al., 1999; Yaklichkin et al., 2007b). Jennings et al. published high-resolution crystal structures of the human Goosecoid (GSC) EH1 motif bound with the WD-repeat domain of the Grg1 human homolog, TLE1. The paper identified the residues involved in stabilizing the helical

conformation of the EH1 motif, and those that physically interact with TLE1. When a single TLE1 residue that interacts with the phenylalanine (F) in the EH1 was mutated, the authors detected complete loss of the EH1-TLE1 interaction. Also, the phenylalanine is 100% conserved in all EH1 motifs of vertebrate Fox proteins (Yaklichkin et al., 2007a), suggesting the importance of phenylalanine in the primary position.

Once optimized, co-IP assays showed that the ability of ^{Myc}Grg4 to co-IP with Foxh1^{mEH1} was prominently reduced compared to the wild-type Foxh1 control, indicating that the EH1 mutation greatly disrupted Foxh1-Grg4 physical interactions (n = 3 independent injection experiments and western blots; Fig. 5.6). It must be noted that there was discrepancy in the results of the co-IP assays, with some experiments detecting no interaction between Foxh1^{mEH1} and Grg4 and others showing a greatly reduced interaction. These assays were performed in *Xenopus* under overexpression conditions. It is possible that the residual binding is an artifact of this overexpression, or that Grg4 interacts indirectly with Foxh1 through an unidentified complex. Foxh1 does not appear to contain other known Grg binding sites. I tried to preform co-IPs with endogenous levels of protein from mouse embryos (E8.25), but was not successful in being able to routinely and reliably pulldown or detect the Foxh1 variants in mouse. This was most likely due to a low abundance of protein at E8.25, and it could not be determined if the FLAG and Foxh1 antibodies specifically detected the FLAG-tagged Foxh1 proteins in mouse. For example, the FLAG antibody detected the same 45 kDa band (expected molecular weight for FLAG-tagged Foxh1) in lysates from wild-type and *Foxh1*^{F} or *Foxh1*$^{F.F>E}$ embryos (data not shown).

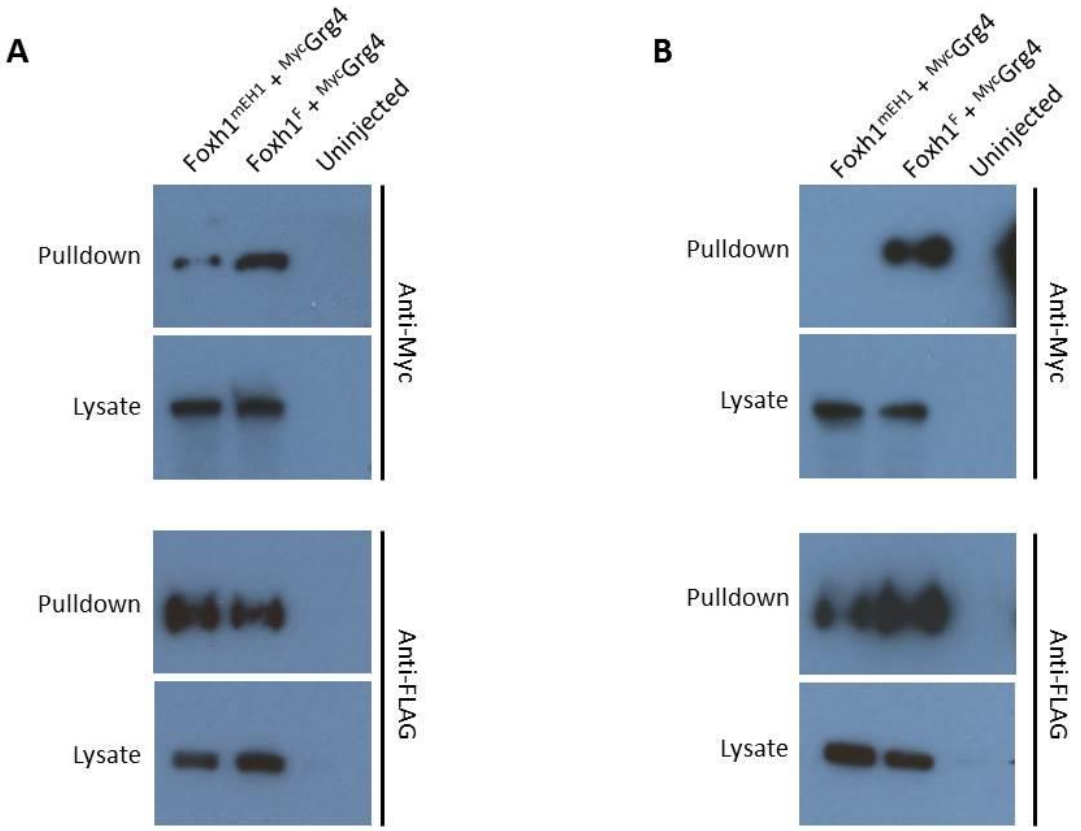

Fig. 5.6 EH1 mutation (F>E) disrupts Foxh1-Grg interaction. (A,B) Protein lysates isolated from gastrula-stage Xenopus embryos injected with RNA encoding Xenopus MycGrg4 (2 ng) and mouse Foxh1F or Foxh1mEH1 (2 ng) were subjected to anti-Foxh1 pulldown. Proteins were detected via western-blot analysis with anti-Myc or anti-FLAG. Two separate experiments are shown to accurately represent the variable results seen with this assay. (A) Greatly reduced ability of Foxh1mEH1 to co-immunoprecipitate with MycGrg4 compared to control Foxh1F. Three minute exposure shown. (B) Separate co-IP analysis confirming that the Foxh1mEH1 - MycGrg4 interaction is disrupted. Thirty second exposure shown. A 10 minute exposure still detects no band in the Foxh1mEH1 + MycGrg4 lane, while the Foxh1mEH1 pulldown band is overexposed (data not shown). Foxh1mEH1 appears to have immunoprecipitated less efficiently than Foxh1F; however, an abundant amount of Foxh1mEH1 was still pulled down and is predicted to be enough to co-IP with mycGrg4 if an interaction existed.

Given the high conservation of the WD-repeat domain among Grg family members (Chen and Courey, 2000), this mutation will likely disrupts potential interactions with other Grg proteins. Based on published *in situ* hybridization expression patterns, Grg3 and Grg4 are the most likely candidates to function in the transcriptional switch because they, like *Foxh1*, are expressed symmetrically within the LPM during stages of asymmetric Nodal signaling (Koop et al., 1996; Leon and Lobe, 1997; Weisberg et al., 1998). A single FLAG tag was also added to Foxh1^{mEH1} to aid in detecting Foxh1^{mEH1} protein over wild-type Foxh1, and to facilitate future chromatin-binding and target gene studies (Fig. 5.3A). As with the EH1 mutation, I characterized whether or not the addition and position (N-terminus vs. C-terminus) of the FLAG tag affected the stability or mesendoderm-inducing potential of wild-type Foxh1. Western blot analysis with a FLAG antibody detected higher levels of N-terminally FLAG-tagged Foxh1 compared to C-terminally FLAG-tagged Foxh1 in lysates of *Xenopus* embryos injected with RNA encoding either Foxh1 variant (Fig. 5.4A). This result suggests that the C-terminal tag location may destabilize or decrease the translational efficiency of Foxh1. To help determine if the C-terminal tag destabilized Foxh1, or if the N-terminal tag over-stabilized Foxh1, I wanted to compare the stability of these variants to the production and stability of untagged Foxh1. Unfortunately, the Foxh1 antibody was not specific enough to permit this experiment (data not shown).

Animal cap elongation assays and qRT-PCR analysis, performed as described above, showed that both FLAG-tagged Foxh1 proteins caused animal cap elongation and induced expression of *Gsc*, *Xbra*, and *Muscle actin* at levels equivalent to that of untagged Foxh1. Therefore, the FLAG

tag location was concluded to not alter the mesendoderm-inducing function of Foxh1. The N-terminus was tagged because N-terminally FLAG-tagged Foxh1 appeared more stable and this location positioned the tag away from the more C-terminally located EH1 motif and SID, hopefully limiting any potential for interference with Grg or p-Smad2/Smad4 binding. A control line, *Foxh1*^{F}, identical to *Foxh1*^{mEH1} except for containing a wild-type EH1 motif, was constructed in parallel, for the most rigorous testing that any abnormal phenotype observed in *Foxh1*^{mEH1} mice was in fact a consequence of the EH1 mutation rather than the presence of the FLAG tag or residual exogenous sequences (Lox, FRT, or restriction enzyme sites) inserted into the *Foxh1* locus that remained after gene engineering (Fig. 5.3A; Fig. 5.2). The *Foxh1*^{mEH1} and *Foxh1*^{F} RMCE replacement constructs were electroporated into the *Foxh1*^{LCA} mESC line, and correctly recombined clonal cell lines were injected into C57BL/6 blastocysts to generate *Foxh1*^{mEH1} and *Foxh1*^{F} chimeras. The FRT-flanked hygromycin resistance (hygro^{R}) cassette, which was used to select for RMCE events, was removed from the *Foxh1* locus by mating chimeras to mice carrying FlpE, the enzyme responsible for recombining FRT sites. Mice homozygous for the *Foxh1*^{mEH1} or *Foxh1*^{F} allele were born at Mendelian ratio, survived to adulthood, and bred normally. The *Foxh1* expression pattern was unchanged in *Foxh1*$^{F/F}$ and *Foxh1*$^{mEH1/mEH1}$ embryos compared to wild-type embryos, indicating that the EH1 mutation and FLAG tag did not disrupt *Foxh1* transcription (Fig. 5.7). *Foxh1*$^{F/F}$ embryos were molecularly and morphologically identical to wild type. Therefore, *Foxh1*$^{F/F}$ and wild-type animals were used interchangeably as control embryos.

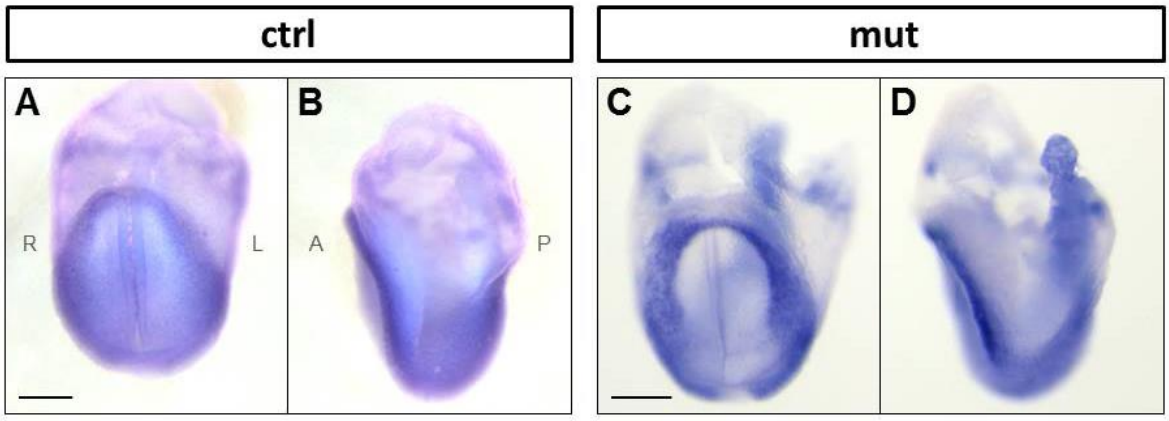

Fig. 5.7 Addition of FLAG tag and EH1 mutation did not alter *Foxh1* expression. (A-D) Whole-mount *in situ* hybridization analysis of *Foxh1* expression in (A,B) E8.0 control compared to (C,D) *Foxh1*$^{mEH1/mEH1}$ embryos. *Foxh1* expression was equivalent in level and distribution in *Foxh1*$^{mEH1/mEH1}$ and control embryos. Embryo orientations: (A,C) Anterior views. (B,D) Lateral views. Scale bars: 200 µm. A, anterior; L, left; P, posterior; R, right.

Gastrulation and A-P patterning are unaffected in Foxh1$^{mEH1/mEH1}$ embryos

Since Foxh1-dependent Nodal signaling is essential for proper gastrulation and A-P patterning, E6.75-7.25 *Foxh1*$^{mEH1/mEH1}$ embryos were analyzed for defects in cell-lineage allocation and axis orientation. Previously characterized Nodal gain-of-function mutants, such as *Lefty2*$^{-/-}$ embryos, present with an expanded primitive streak and excess mesoderm (Meno et al., 1999). If Foxh1-Grg–mediated repression is an important negative regulator of Nodal signaling at this stage, loss of the Grg interaction would be expected to cause increased and/or prolonged Nodal signaling within the epiblast, resulting in defects similar to those seen in *Lefty2*$^{-/-}$ embryos. However, *Foxh1*$^{mEH1/mEH1}$ embryos appeared morphologically normal (Fig. 5.8; see Table 5.1 for *n* values). Any size difference between wild-type and *Foxh1*$^{mEH1/mEH1}$ embryos is attributed to the size and stage variation routinely seen within and between litters at these early developmental stages (Downs and Davies, 1993). The morphological observations were confirmed molecularly by *in situ* hybridization analyses of *Nodal,* its downstream targets, and early patterning genes. No spatial or temporal defects in the expression of *Nodal* (Fig. 5.8A,B) or its downstream target *Lefty2* (Fig. 5.8C,D) were observed. *Otx2* expression, which begins in the visceral endoderm and shifts anteriorly to mark the anterior ectoderm as gastrulation progresses (Zakin et al., 2000), was not altered in mutant embryos, suggesting that regionalized lineage allocation was normal in these embryos (Fig. 5.8G,H). Additionally, expression of the mesoderm and primitive-streak markers, and targets of Foxh1-dependent transcription, *Brachyury/T* and *Goosecoid* were unaffected in *Foxh1*$^{mEH1/mEH1}$ embryos, confirming that the primitive streak was correctly patterned (Fig. 5.8E,F,I,J). Finally, the definitive endoderm marker *Foxa2*, whose expression is dependent on Foxh1 (Hoodless et al., 2001) and is disrupted

In situ Hybridizations				
			Control	
Probe	**Stage**	**Foxh1$^{mEH1/mEH1}$**	**WT**	**Foxh1$^{F/F}$**
Nodal	E6.75	3	13	1
Lefty2	E6.75	10	16	4
T	E7.25	9	7	7
Otx2	E7.25	9	14	6
Gsc	E7.25	8	22	0
Foxh1	E7.75-8.25	14	11	2
Nodal	E8.25	10	8	6
Lefty2	E8.25	8	7	2
Pitx2	E8.25	7	7	5
Foxa2	E8.25	6	7	2
Morphological Analyses				
Analysis	**Stage**	**Foxh1$^{mEH1/mEH1}$**	**WT**	**Foxh1$^{F/F}$**
Heart looping	E9.5-10.5	8	12	7
Latex injection	E15.5	12	1	2
Overall morphology	E13.5-15.5	12	23	6

Table 5.1 Number of embryos analyzed for each experiment.

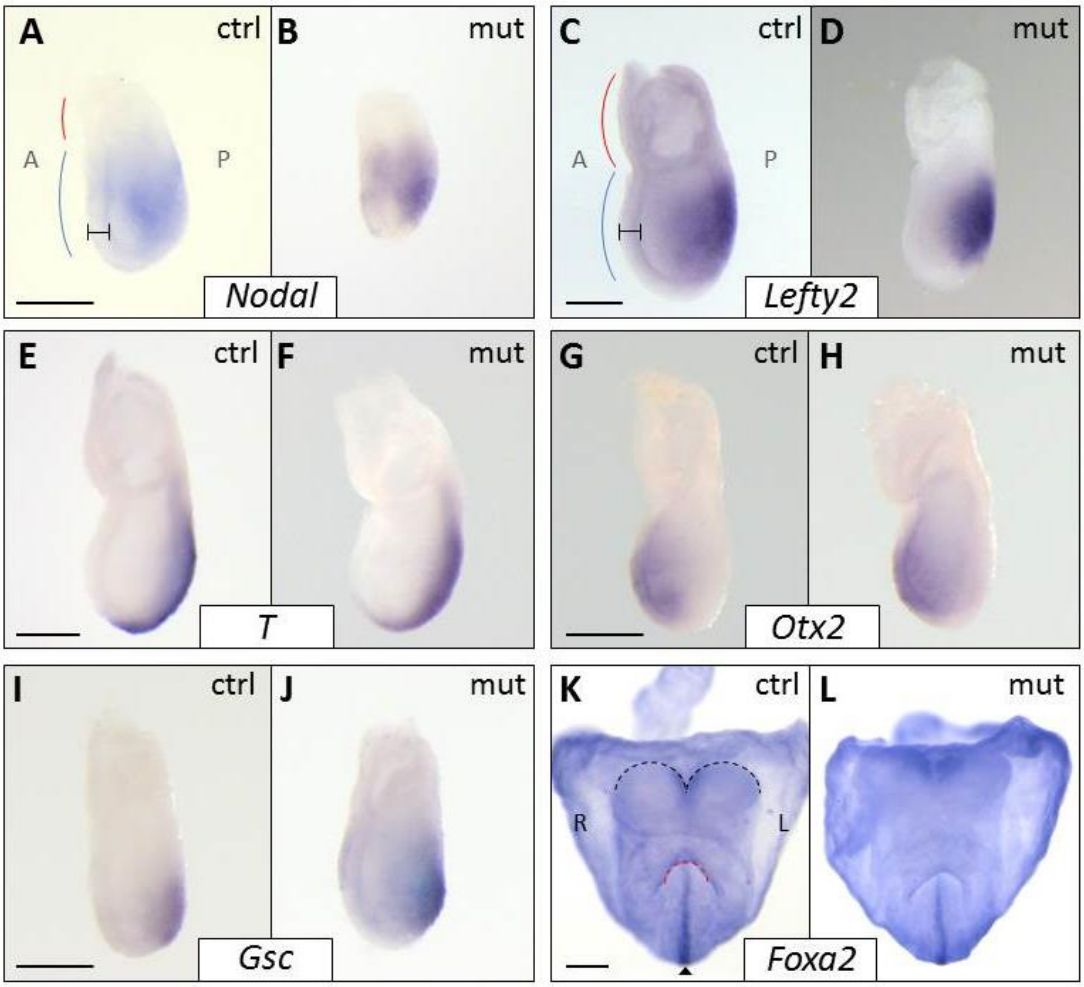

Fig. 5.8 A-P patterning and gastrulation were unaffected in *Foxh1*$^{mEH1/mEH1}$ embryos. Expression of multiple A-P patterning genes was examined by whole-mount *in situ* hybridization in control (ctrl represents wild-type or *Foxh1*$^{F/F}$) or *Foxh1*$^{mEH1/mEH1}$ (mut) E6.75-E7.25 embryos. The expression patterns of *Nodal* (A,B), *Lefty2* (C,D), *Brachyury/T* (E,F), *Otx2* (G,H), and *Gsc* (I,J) were similar between control and *Foxh1*$^{mEH1/mEH1}$ embryos. Red and blue lines mark representative location of extraembryonic tissue and embryo proper, respectively, in (A) E6.75 and (C) E7.25 embryos. Hash marks denote definitive endoderm. (K,L) *Foxa2* expression was unaffected in *Foxh1*$^{mEH1/mEH1}$, confirming midline (arrowhead) integrity in mutant embryos. Black and red lines outline headfolds and foregut pocket, respectively. Embryo orientations: (A-J) Lateral views. (K-L) Anterior views. Scale bars: 200 µm. A, anterior; L, left; P, posterior; R, right.

in both loss- and gain-of-function Nodal mutants (Perea-Gomez et al., 2002; Vincent et al., 2003), was clearly expressed in the axial midline of early somite mutant embryos (Fig. 5.8K,L). Combined, these results show that early cell specification and patterning were not altered in *Foxh1*$^{mEH1/mEH1}$ embryos, and that Foxh1-Grg–mediated repression is not a primary regulator of Nodal signaling at this stage.

L-R patterning is unaffected in Foxh1$^{mEH1/mEH1}$ embryos

We next investigated if Foxh1-Grg–mediated repression regulates Nodal signaling during stages of L-R patterning. As discussed in the Introduction, *Nodal* expression, as well as that of *Lefty2* and *Pitx2*, is strikingly left-sided, quickly moving through the L LPM in a dynamic posterior-to-anterior wave of expression (Collignon et al., 1996; Lowe et al., 1996; Meno et al., 1996; Ohi and Wright, 2007). Bilateral expression of Foxh1, Smad2/4, and Groucho co-repressors in the LPM (Koop et al., 1996; Leon and Lobe, 1997; Waldrip et al., 1998; Weisberg et al., 1998) suggests that Foxh1 transcriptional switching may regulate the spatiotemporal expression of Nodal circuit genes by initiating their expression in the L LPM and suppressing it in the R LPM. If the Foxh1-Grg repression arm negatively regulated Nodal signaling, it was predicted that disrupting this interaction would result in premature, prolonged, and/or R-sided expression of *Nodal* and its downstream targets. In all *Foxh1*$^{mEH1/mEH1}$ embryos assayed, *Nodal* was solely L-sided, and not detected in the L LPM prior to 2-3 somites or beyond 8 somites (Fig. 5.9A,B). As expected, *Nodal* expression in the node, which is controlled by a Foxh1-independent enhancer, was not altered (data not shown). In accordance with *Nodal* expression, no spatial or temporal defects were detected in *Lefty2* and *Pitx2* expression (Fig. 5.9C-F). From these results we

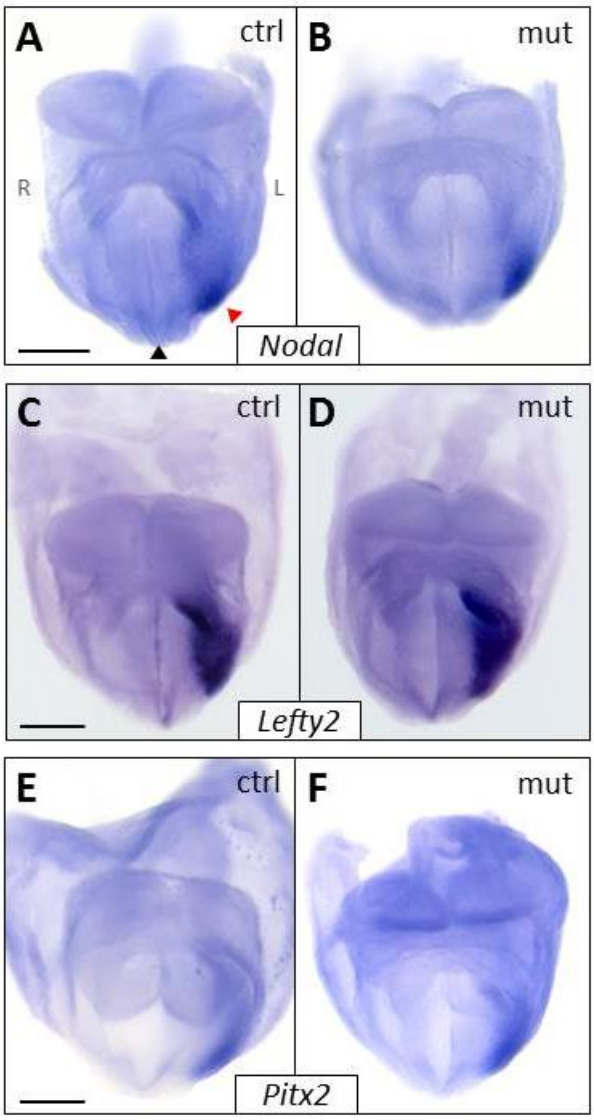

Fig. 5.9 Expression of L-R patterning genes was unaffected in *Foxh1*$^{mEH1/mEH1}$ embryos. (A-F) Whole-mount *in situ* hybridization analysis of L-R patterning genes (A,B) *Nodal*, (C,D) *Lefty2*, and (E,F) *Pitx2* in the left LPM of control or *Foxh1*$^{mEH1/mEH1}$ embryos at E8.25. No aberrant expression of L-R patterning genes was detected in mutant embryos. Black and red arrowheads indicate midline and LPM, respectively. Embryos orientations: (A-F) anterior views. Scale bars: 200 µm. L, left; R, right.

conclude that loss of Foxh1-Grg–mediated repression during L-R patterning can be overcome without compromising development.

Foxh1$^{mEH1/mEH1}$ embryos display normal L-R situs

Nodal signaling (*Nodal*, *Lefty2*, *Pitx2*) in the L LPM directs proper placement and anatomy of the visceral organs (Nakamura and Hamada, 2012). Alterations in *Nodal* expression, and thus signaling, such as right-sided or bilateral expression, can lead to multiple heart abnormalities, pulmonary isomerism, intestinal malrotation, and misplacement of visceral organs with respect to the midline. Heart abnormalities commonly observed in Nodal signaling mutants include dextrocardia, reversed heart looping, transposition of the great arteries, and ventricular septation (Bisgrove and Yost, 2001). Analysis of heart morphology and placement in mutantE9.5-10.5 embryos revealed, in all embryos analyzed, stereotypically normal rightward looping and correct cardiac positioning left of midline (Fig. 5.10A,B). Functional assessment of heart morphology for septal and vessel-transposition defects was done by injecting blue and yellow liquid latex, respectively, into the left and right ventricles of E15.5 *Foxh1*$^{mEH1/mEH1}$ embryos to highlight the vasculature and aid in detecting cardiovascular defects. As seen in wild-type embryos, the pulmonary trunk passed ventrally to the aorta in all *Foxh1*$^{mEH1/mEH1}$ embryos analyzed, indicating no transposition of the great arteries. Also, no ventricular septations were identified, as mixing of the yellow and blue latexes was not observed in the ventricles of these embryos (Fig. 5.10C,D). Overall morphology of visceral organs (lungs, liver, gut, stomach) appeared normal in *Foxh1*$^{mEH1/mEH1}$ embryos (Fig. 5.10E-H). These results corroborate our early findings that showed no molecular defects in L-R patterning. Together,

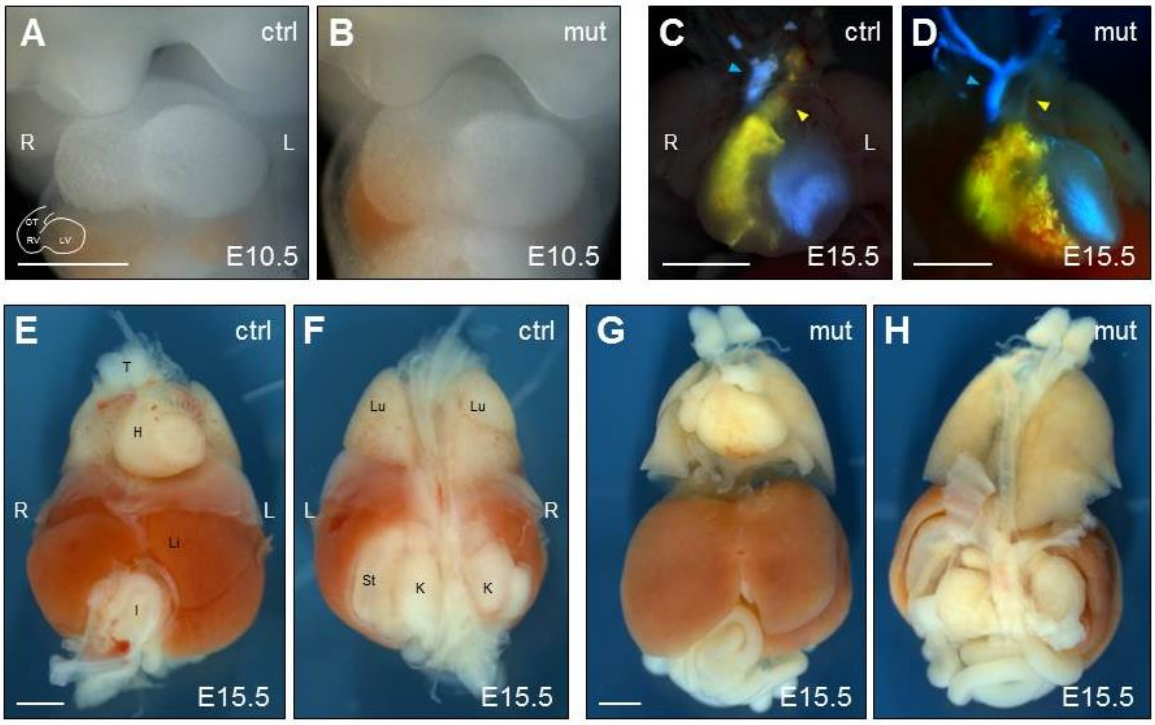

Fig. 5.10 Internal organ situs and morphology was normal in *Foxh1*$^{mEH1/mEH1}$ embryos. (A,B) Normal dextral looping of the heart was observed in E10.5 *Foxh1*$^{mEH1/mEH1}$ embryos. (C,D) Different colors of liquid latex were injected into the right (yellow) and left (blue) ventricles of E15.5 control and *Foxh1*$^{mEH1/mEH1}$ embryos to highlight potential defects in ventricular septation, formation and positioning of the great arteries and aortic arch. No latex mixing, which would have indicated septation defects, was observed in *Foxh1*$^{mEH1/mEH1}$embryos. Also, the pulmonary trunk (yellow arrowhead) always appeared ventral to the aorta (blue arrowhead), and aortic branching was equivalent to control embryos. (E-H) Overall organ placement and morphology was unaffected in *Foxh1*$^{mEH1/mEH1}$ embryos at E15.5. Embryo orientations: (A-E, G) Ventral views. (F, H) Dorsal views. Scale bars: (A,B) 500 µm; (C-H) 1 mm. H, heart; I, intestine; K, kidney; L, left; Li, liver; Lu, lung; LV; left ventricle; OT, outflow tract; RV, right ventricle; St, stomach; T, thymus.

these data show that major disruption of the Foxh1-Grg interaction alone does not alter Nodal signaling in the mouse, and that, possibly, the role Foxh1-Grg–mediated repression plays in regulating *Nodal* transcription is masked by a highly buffered regulatory system, which compensates for its loss in an effort to maintain the spatiotemporal dynamics of Nodal signaling.

Discussion

This is the first study to use a precise amino acid alteration to address the role of Foxh1-Grg–mediated repression in regulating Nodal signaling during early mouse development. We altered the endogenous *Foxh1* locus so that our experiments were performed under endogenous levels of gene and protein expression, rather than in an overexpression context, providing the most rigorous way to assay the direct influence of Grg-based repression acting through Foxh1 on Nodal signaling. The minor modifications made to create the $Foxh1^{mEH1}$ allele were carefully controlled for by the parallel construction of the "wild-type" $Foxh1^{F}$ allele (noting that both proteins also contained an N-terminal FLAG tag). We conclude that the blocked interaction between Foxh1 and Grg can be accommodated by adaptable gene regulatory mechanisms, such that there are no major effects on Nodal signaling at the level of target gene readout, or overall body axis formation, anterior-posterior or left-right patterning. Our results suggest that there is substantial robustness in the mechanisms that have evolved to stabilize Nodal regulatory systems and lead to successful germ-layer development and embryonic patterning.

Buffered regulatory system potentially compensates for loss of Foxh1-Grg–mediated repression

Cell fate determination is qualitatively influenced by the level and duration of Nodal signaling. Experiments in *Xenopus* embryos showed that higher Nodal/Activin signaling induced the mesendoderm marker *gsc*, while lower levels induced the pan-mesodermal marker *xbra* (Agius et al., 2000; Gurdon et al., 1994; Jones et al., 1995). Dose-dependent responses also control mouse development (Robertson, 2014). In *Nodal* null embryos, little mesodermal differentiation occurs and there is subsequent failure to gastrulate, causing developmental arrest (Conlon et al., 1994; Zhou et al., 1993). Mesoderm induction is restored in mutants with reduced *Nodal* expression, but definitive endoderm is still absent (Norris et al., 2002; Vincent et al., 2003). Left-right patterning also depends upon the level of the Nodal signaling component *Pitx2,* a transcriptional effector that is essential for asymmetric organogenesis (Nakamura and Hamada, 2012). Experiments with *Pitx2* revealed a progressive gene-dosage requirement in organ formation and L-R patterning: lung and gut required the highest level of *Pitx2* expression, followed by the heart, with the stomach requiring the least (Gage et al., 1999; Liu et al., 2001). Because proper embryonic patterning depends upon the precise titration of Nodal signaling, it is likely that buffered regulatory systems were developed to provide stability but also rheostat-like level control. The employment of such a system may be one explanation for the lack of phenotype in $Foxh^{mEH1/mEH1}$ embryos.

Tissue-specific expression of *Nodal* is, in part, regulated by five different enhancers that drive expression in the epiblast, node, and LPM (Adachi et al., 1999; Papanayotou et al., 2014; Saijoh et al., 2005; Vincent et al., 2003). The dynamic expression in the epiblast and LPM is also

strongly affected by a self-enhancement and lateral-inhibition (SELI) system through which Nodal enhances its own expression with a positive feed-forward loop that activates the ASE. Nodal then rapidly initiates expression of its feedback antagonist Lefty2 (Nakamura et al., 2006). Lefty2 molecules, which have an inherent ability to travel faster and farther than Nodal, and have greater stability, help terminate N*odal* expression in the L LPM, as well as prevent the Nodal autoregulatory loop from fully initiating in the R LPM (Marjoram and Wright, 2011; Müller et al., 2012; Nakamura et al., 2006). Lefty2 inhibits Nodal signaling by either binding directly to the Nodal dimer, or competitively blocking access to the obligate EGF-CFC co-receptors (Chen and Shen, 2004). Such inhibition by Lefty2 prevents phosphorylation and prevents Smad2 shuttling to the nucleus, shutting down Foxh1-dependent transcription of target genes.

We speculate that the *Nodal* locus could be more "open" in *Foxh1*$^{mEH1/mEH1}$ embryos because of impaired interaction with Grg co-repressors. However, attenuation of Smad2 phosphorylation by Lefty2 inhibition at the cell surface should still occur in mutant embryos, dampening the potential over-activation of *Nodal* expression. Thus Lefty2 would be an especially important component of the buffered regulatory system that compensates for the reduction/loss of Foxh1-Grg–mediated repression in *Foxh1*^{mEH1} mutant mice, preventing a mutant phenotype. Original studies in *Xenopus* suggesting that Foxh1 represses *Nodal* transcription (D. S. Kessler, personal communication) may have overcome this degree of buffering by overexpressing mutant Foxh1, unlike in this study with *Foxh1*^{mEH1} being expressed from the endogenous locus.

The existence of a system that exerts meticulous control over Nodal signaling is suggested by the multiple Nodal signaling loss- and gain-of-function mutations that display incomplete penetrance or variable expressivity. For example, the severity of defects in *Foxh1*$^{-/-}$ embryos varies greatly, from completely failed development of the embryo proper, to a less severe phenotype without midline structures (Hoodless et al., 2001; Yamamoto et al., 2001). Similarly, embryos lacking the co-receptor *Cryptic* have numerous defects in asymmetric organogenesis, but the specific organs affected differ among mutant embryos (Yan et al., 1999). Incomplete penetrance is seen in embryos that lack *Lefty2* in the LPM, with two-thirds of the animals dying a few days after birth from cardiac defects, which were not detected in mutants that survived to adulthood (Meno et al., 2001). Homozygous mutations in the Nodal antagonists *Lefty1* and *Cerl* alone do not cause defects in gastrulation (Meno et al., 1998; Simpson et al., 1999), but the double homozygous *Lefty1*$^{-/-}$*;Cerl*$^{-/-}$ mutants are 100% embryonic lethal (Perea-Gomez et al., 2002). These results demonstrate that loss of a single negative regulator of Nodal signaling can be compensated for, and that removal of additional members of the buffered regulatory system is required to manifest an abnormal phenotype.

Therefore, it is possible that this new *Foxh1*$^{mEH1/mEH1}$ condition represents a sensitized state in which relatively subtle manipulation of other components of the buffered system could reveal patterning defects. Future experiments could test how the loss of Foxh1-Grg–mediated repression is compensated. For example, loss of Lefty2 in the *Foxh1*^{mEH1} background may yield patterning deficits that remain hidden under disruption of only the Foxh1-Grg interaction. Introducing a *Foxh1* null allele (*Foxh1*$^{mEH1/-}$) may also sensitize mice to the EH1 mutation by further reducing the potential of the Foxh1-Grg interaction, and produce a mutant phenotype.

While our Foxh1^{mEH1} amino-acid alteration removes a residue that is essential for tight Grg interaction (Jennings et al., 2006), we must remain open to the possibility that the primary explanation for the lack of abnormal phenotype is that some low-level Foxh1^{mEH1}-Grg association is sufficient to effect substantial repression of *Nodal* transcription. The strength of the data indicating the importance of the phenylalanine residue for Grg interaction strongly suggest that any residual Grg binding might occur not through the highly disrupted EH1 motif, but indirectly through some other member of the as-yet-uncharacterized transcriptional complex. An even simpler interpretation is that Grg-mediated repression of Nodal signaling is not conserved in the mouse. The sensitization experiments described above are pertinent and use our findings here as the foundation. In addition, experiments investigating the type of epigenetic repression marks present at the *Nodal* locus in *Foxh1*^{mEH1} mutant embryos compared to control embryos could help determine the extent of repression that remains in *Foxh1*^{mEH1} embryos.

Epigenetic regulation of Nodal signaling

The epigenetic landscape provides critical input onto a gene's transcriptional state, but almost nothing is known about such landscape alterations at the *Nodal* locus during development, or the degree to which epigenetic modifications contribute to Nodal signaling regulation. It is well documented that pSmad2/Smad4 recruits the co-activators p300 and CREB binding protein (CBP), which use their intrinsic histone acetyltransferase activity to promote an open-chromatin conformation (Attisano and Wrana, 2000). The ability of Foxh1 to interact with factors that recruit HDACs, which are capable of reversing the pSmad2/Smad4-founded markings, further

supports Foxh1 transcriptional switching as a plausible epigenetic mode of modulating Nodal signaling.

Recent studies report roles for histone acetylation and methylation in the positive and negative regulation of Nodal signaling in mouse ESCs and in embryos. In mouse ESCs, Nodal-Smad2/3 signaling recruits Jmjd3, a $H3^{k27me3}$-specific demethylase, to Nodal target-genes to counteract the repressive effect of Polycomb repressive complex 2 (PRC2) (Dahle et al., 2010). On the other hand, studies in Medaka fish report physical interaction of Foxh1with the PRC2 histone-modifier Ezh1, with *Ezh1* knockdown producing bilateral *Nodal* expression and L-R patterning defects (Arai et al., 2010). Because PRC2 can be recruited by Grg co-repressors (Patel et al., 2012), Foxh1, through interaction with Grg, could initiate longer-term transcriptional repression. Also, others have already implied that HDACs could be part of the repression mechanism for *Nodal* expression in the R LPM (Carneiro et al., 2011).

Understanding whether or not the *Nodal* locus remains poised or repressed during time points when *Nodal* is not expressed may provide insight into the flexible regulation of Nodal signaling during embryogenesis, and the specific levels of signaling that transcriptionally activate the various sets of downstream targets. We also speculate that the Grg-mediated long-term repression of *Nodal* expression might be essential in preventing neoplastic reactivation of the Nodal signaling pathway. The $Foxh1^{F}$ line will be useful for studying the epigenetic regulation occurring at the *Nodal* locus, and other ASE-containing loci, as well as for identifying novel targets of Foxh1.

CHAPTER VI

SUMMARY AND FUTURE DIRECTIONS

Summary

Nodal signaling is a highly conserved pathway in vertebrate development that is required for gastrulation, anterior-posterior (A-P) patterning, and the derivation of left-right (L-R) asymmetry. Since the discovery of Nodal almost 20 years ago, much has been learned about its regulation and function in development. Particular topics of intense research have included identifying the molecular components of the Nodal signaling pathway, the mechanisms that drive *Nodal* expression, the factors that regulate ligand dynamics, and understanding how Nodal regulates cell-fate determination and patterning. Despite reaching such a significant level of understanding in a relatively short time period, certain equivalently important aspects of Nodal signaling regulation and function still represent mysteries. In identifying mechanisms that drive *Nodal* expression, primary emphasis was placed on understanding the activation of *Nodal* transcription during development. Little work has been done to understand the role that transcriptional repression of *Nodal* has in the overall negative regulation of Nodal signaling. Instead, much of our knowledge on how Nodal signaling is attenuated in the embryo comes from work detailing how the Nodal ligand is blocked from activating cell-surface receptors, often by the use of extracellular inhibitors that physically interact with Nodal and prevent function. In terms of embryonic patterning, it is still unknown how Nodal signaling in the left lateral plate mesoderm (L LPM) establishes and directs the individual asymmetric morphogenetic programs of multiple organ anlagen.

Therefore, the aims of my thesis research were established to help move us to a better understanding of three basic aspects of Nodal signaling: (1) how cells in the L LPM interpret Nodal signaling dynamics (i.e. duration, levels) during stages of asymmetric gene expression, (2) how Nodal signaling in the L LPM influences tissue architecture prior to gut looping, and (3) how *Nodal* is negatively regulated (repressed, or prevented from over-activity) at the transcriptional level. In order to understand how active Nodal signaling dynamics relate to those of the *Nodal* expression pattern in the L LPM, one of my goals was to generate a spatiotemporal map of pSmad2 localization across the LPM of *Xenopus* embryos during stages of asymmetric gene expression. Knowing the location, duration, and levels of active Nodal signaling in the LPM, using pSmad2 as the active readout, could provide insight into how Nodal signaling becomes a morphogenetic cue. For example, pSmad2 localization patterns might have revealed that not all cells experience the same level of signaling, and that the level of signaling experienced determines which cells actively engage in tissue morphogenesis (i.e. undergo cell shape, ECM remodeling) and those that do not, the latter becoming 'follower' cells after the pioneer cells initiate tissue morphogenetic movements.

To generate such a precise map of pSmad2 localization, a specific and sensitive antibody was needed. However, none of the currently available antibodies fit these criteria. Therefore, we generated a new antibody against pSmad2. Unfortunately, my characterization studies, detailed in Chapter III, revealed that the antibody did not specifically recognize pSmad2 on tissue sections of *Xenopus* tailbud-stage embryos. From this, we concluded that the antibody could not be used to generate a spatiotemporal map of Nodal signaling. I, therefore, strongly deprioritized the project in order to focus on other aspects of my thesis. For this reason, I do

not discuss the future directions of this project below, because I already included some potential alternative methods for detecting active Nodal signaling in frog in the Discussion section of Chapter III.

Current studies in the chicken and frog have begun to address the general mechanisms of asymmetric organogenesis by identifying molecular and architectural asymmetries occurring within the gut mesoderm. Although seminal, these studies in fact have rather a narrow focus, beginning analysis after the start of asymmetric morphogenesis, and characterizing only a limited region of the gut—the midgut. In Chapter IV, I described how I was aiming to expand on these studies by characterizing potential changes in the LPM architecture (cell shape, ECM and cytoskeletal composition) during the time period between the end of asymmetric *Nodal* expression (stage 25) and the first time of noticeable, incipient gut looping in *Xenopus* (stage 38). I also wanted to investigate how Nodal signaling is linked to these changes, and how these architectural changes guide the direction of gut looping.

This project was initiated by a previous graduate student in the lab, Lindsay Marjoram. In her preliminary findings, she detected tighter bundling and more contracted F-actin in the R LPM compared to the L LPM. I confirmed her results and identified a potential asymmetry in the localization of β-1 integrin, in which there was more intense immunodetection in the R vs. L LPM (Fig. 4.1; Fig. 4.2). The caution here is that additional analysis of more embryos will be needed to determine if the asymmetric localization is reproducible and then find a way to quantify the difference, and understand, again, if it is focal or more widespread across the LPM. My biggest contribution to this project was the optimization of a whole-mount immunolabeling

and Technovit sectioning protocol that had not been used yet by the lab (detailed in Materials and Methods; Chapter II). Previously, the lab analyzed LPM architecture by immunolabeling cryosections of *Xenopus* embryos. This technique often resulted in large chunks of missing tissue and distorted (that is, compressed or stretched) tissue architecture. With the new whole-mount immunolabeling and Technovit embedding/sectioning protocol, tissue architecture was immaculately preserved (Fig. 4.3). The improvement in tissue preservation would greatly enhance our ability to obtain high-resolution images of, and identify changes in, cell morphology and architecture within the LPM and underlying endoderm that give rise to the gut. Also, being able to perform whole-mount immunolabeling on *Xenopus* embryos would allow us to pursue 3-D rendering of LPM tissue architecture, which was not possible with our previous cryosectioning method due to poor tissue architecture quality and registration problems with putting whole 3-D images into place from multiple sections.

The bulk of my thesis work, as detailed in Chapter V, focused on identifying whether or not the transcription factor Foxh1 acts as a transcriptional repressor of *Nodal* expression. It is well established that Foxh1 is necessary for the initiation of *Nodal, Lefty2*, and *Pitx2* expression in response to Nodal signaling. Unpublished work from our collaborator, Dr. Dan Kessler at the University of Pennsylvania, suggests that Foxh1 could regulate *Nodal* expression by acting as a transcriptional switch. In this type of regulatory mode, Foxh1 toggles between positive and negative transcriptional activity by switching between binding partners – the pSmad2 activator and Groucho co-repressor, respectively (Fig. 5.1). To test the conservation of the Foxh1 transcriptional switch in mouse, and to determine the consequences of its removal, I derived a

mouse line in which the Groucho binding motif, the Engrailed-homology 1 (EH1) motif, of Foxh1 was mutated to prevent binding with Groucho (Grg) co-repressors.

I began by constructing a loxed-cassette acceptor allele (LCA) of the *Foxh1* locus. The *Foxh1*^{LCA} allowed the insertion of variant Foxh1 protein-encoding sequences into the endogenous locus. Two alleles were created: *Foxh1*^{mEH1}, which encoded an N-terminally FLAG-tagged Foxh1 with a single amino acid (F-to-E) substitution in the EH1, and *Foxh1*^{F}, which is identical to *Foxh1*^{mEH1} except for its wild-type EH1 motif. Molecular and morphological analyses found no Nodal signaling or embryonic patterning defects in *Foxh1*$^{mEH1/mEH1}$ embryos (Figs. 5.8-5.10), and these mice survived to adulthood. The absence of a mutant phenotype could have, in principle, several explanations. First, some of the co-immunoprecipitation assays, on the surface, suggest that the F-to-E substitution does not always cause the complete abolition of Foxh1^{mEH1} and Grg interaction (Fig. 5.6). Although we argue against this possibility (see Chapter V for details, but primarily we think it reflects the heterologous and overexpression conditions of the assay), it is difficult to rule out completely the explanation that the little interaction remaining was sufficient to effect substantial repression of *Nodal* transcription. Second, it is possible that Foxh1-Grg–mediated repression is not conserved, and unlike in Xenopus tissue, does not regulate Nodal signaling in mouse. Finally, we prefer the idea that Nodal signaling is regulated by a highly buffered system capable of compensating for the loss of the Foxh1-Groucho interaction and maintaining normal spatiotemporal dynamics of Nodal signaling in mutant mice. Experiments that can distinguish between these possibilities have been devised and are discussed in detail below. Also discussed below are additional experiments and tools that could

help us gain a deeper understanding of how the spatiotemporal dynamics of *Nodal* transcription are epigenetically regulated during embryonic development.

Chapter IV Future Directions

Mapping F-actin foci

The presence of L-R differences in the actin cytoskeleton between the L and R LPM in *Xenopus* may be significant with regard to asymmetric gut looping considering studies in fly, chicken, and mouse have noted an increase in actin cytoskeleton regulators in regions of the gut undergoing active looping. Furthermore, the increase in F-actin bundling that we have observed in the R LPM was not uniform along the A-P axis, but seemed more focal. The focal nature of increased F-actin bundling/tightening supports the hypothesis that these F-actin foci might mark future sites of cell-architectural rearrangements, such as constriction, which could lead to incipient bending of the gut. Before a conclusion can be made about their potential role in gut looping, it must first be determined if the F-actin foci appear reproducibly in the same locations along the A-P and D-V axes in embryos of the same stage. General conservation of the locations of F-actin foci across different embryos would further indicate the importance and a possible instructive role in tissue morphogenesis of the LPM. I speculate that mapping of the foci will eventually be achievable by analyzing the actin cytoskeleton in whole mounts. As discussed in the Results section of Chapter IV, methods for labeling and imaging embryos in whole mount still need to be finessed, but initial attempts showed promise.

If F-actin foci in the R LPM appear reproducible in their location along the A-P and D-V axes, it may be possible to trace the cells near the foci to determine if they become incorporated into

specific concavity or convexity regions of the gut. In a method similar to that performed by Muller et al. (2003) to determine the contribution of specific regions of the LPM at stage 23 to gut-derived organs at stage 45/46, fluorescent dyes or dextrans could be injected into regions of the LPM that have been reproducibly pre-determined to contain F-actin foci (from the whole-mount mapping proposed above). Embryos would then be analyzed during stages of gut looping to determine where labeled cells localize in the mesoderm (concavity, convexity, linear region) surrounding the gut endoderm (Fig. 6.1).

Identifying additional LPM architecture asymmetries

The identification of L-R asymmetries in the actin cytoskeleton within the LPM between stages 35-43 provides a launching point for the identification of other cytoskeletal or ECM components, which connect to the actin cytoskeleton, that also display asymmetric characteristics. For example, adherens junctions link directly to actin, and the adherens junction component α-catenin has been shown to be increased on the left of the gut bending in chicken (Welsh et al., 2013). Catenins help connect the cadherin family of transmembrane proteins to the actin cytoskeleton, which in turn promote cell-cell adhesion by binding with other cadherins, such as N-cadherin, on neighboring cells. Given its importance in influencing tissue architecture changes in the chicken dorsal mesentery and in multiple other systems (Davis et al., 2008; Kurpios et al., 2008; Leonard et al., 2011; Plageman Jr. et al., 2011; Welsh et al., 2013), determining the localization pattern of N-cadherin in the LPM has been an interest of the Wright lab for some time. Unfortunately, multiple antibodies against N-cadherin had been tested in the lab and none showed reactivity in *Xenopus*. Towards the end of my work on this

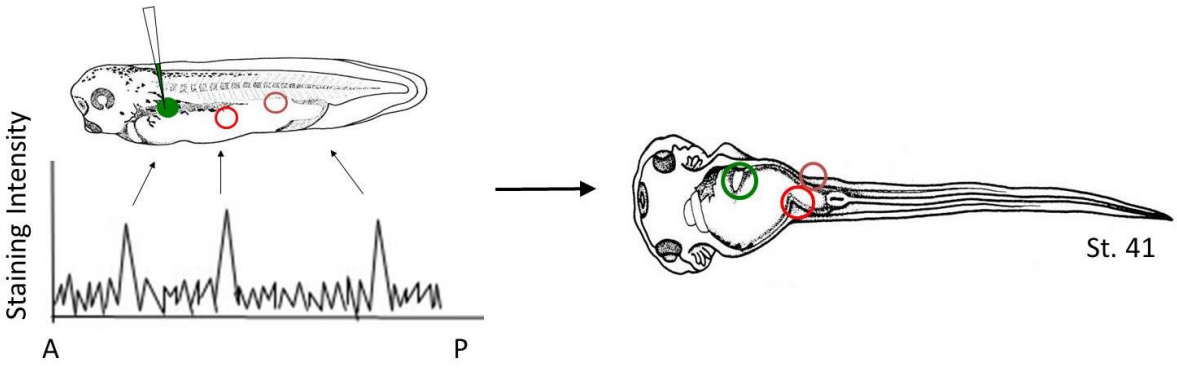

Fig. 6.1 Schematic of tissue architecture tracing experiment. Regions of LPM tissue containing architectural features of interest (circles), such as F-actin foci, will be mapped along the A-P axis to determine if the features localize to the same regions in every embryo. If so, these regions of the embryo can then be injected with a fluorescent dye or dextran (filled-in circle) to determine if these cells localize to regions of active gut looping at later stages.

project, I obtained possible signal with a rabbit anti-N-cadherin antibody (Abcam) when used for whole-mount immunolabeling of a stage 23 embryo. Although the specificity of the localization pattern was not certain as a confounding signal was detected in the nucleus in addition to cell borders. It is possible that with further optimization it would be able to investigate if asymmetries in N-cadherin localization exist between the L and R LPM.

A major determinant for the importance of the observed asymmetries in LPM cytoskeleton architecture in shaping the gut is whether or not they actually lead to defined inductions in cell shape change. For example, increased deposition of ECM and cytoskeleton components in the chicken dorsal mesentery cause increased cell-cell adhesion, increased tissue condensation, and promote adoption of a columnar cell shape (Davis et al., 2008; Kurpios et al., 2008). The use of Technovit 7100 greatly enhances the feasibility of characterizing cell morphology given its accurate preservation of cell architecture. Cell shape within the L and R LPM would be assayed in stages preceding actual gut looping by whole-mount immunolabeling *Xenopus* embryos with antibodies against E-cadherin, β-1 integrin, and β-catenin, all of which demarcate cell boundaries in the endoderm and LPM. Using fate mapping described above, F-actin foci or cells with increased adherens junctions could be labeled and followed further along in embryogenesis to determine if alterations in the cytoskeletons lead to cell-shape changes. For example, it would be interesting to investigate if the columnar architecture of splanchnic mesoderm cells is maintained in regions near F-actin foci, and if cells adopt a more squamous architecture in regions of the R LPM where such foci are absent.

In addition to characterizing the physical changes occurring to LPM tissue architecture and how these changes influence gut chirality, we also need to know what lies upstream of the physical changes. The recent identification of an upregulation in Wnt signaling components and formins (Daam2) in the left dorsal mesentery of chicken and mouse (Welsh et al., 2013) provides an interesting starting point. The lack of nuclear β-catenin and changes in the cytoskeleton suggested that non-canonical Wnt signaling was activated in the left dorsal mesentery (Welsh et al., 2013). It could be worth investigating the expression of Wnt signaling components and effectors (Daam1/2), especially those belonging to the planar cell polarity (PCP) pathway, via in *situ* hybridization in the LPM of *Xenopus*.

Another pertinent pathway to investigate is the Rho GTPase signaling pathway. When *Pitx2a* was misexpressed in HeLa cells, the Rho GTPases Rac1 and RhoA were activated, causing changes in the actin cytoskeleton and increasing cell-cell adhesion (Wei and Adelstein, 2002). Daam2, a Wnt effector, has also been suggested to activate Rho GTPases (Welsh et al., 2013). Unfortunately, the currently available antibodies against Rac1 and RhoA do not work on *Xenopus* tissue. Several years ago, the Nascone-Yoder lab published a caged Rockout-derivative that allowed for the spatiotemporal control of Rho kinase in live *Xenopus* embryos (Morckel et al., 2011). Caged Rockout consists of a photolabile caging group attached to the small-molecule inhibitor of Rho kinase, Rockout. When caged Rockout is exposed to a short pulse of UV light of 30-120 seconds, Rockout becomes uncaged and free to repress Rho kinase. *Xenopus* embryos take up caged Rockout through simple diffusion when incubated in a solution. Embryos in which caged Rockout was UV-activated on the right side between stages 35-39 displayed

reversed midgut curvature and disorganization of the normal columnar epithelial architecture when analyzed at stage 45/46 (Morckel et al., 2011).

This technique could be used to investigate the importance of Rho GTPases in the regulation of the actin cytoskeleton in LPM. In Morckel et al. (2011), uncaging of Rockout was done at stages just prior to, or immediately following, the first visual sign of gut looping, and embryos were not analyzed until later stages of gut looping. I propose, therefore, treating embryos with caged Rockout at various, earlier stages following asymmetric *Nodal* expression and analyzing before stage 38. Such manipulations could help determine if and when Rho GTPase signaling has a role in initiating rearrangements of the actin cytoskeleton in the LPM.

Connecting Nodal signaling to changes in LPM architecture

A primary goal of my project here was to learn how Nodal signaling influences the observed tissue architecture asymmetries in the LPM. To determine if Nodal signaling could alter actin cytoskeleton architecture, in experiments performed by Lindsay Marjoram , a *Nodal*-expressing tissue graft was placed in the right LPM of a stage 17 *Xenopus* embryo, and F-actin was subsequently analyzed by labeling with fluorescently conjugated phalloidin at stage 38. Increases in F-actin labeling intensity were detected in the left LPM, to a level equaling that in the right LPM of unmanipulated embryos. Analysis at higher magnification showed that the increase in labeling was reflective of increased F-actin bundling and contraction. Interestingly, no changes in F-actin bundling or contraction were detected on the right LPM, the side receiving the Nodal-producing graft (Marjoram and Wright, unpublished data). It was expected that F-actin characteristics on the right would have mimicked those in the L LPM of an

unmanipulated embryo (that is: diffuse, relaxed) when exposed to *Nodal,* if there was a reversal of the normal situation. These results suggest that actin cytoskeleton dynamics, at least in the L LPM, may be responsive to Nodal signaling. However, the results are preliminary and must be repeated before any instructive role for Nodal signaling in altering actin cytoskeleton dynamics could be deduced.

In the experimental setup used above, endogenous Nodal signaling was still able to occur in the L LPM. A cleaner experiment, in my view, would be to first eliminate Nodal signaling in the LPM by posteriorly cropping of the embryos at stage 17 to remove the first inductive signals from the L-R organizer, and thereby preventing any L-sided *Nodal* expression. A *Nodal* expressing graft could then be placed in the R LPM of these embryos to initiate Nodal signaling only on the right. This manipulation could determine if Nodal signaling instructs F-actin to become more diffuse and not as tightly bundled on the left, compared to the right – that is, the instruction passed by Nodal would be to become more relaxed and not as contracted in cell shape. Alternatively, actin cytoskeleton characteristics could be analyzed in normal, ungrafted embryos that completely lacked asymmetric *Nodal* expression, either as a result of posterior cropping or by treatment with the ALK4/5/7 inhibitor SB505124. It would be expected that, if Nodal signaling affects actin cytoskeleton dynamics, F-actin in the L and R LPM would become equivalent, remaining equally constricted and tightly bundled as seen in the right-sided non-*Nodal*-expressing LPM of normal embryos. However, ectopic Nodal signaling could still fail to alter actin cytoskeleton dynamics on the right, while dynamics on the left respond to loss of Nodal signaling, as was seen in preliminary experiments. This could signify that additional,

unidentified pathways, and which are absent from the right-side LPM, cooperate with Nodal signaling in the L LPM to cause F-actin to become more diffuse and loosely bundled.

Another avenue to investigate is whether or not changes in endoderm architecture (i.e. thickness) or length are major contributors to chiral formation of the gut, and if differences between the left and right endoderm are dependent on Nodal signaling. It has been reported that *Pitx2* overexpression in *Xenopus* causes shortened gut tubes (Muller et al., 2003), suggesting that Pitx2 can slow the rate of gut tube elongation. The changing thickness of the underlying endoderm, which in Xenopus is composed of large yolky cells essentially acting as relatively solid 'blocks' of tissue, may also influence the rate of LPM elongation. Cells in the endoderm undergo radial intercalation as the gut lumen forms, causing the endoderm to lengthen (Chalmers and Slack, 2000). My own Technovit sections of stage 35/36 embryos showed increased thickening of the endoderm on the left compared to the right (Fig. 4.5), an observation that was noted by others (Muller et al. 2003). It is possible that the difference in thickness is due to asymmetry in either the rate of radial intercalation, being faster on the right than the left, or the number of cells that intercalate on the right versus the left. It could be imagined that such asymmetry would cause endoderm on the right to become slightly thinner and more elongated along the A-P axis compared to on the left. The LPM would then have to asymmetrically increase its length, most likely through cell shape changes or spreading, to maintain coverage of the endoderm, resulting in a longer R LPM than L LPM. Differential rates of LPM elongation have already been shown in *Xenopus*, with the R LPM lengthening faster than the L LPM (Muller et al., 2003). Shortened guts in *Pitx2* overexpression embryos and the observation of asymmetries in gut thickness suggest that Nodal signaling may also affect the

endoderm. The gain- and loss-of-function assays used to manipulate actin cytoskeleton dynamics could also be used to determine if Nodal signaling affects the thickness of the endoderm. It may also be possible that Nodal signaling works in parallel with pathways in the endoderm, which function to control intercalation dynamics and/or endoderm thickness, to direct gut looping.

It is thought that the use of differential elongation as part of the mechanism to drive gut looping is not relevant in higher vertebrates because the mouse and chicken gut tube appear symmetric in cross-section (Welsh et al., 2013), and the gut endoderm is not rigidly supported on either side, by LPM, as it is in *Xenopus*. Although there are likely species-specific variations in the mechanisms that control gut looping, and embryonic development as a whole, it is important to continue studies like this one and those investigating Nodal ligand properties in the *Xenopus* model system. Such studies should not be looked at as just providing information about a specific process in *Xenopus*, but should instead be seen as contributing to the overall fundamental understanding of morphogen dynamics and tissue morphogenesis.

Chapter V Future Directions

Determining why Foxh1$^{mEH1/mEH1}$ mice do not have patterning defects

There are three possibilities as for why *Foxh1*$^{mEH1/mEH1}$ mice did not display a phenotype: 1) the Foxh1 transcriptional-switch mechanism is not conserved, 2) the EH1 mutation does not fully disrupt Foxh1-Grg binding, or 3) components of a buffered regulatory system can compensate for loss of Foxh1-Grg–mediated repression. I first wanted to test if the loss of Foxh1-Grg–mediated repression was being compensated for by a buffered regulatory system by reducing

the levels of a presumed major contributor to the system, Lefty2, in the Foxh1$^{mEH1/mEH1}$ background. To do this, I obtained the *Lefty2*$^{\Delta ASE}$ mouse line from Dr. Yukio Saijoh at the University of Utah. The *Lefty2*$^{\Delta ASE}$ allele lacks the asymmetric enhancer (ASE) of Lefty2, thus preventing *Lefty2* expression in the LPM. We chose the *Lefty2*$^{\Delta ASE}$ allele over the *Lefty2* null allele because, unlike the null, it is not embryonic lethal. *Lefty2*$^{-/-}$ embryos die because of gastrulation defects (Meno et al., 1999), preventing analysis of L-R patterning in these embryos. *Lefty2*$^{\Delta ASE/\Delta ASE}$ embryos bypass gastrulation defects because the enhancer responsible for driving *Lefty2* expression at this stage is unaffected by the ASE deletion. *Lefty2*$^{\Delta ASE/+}$ appear phenotypically normal comparable to wild-type mice, while two-thirds of *Lefty2*$^{\Delta ASE/\Delta ASE}$ mice die shortly after birth because of heart defects. The other one-third survives to adulthood with no detectable heart defects (Meno et al., 2001). Breeding *ΔASE* mice to mEH1 would test for a sensitization of the Foxh1$^{mEH1/mEH1}$ background to alterations in Nodal signaling, either in the heterozygous or homozygous condition for *ΔASE.*

So far, however, *Foxh1*$^{mEH1/mEH1}$*;Lefty2*$^{\Delta ASE/+}$ embryos at E15.5 show no defects in organ *situs* or morphology, although because these experiments were begun towards the end of my thesis research period, the number of these embryos is low (n = 2). Because most Nodal signaling mutants display incomplete penetrance or variable expressivity (see Chapter V for further details), more embryos and stages need to be analyzed before conclusions can be drawn. It is possible that *Foxh1*$^{mEH1/mEH1}$ mice may need to crossed to *Lefty2*$^{\Delta ASE/\Delta ASE}$ mice before a mutant phenotype is seen. In this situation, we would look for enhancement of the Lefty2$^{\Delta ASE/\Delta ASE}$ phenotype, which would suggest synergy between the mEH1 mutation and loss of Lefty2. For example, there might be embryonic lethality (*Lefty2*$^{\Delta ASE/\Delta ASE}$ pups die just after birth), fewer

mice might survive to adulthood without defects, and/or there could be an increase in the severity of *situs* defects. If an increase in the severity of the Lefty2$^{\Delta ASE/\Delta ASE}$ phenotype were not observed, the lack of any sensitization in the mEH1 condition could provide even stronger evidence that Foxh1-Grg–mediated repression is not important in regulating Nodal signaling.

It has also been suggested that a *Foxh1* null allele could be introduced into the Foxh1^{mEH1} background (to create Foxh1$^{mEH1/-}$ animals) as another test of a sensitized condition, this time by reducing the level of Grg binding—here we are assuming that the Foxh1-Grg interaction is not fully disrupted in *Foxh1*$^{mEH1/mEH1}$ mice—and reducing the activator functions in the Foxh1^{mEh1} protein. It is uncertain if a null plus EH1 mutation will result in a mutant phenotype, as both *Foxh1*$^{+/-}$ (Hoodless et al., 2001; Yamamoto et al., 2001) and *Foxh1*$^{mEH1/mEH1}$ animals are normal.

In principle, analyzing *Groucho* mutant mice for gastrulation or L-R patterning defects could be a complementary way of addressing the function of Grg-mediated repression in the regulation of Nodal signaling. *Grg4/Tle4* null mice were just recently reported (Wheat et al., 2014). The authors made a conditional *Grg4*^{fl} allele, and inactivated it in all tissues using *β-actin:Cre*. This "global null" had defective hematopoiesis and bone development, but no "obvious organ abnormalities." The Groucho domain (WD-repeats domain) that is largely responsible for Fox or other protein interactions via binding to the EH1 motif is highly conserved (>80% amino-acid sequence identity) among Groucho family members (Jennings and Ish-Horowicz, 2008). Several Grg members are expressed during gastrulation and L-R patterning when Nodal signaling is active, raising the possibility that Grg proteins function redundantly and that no Nodal signaling

defects would exist in single *Grg* knockouts. To my knowledge, *Grg* double, triple, or quadruple knockouts have not been reported.

Epigenetic control of Nodal transcription

Recent work has begun to uncover the type of epigenetic marks that exist at the *Nodal* locus in embryonic stem cells (ESCs; mouse and human) and how such marking compares to those in differentiated lineages such as endoderm. However, very little is known about the epigenetic markings at the *Nodal* locus in the embryo during A-P axis formation, gastrulation and L-R patterning. Identifying the types of active and repressive marks at the *Nodal* locus at various developmental stages could provide deeper insight into how *Nodal* expression is spatiotemporally regulated in such a dynamic fashion. Analyzing the epigenetic marking could also serve as another way to investigate whether or not Foxh1-Grg–mediated repression has a role in regulating *Nodal* transcription. Below, I focus only on describing experiments that will help identify the types of active and repressive marks associated with the *Nodal* locus ASE, as the *Nodal* enhancer is bound by Foxh1.

To facilitate such an investigation, I obtained a fluorescent reporter of Foxh1-dependent Nodal signaling, which was generated in the lab of Jérôme Collignon (Université Paris-Diderot, France). The reporter consists of the *Nodal* ASE sequence linked to a destabilized eYFP (Granier et al., 2011), and ASE activation causes *YFP* expression (Fig. 6.2). Because *Nodal*, *Lefty2*, and *Pitx2* all have an ASE, YFP will be produced in a cell when any of these three genes are transcribed, therefore, the transgene represents Nodal signaling as a whole, and is not just a read out of *Nodal* transcription. This is exemplified by symmetrical *YFP* expression in the head

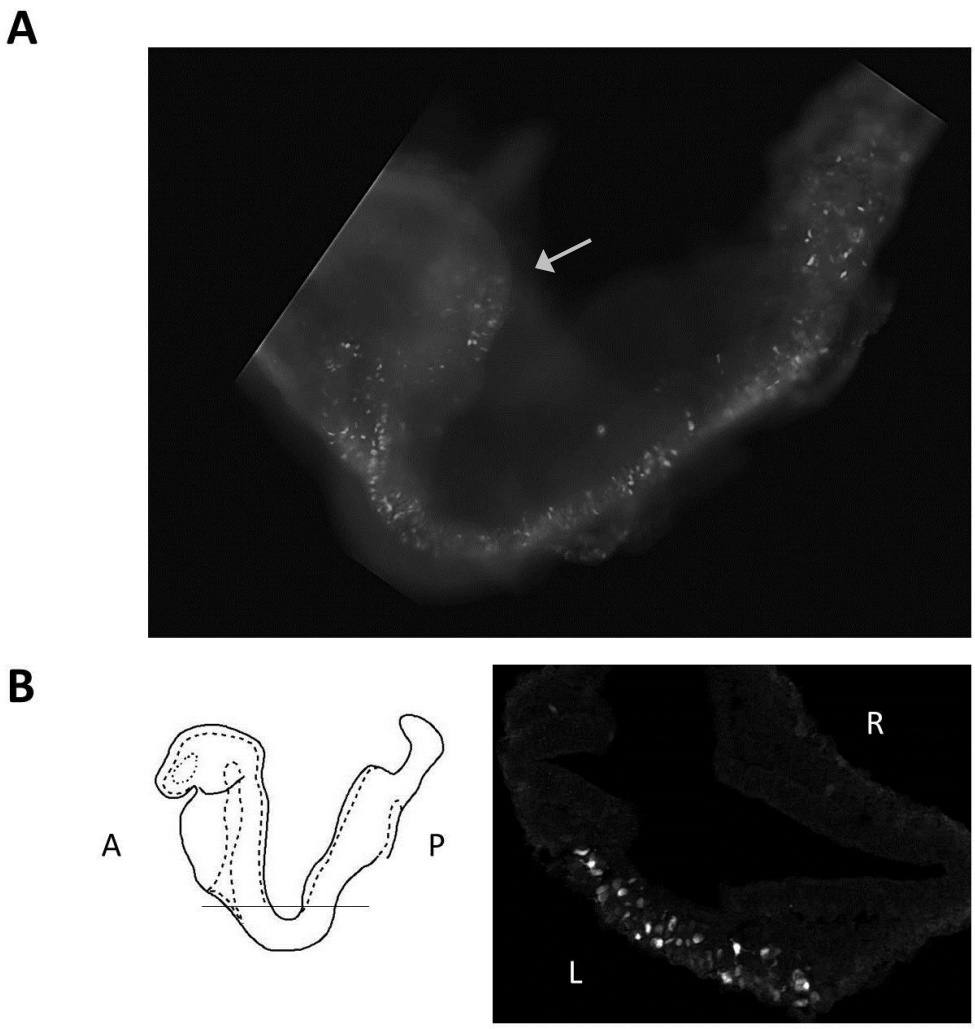

Fig. 6.2 ***ASE-YFP*** **transgene expression in E8.25 embryos.** (A) Immunolabeling for YFP in a whole-mount E8.25 embryo. YFP localization is seen in the L LPM and the head fold (arrow). (B) Schematic shows sectional plane (line) of the cryosection to the left. YFP localizes to the L LPM and not the R LPM. (A) Left lateral view. A, anterior; L, left; P, posterior; R, right.

mesenchyme, where symmetrical P*itx2* expression is observed (Ryan et al., 1998). With this tool, cells actively undergoing Nodal signaling (YFP^+) can be separated from non-signaling cells (YFP^-) by flow sorting of cells from mouse embryonic tissues dissected during stages of Nodal signaling (i.e. E5.5-7.25, E8.25). Wild-type YFP^+ and YFP^- populations, as well as $Foxh1^{mEH1/mEH1}$ YFP^+ populations, would then be analyzed via chromatin immunoprecipitation (ChIP) to determine the types of active or repressive marks on the ASE, and results compared between various tissues. If both wild-type and $Foxh1^{mEH1/mEH1}$ YFP^+ populations share the same epigenetic markings, it could imply the Foxh1-Grg–mediated repression is not disrupted in mEH1 mutant embryos, or that it is not a conserved regulator of the epigenetic state of the *Nodal* locus in mouse. If different markings were to be observed between the two cell populations, we would have evidence that the Foxh1-Grg interaction is disrupted, but is functionally compensated for by a component of the buffered regulatory system. For example, the buffered system could offset the loss of epigenetic repression at the *Nodal* locus by inhibiting nuclear translocation of the co-activator pSmad2. These analyses could be extended to *Lefty2* and *Pitx2* to determine if Foxh1-Grg–mediated repression is involved in their epigenetic regulation.

Infertility and thymus growth defects in $Foxh1^{mEH1/mEH1}$ mice

Although defects in embryogenesis were not detected in $Foxh1^{mEH1/mEH1}$ mice, some adult mice displayed abnormalities not seen in $Foxh1^{F/F}$ control ("F" refers to FLAG tag) or wild-type animals. For example, $Foxh1^{mEH1/mEH1}$ males homozygous for the *ASE-YFP* transgene ($Foxh1^{mEH1/mEH1}$;*ASE-YFP/ASE-YFP*) are presumed infertile. Because the genomic insertion site of

the *ASE-YFP* transgene has not been mapped, locus specific primers cannot be designed and transgene homozygosity is determined by crossing the mouse in question with a wild-type mate. If all pups from this cross have the *ASE-YFP* transgene, the non-wild-type parent can be considered transgene-homozygous. A total of four *Foxh1*$^{mEH1/mEH1}$ males carrying the transgene have been tested for transgene homozygosity. *Foxh1*$^{mEH1/mEH1}$ male mice carrying the transgene always produce offspring with and without the transgene (n = 2/2; each male mated at least four times), indicating that these males are heterozygous for the transgene. Therefore, I am proposing that the infertile *Foxh1*$^{mEH1/mEH1}$ mutant male mice carrying the *ASE-YFP* transgene are transgene-homozygous (n = 2/2; one mated twice, the other mated six times without impregnating females). Males of the following genotypes are all fertile: *Foxh1*$^{mEH1/mEH1}$, *Foxh1*$^{mEH1/+}$;*ASE-YFP/ASE-YFP*, *Foxh1*$^{mEH1/mEH1}$;*ASE-YFP*/+, *Foxh1*$^{+}$/*Foxh1*$^{+}$;*ASE-YFP/ASE-YFP*, *Foxh1*$^{F/F}$, and *Foxh1*$^{F/F}$;*ASE-YFP*/*ASE-YFP*. Nodal was recently discovered to regulate germ-cell potency during testis development (Spiller et al., 2012), as reviewed in the introduction to this thesis (Chapter I). It is possible that the *ASE-YFP* transgene insertion disrupts a gene that synergizes with the *Foxh1*^{mEH1} mutation to disrupt specification of male germ cells. Male germ-cell development will need to be analyzed in these embryos. To date, no other defects have been identified in the presumed *Foxh1*$^{mEH1/mEH1}$*;ASE-YFP/ASE-YFP* males. The fertility of *Foxh1*$^{mEH1/mEH1}$*;ASE-YFP/ASE-YFP* females has not yet been studied in detail. If *Foxh1*$^{mEH1/mEH1}$*;ASE-YFP/ASE-YFP* male infertility arises from disruption of germ-cell maturation, females should be unaffected, as Nodal signaling occurs only in the XY germline (Spiller et al., 2012).

Some *Foxh1*$^{mEH1/mEH1}$ mice have died prematurely from a very enlarged thymus. Prior to death or euthanasia, mice presented with weight loss, ruffled fur, and labored breathing. In total, six *Foxh1*$^{mEH1/mEH1}$ mice died between 2-4 months of age. Three mice were autopsied and found to have a grossly enlarged thymus that completely eclipsed the lungs and heart (Fig. 6.3A), with cause of death likely being internal strangulation from the thymus occupying most of the chest cavity, restricting lung inflation. In healthy animals of this age, the thymus is a bilobed organ positioned just anterior of the heart, typically only obscuring the aortic arch. One of the enlarged thymi, along with the attached heart and lungs, was collected for histological analysis. The enlarged thymus did not have morphologically defined lobes, and hematoxylin and eosin staining on a small portion of this tissue did not detect the expected distinct tissue architecture of capsule, medulla, and cortex. Instead, the tissue was composed of fairly homogeneous fields of small, rounded cells with little cytoplasm (Fig. 6.3B).

We currently think that the enlarged thymi represent tumors of some sort, although the analysis is still ongoing. We first tested if the tissue was a thymoma derived from thymic epithelium, but none of the 'overgrown tissue' was positive for any markers of the thymic epithelium, such as CD205 and keratin-14 (Fig. 6.3C). We sent paraffin and cryosections of the enlarged thymus to Nancy Manley (University of Georgia, Athens), an expert in parathyroid and thymus development, to further analyze this tissue. Her lab is in the process of immunolabeling for additional informative proteins such as CD45 (marking all hematopoietically derived cells), Ikaros (lymphocytes), CD4 (helper T cells), CD8 (cytotoxic T cells), PDGFRa (capsule), and CD31 (vasculature).

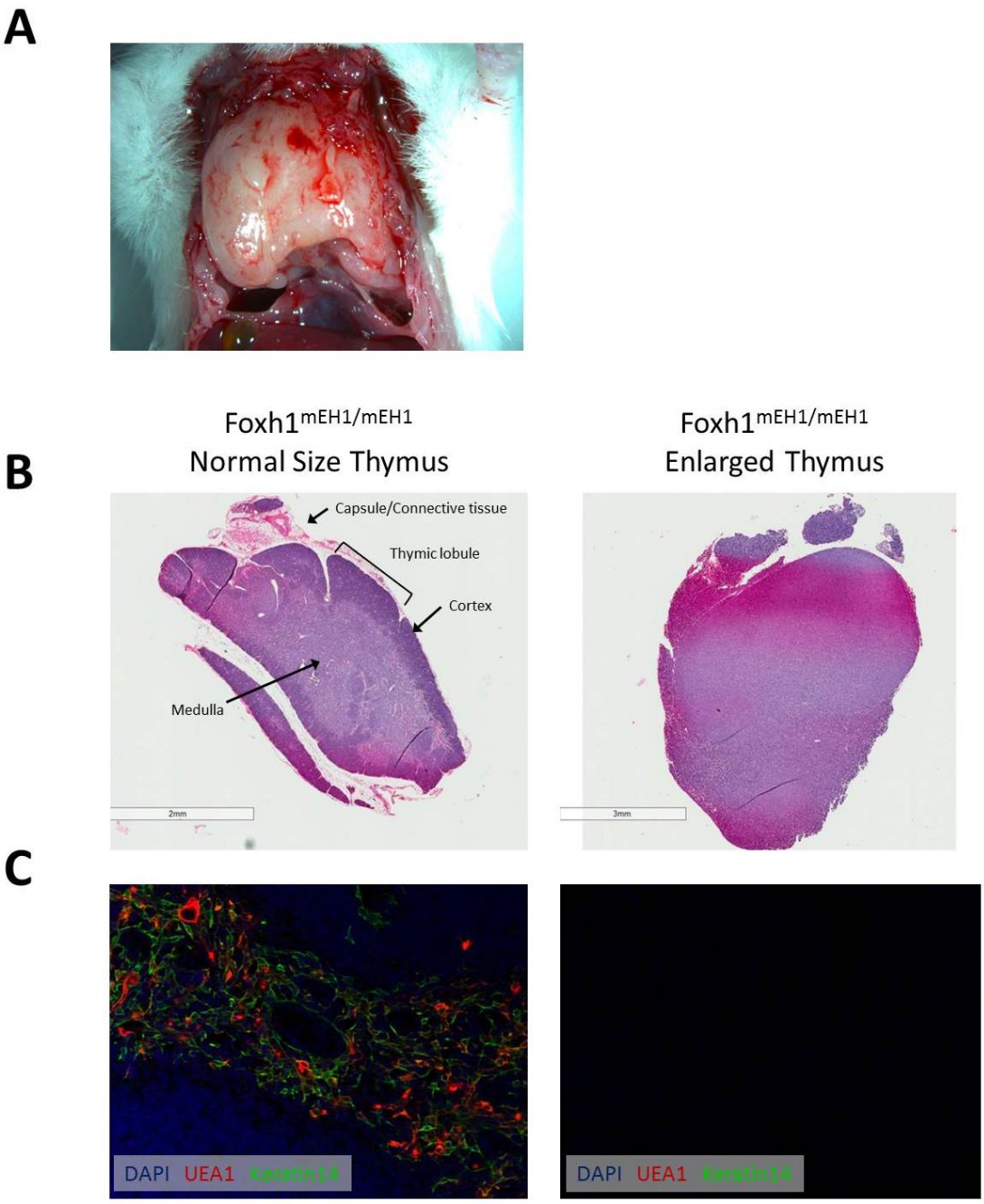

Fig. 6.3 ***Foxh1*$^{mEH1/mEH1}$ mice have enlarged thymi.** (A) Enlarged thymus in a female *Foxh1*$^{mEH1/mEH1}$ mouse. The thymus completely eclipses the heart and lungs, which are normally visible in a wild-type mouse. (B) H&E staining on paraffin sections of a normal-sized thymus from a *Foxh1*$^{mEH1/mEH1}$ mouse and a piece of the enlarged thymus. Typical thymic architecture is lost in the enlarged thymus (staining by Jeff Duryea). (C) Immunostaining for UEA1 (endothelial cells) and Keratin14 (thymic epithelium). The normal-sized thymus stains with both markers, while tissue from the enlarged thymus does not (staining by Caroline Wiser). This suggests that the enlarged thymus is not a thymoma, a tumor originating from the thymic epithelial cells.

A thymoma is just one example of thymic neoplasia. Hyperplasia, thymic carcinoma, thymolipoma, and lymphomas can all present with an enlarged thymus. True thymic hyperplasia is an increase in the size of the thymus, but the overall structure is preserved (Strollo et al., 1999). The enlarged mutant thymus is most likely not hyperplasia, as the structural organization of the thymus is lost. It is also most likely not thymolipoma, which is a slow-growing benign neoplasm that is encapsulated and contains adipose tissue (Strollo et al., 1999). Hematoxylin and eosin staining did not detect adipose tissue in sections of the enlarged mutant thymus. Thymic carcinoma arises from the epithelium of the thymus and outwardly resembles a thymoma. However, like the enlarged mutant thymus, a carcinoma is not encapsulated, and it is identified by the absence of normal histologic and immunohistochemical characteristics of thymic epithelial cells (Goldstein et al., 2014; Strollo et al., 1999). It is also possible that the enlargement of the thymus is due to a lymphoma. Primary mediastinal large B-cell lymphoma typically occurs in young adult females. It is thought to arise from thymic medullary B cells, which present as large-to-medium cells with indistinct borders. The thymus is also not encapsulated in this condition. Another lymphoma, lymphoblastic lymphoma, is unencapsulated and contains small immature lymphoblastic T cells. This condition is more common in males.

Based on these histological and morphological descriptions, the enlarged thymi from Foxh1$^{mEH1/mEH1}$ mice most resemble thymic carcinoma or lymphoma. The additional immunohistochemical analyses being performed by Dr. Manley's lab will help determine if the cells comprising the enlarged thymus are T or B cells. However, from the initial hematoxylin and eosin analysis, these cells appear small with little cytoplasm, suggesting that these cells

may be T cells. Also, several of these thymic neoplasms (i.e. carcinoma and lymphoma) result in metastases to other organs like the lungs (Strollo et al., 1999). Therefore, it could be useful to analyze the lungs from the Foxh1 mutant animal for metastatic lesions (lungs were collected with the enlarged thymus). This will help determine if the thymic growth is cancerous or benign, and potentially pinpoint a condition.

So far, only the *Foxh1*$^{mEH1/mEH1}$ females have been found with an enlarged thymus. It is not known if this correlation is significant, or coincidental because my mouse colony has many more females than males. Of the three mice autopsied, two were siblings and the third from a distinct litter had a sibling that died around 2-3 months of age, but was not autopsied. Two additional *Foxh1*$^{mEH1/mEH1}$ females, both siblings in another litter, died unexpectedly at 3-4 months of age, but were quickly disposed of by Division of Animal Care technicians, preventing analysis. Although the enlarged thymus phenotype could therefore have potentially occurred in only six mice so far, I have not witnessed any unexpected deaths at these ages (2-4 months) in *Foxh1*$^{F/F}$ mice, or any other genotype in my mouse colony, which carried an average of 45 cages for the past three years. The appearance of this phenotype in siblings suggests some form of genetic underpinning. Its absence in *Foxh1*$^{F/F}$ mice, which have essentially the same mixed background as *Foxh1*$^{mEH1/mEH1}$ mice, suggests that the phenotype is specifically coupled to their *Foxh1*$^{mEH1/mEH1}$ status.

To my knowledge, Nodal signaling has not been implicated in thymus development. Other members of the TGF-β superfamily, primarily the TGF-β ligands themselves, are thought to have important roles in differentiation and proliferation of T-cells (reviewed in Licona-Limón and

Soldevila, 2007). In addition, expression of Activin, ALK4, Smad2, Smad3, and Smad4 has been described in the developing thymus and in thymocytes from adult mice (Licona et al., 2006), but much work is still needed to elucidate the function of Activin signaling in the thymus. It is possible that Nodal has a yet-unidentified function in the thymus, or that Foxh1 functions independently of Nodal, perhaps within the highly related Activin-signaling pathway. The potential role for Grg proteins in thymus development/homeostasis is also still emerging. The recent characterization of *Grg4*$^{-/-}$ mice revealed thymic atrophy and a reduced number of lymphocytes (Wheat et al., 2014). This phenotype differs from what is seen in *Foxh1*$^{mEH1/mEH1}$ mice (atrophy vs. enlargement). It is possible that multiple Grg co-repressors are involved in thymus development and that they function in different pathways. Therefore, Foxh1 may be interacting with Grgs other than Grg4 in the thymus (mEH1 mutation should disrupt binding with all Grg proteins). A primary level of analysis would include *in situ* hybridization analysis on sections of the enlarged thymus to determine if *Foxh1* and Nodal circuit members (*Nodal*, *Lefty2*, and *Pitx2*) are expressed in comparison to wild-type thymus.

Also, it is plausible that mutations in additional genes in the Foxh1$^{mEH1/mEH1}$ background are contributing to the enlarged thymus phenotype. Since only 2-3% of Foxh1$^{mEH1/mEH1}$ mice have this defect, the gene(s) may act as a modifier of Foxh1/Nodal signaling function, or could even function independent of Foxh1. Whole exome sequencing could be used to determine if and what other genetic lesions exist in enlarged Foxh1$^{mEH1/mEH1}$ thymi, in addition to the EH1 mutation, compared to wild-type thymi. Comparison to Foxh1$^{F/F}$ thymi may also be beneficial in determining if additional point mutations were introduced into the genome during RMCE in ESCs, prior to the generation of chimeras.

It is interesting to speculate as to why *Foxh1*$^{mEH1/mEH1}$ mice have thymus defects and apparently infertility issues, but not in A-P axis formation, gastrulation, or L-R patterning. It is possible that Nodal signaling may not be as heavily buffered in these tissues as it is in embryonic tissue patterning and body axis formation. For example, in metastatic melanoma cells, *Lefty2* is not expressed, and Nodal signaling goes unchecked (reviewed in Strizzi et al., 2012). Therefore, the loss of Foxh1-Grg–mediated repression may be less easily compensated for in the thymus and male germline.

Characterization of novel Foxh1 hypomorphs

During my analysis of *Foxh1*$^{mEH1/mEH1}$ mice, we discovered that one *Foxh1*$^{mEH1/mEH1}$ embryo still carrying the hygromycin^{R} (hygro^{R}) cassette (Foxh1$^{mEH1+hygro/mEH1+hygro}$) displayed bilateral *Nodal* expression at E8.25 (Fig. 6.4A,B). Further analysis revealed that *Foxh1*$^{mEH1+hygro/mEH1+hygro}$ embryos and those homozygous for the wild-type *Foxh1*^{F} allele but still containing a hygro^{R} cassette (Foxh1$^{F+hygro/F+hygro}$), phenotypically resembled the least severe phenotype observed in *Foxh1*$^{-/-}$ embryos at E9.5 (Hoodless et al., 2001; Yamamoto et al., 2001). These embryos had underdeveloped anterior structures, fused heads, enlarged pericardiums, and delayed turning (n = 3/3 of Foxh1$^{F+hygro/F+hygro}$ embryos; n = 3/4 Foxh1$^{mEH1+hygro/mEH1+hygro}$ embryos) (Fig 6.4C-E). Because one *Foxh1* mutant hygro^{R}-containing embryo appeared morphologically normal at E9.5, I analyzed embryo morphology at E15.5 to determine how late into development these embryos could survive and if they exhibited abnormal L-R asymmetry. The single Foxh1$^{mEH1+hygro/mEH1+hygro}$ embryo recovered at this stage was reabsorbing and the single Foxh1$^{F+hygro/F+hygro}$ embryo was severely holoprosencephalic, with a large ‘proboscis’ and a single

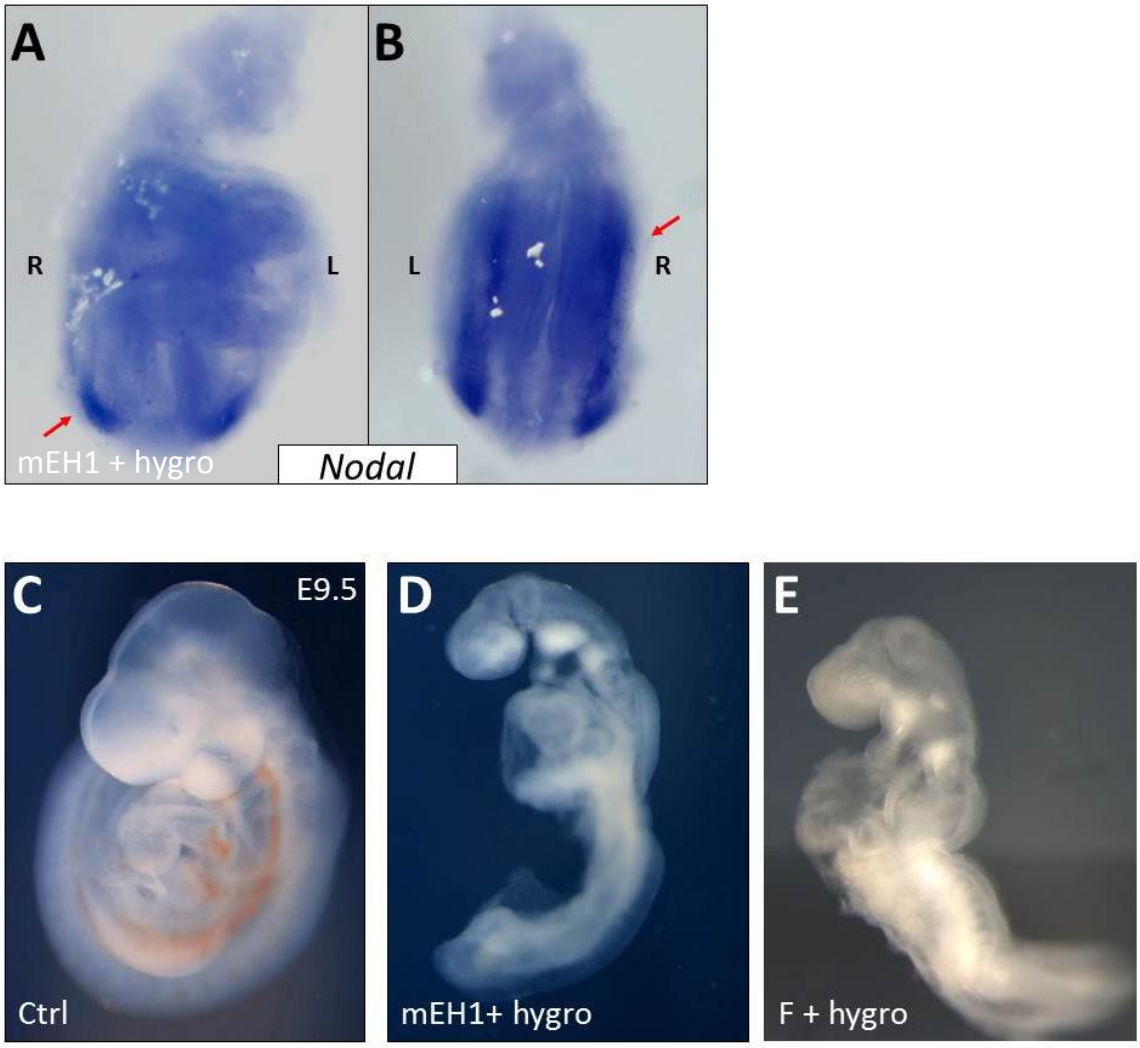

Fig. 6.4 Insertion of hygromycin^{R} cassette in *Foxh1* locus disrupts embryonic development. (A,B) *Nodal* expression in a *Foxh1*$^{mEH1+hygro/mEH1+hygro}$ E8.25 embryo. Ectopic R-sided expression is seen within the R LPM (red arrows). (C-E) E9.5 morphology of a (C) wild-type embryo, (D) *Foxh1*$^{mEH1+hygro/mEH1+hygro}$ embryo, and a (E) *Foxh1*$^{F+hygro/F+hygro}$ embryos. Mutant embryos display underdeveloped anterior structure and delayed turning, among other defects. (A) anterior view; (B) posterior view; (C-D) left lateral views. L, left; R, right.

eye field directly below it (Fig 6.5A). Further analysis of this embryo revealed right pulmonary isomerism and an abnormal heart (Fig. 6.5B-D). No animal homozygous for the *Foxh1*$^{mEH1+hygro}$ or *Foxh1*$^{F+hygro}$ allele has been born; therefore, it is assumed that these alleles cause embryonic lethality.

These defects, as well as those seen at stage E9.5, are classic indicators of decreased levels of Nodal signaling. However, the bilateral *Nodal* expression seen in one of the E8.25 embryos (n = 1/1) can be attributed to increased Nodal signaling associated with the loss of inhibitors (i.e.*Lefty1*$^{-/-}$), defects in the midline thereby allowing right-sided development of *Nodal* expression, or defects in cilia-based flow at the node, which can randomize or cause bilaterally symmetric *Nodal* expression. Despite the low number of cases so far analyzed, taking the results together, however, is somewhat suggestive of defects in Nodal signaling during gastrulation, which affect the patterning of the anterior primitive streak and its derivatives such as the node and prechordal plate. The lack of proper specification of these tissues then affects L-R patterning. Cyclopia, which is most commonly associated with defects in Shh signaling, could be caused by reduced and abnormal specification of the prechordal plate and midline tissues where *Shh* is normally expressed during development (for a review of holoprosencephaly mouse models, see Hayhurst and McConnell, 2003). Additional sectional and *in situ* hybridization analyses of *Shh* in E8.25 embryos will be needed to determine the cause of holoprosencephaly in the *Foxh1* hygro^{R}-containing hypomorphs.

The presence of the hygro^{R} cassette upstream of the *Foxh1* transcriptional start site likely creates a fairly strong hypomorphic allele with reduced capacity to activate downstream target

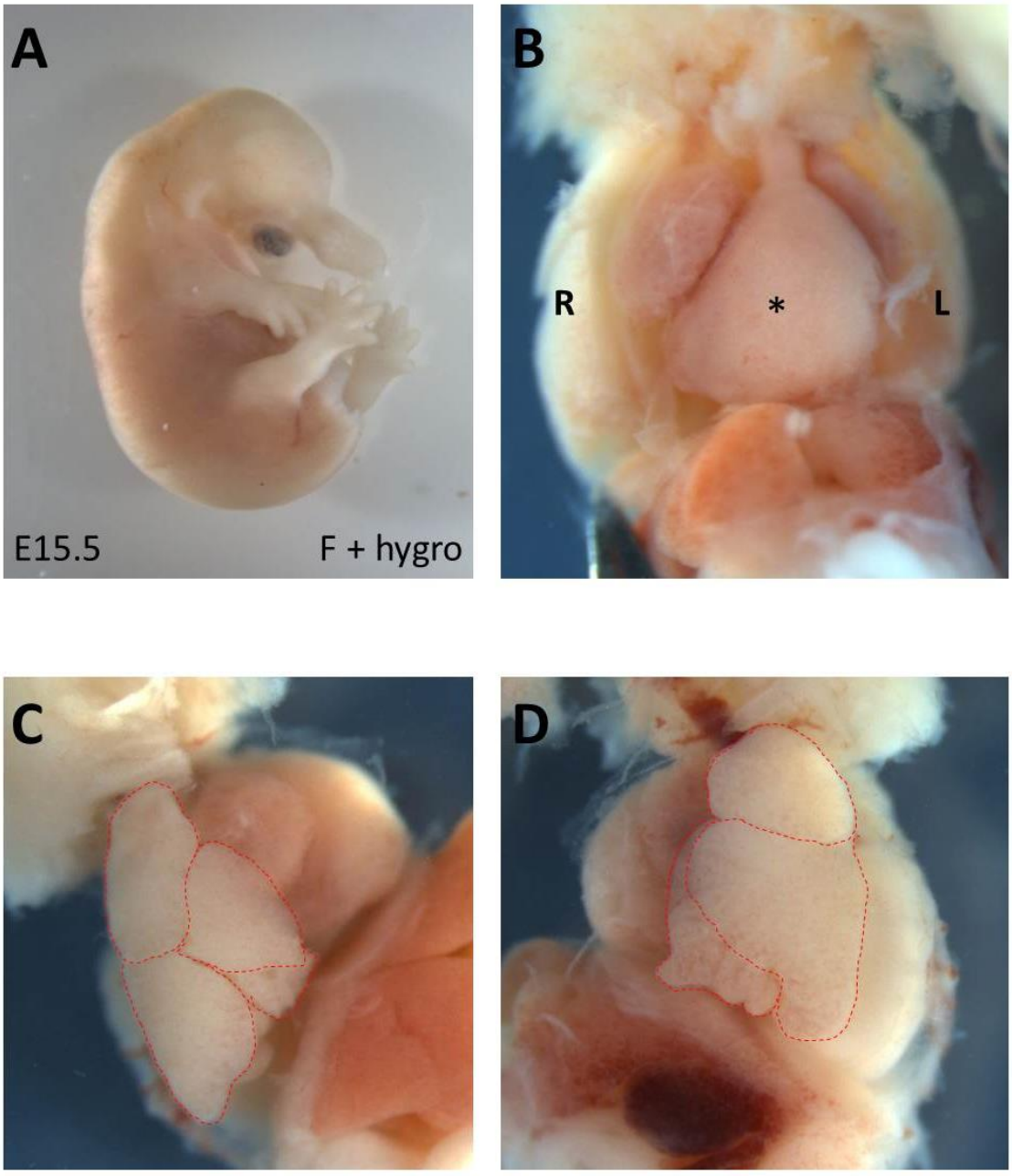

Fig. 6.5 *Foxh1*$^{F+hygro/F+hygro}$ E15.5 embryo displays holoprosencephaly and *situs* defects. (A) Left lateral view of a *Foxh1*$^{F+hygro/F+hygro}$ embryo with severe holoprosencephaly. A presumed single eye field is located directly below a large proboscis. (B-D) This embryo also had (B) abnormal positioning and morphology of the heart (asterisk), in addition to (C,D) right pulmonary isomerism. (C) The right lung has four lobes as usual, but the (D) left lung had multiple lobes, at least three could be distinguished. A left, wild-type lung has one lobe. Red dashed lines outline the individual lobes.

genes of Nodal signaling (i.e. *Nodal*, *Lefty2*, *Pitx2*). My preliminary *in situ* hybridization analysis detected lower *Foxh1* expression levels in E8.0 *Foxh1*$^{mEH1+hygro/mEH1+hygro}$ embryos compared to heterozygotes or wild-type embryos of the same stage. This result needs to be confirmed with qRT-PCR to quantify the degree of reduction. Expression levels of *Nodal* and its downstream targets in embryos homozygous for the *Foxh1*^{mEH1} and *Foxh1*^{F} hypomorphic alleles would also need to be determined.

We are currently testing if partial release of genetic repression—that there could be a "more positively functioning" Foxh1 when it carries the EH1 mutation—can partially compensate for a reduced level of *Foxh1* expression from the *Foxh1*^{mEH1} *hygro*^{R}-containing hypomorphic allele. In this situation, Nodal signaling levels might be restored and lead to a less severe phenotype compared to the *Foxh1*^{F} *hygro*^{R}-containing hypomorphic allele. This comparison would require precise measurement of Nodal circuit gene levels by qRT-PCR. To my knowledge, very little is known about the regulation of *Foxh1* expression, and further investigation would be needed to determine how the hygro^{R} cassette causes the hypomorphic condition, perhaps by disrupting a currently unidentified *cis*-regulatory region (interestingly, this region is not conserved among vertebrates), or interfering with more fundamental aspects of the transcriptional machinery (Fig. 6.6). Analysis of promoter occupancy by components of the transcriptional-initiation complex, or determining the location of important *cis*-regulatory elements could distinguish between these two scenarios.

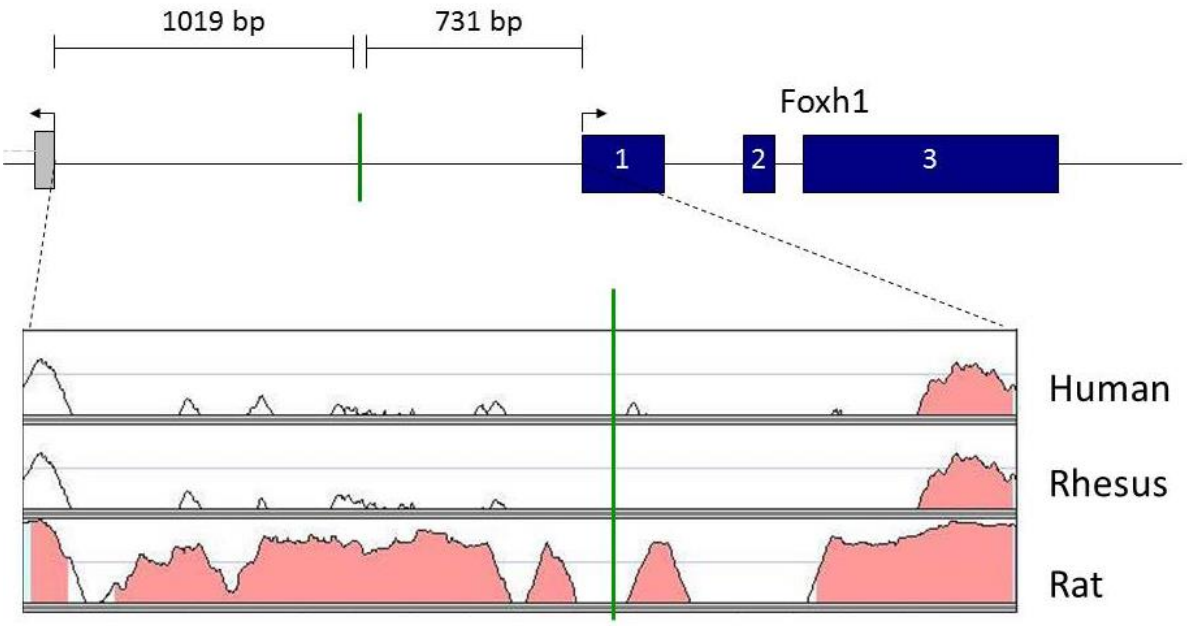

Fig. 6.6 Hygromycin^R cassette inserted into non-conserved region of *Foxh1* locus. Genomic region between the transcriptional start sites of *Foxh1* and its 5' neighboring gene (gray box) is shown in multiple species. Pink shading represents conserved non-coding regions between mouse and the species shown. The green line is the insertion site of the hygro^R cassette.

REFERENCES

Adachi, H., Saijoh, Y., Mochida, K., Ohishi, S., Hashiguchi, H., Hirao, A. and Hamada, H. (1999). Determination of left/right asymmetric expression of Nodal by a left side-specific enhancer with sequence similarity to a Lefty-2 enhancer. Genes Dev. 13, 1589-1600.

Agius, E., Oelgeschläger, M., Wessely, O., Kemp, C. and De Robertis, E. M. (2000). Endodermal Nodal-related signals and mesoderm induction in *Xenopus*. Development 127, 1173-1183.

Arai, D., Katsura, H., Shindo, N., Matsumoto, M. and Higashinakagawa, T. (2010). Polycomb group protein Ezh1 represses *Nodal* and maintains the left-right axis. Dev. Biol. 341, 459-463.

Arnold, S. J. and Robertson, E. J. (2009). Making a commitment: cell lineage allocation and axis patterning in the early mouse embryo. Nat. Rev. Mol. Cell Biol. 10, 91-103.

Attisano, L., Silvestri, C., Izzi, L. and Labbé, E. (2001). The transcriptional role of Smads and FAST (FoxH1) in TGFβ and Activin signaling. Mol. Cell. Endocrinol. 180, 3-11.

Attisano, L. and Wrana, J. L. (2002). Signal transduction by the TGF-beta superfamily. Science. 296, 1646-1647.

Attisano, L. and Wrana, J. L. (2000). Smads as transcriptional co-modulators. Curr. Opin. Cell Biol. 12, 235-243.

Aw, S., Koster, J. C., Pearson, W., Nichols, C. G., Shi, N. Q., Carneiro, K. and Levin, M. (2010). The ATP-sensitive K+-channel (KATP) controls early left–right patterning in Xenopus and chick embryos. Dev. Biol. 346, 39-53.

Belo, J. A., Bouwmeester, T., Leyns, L., Kertesz, N., Gallo, M., Follettie, M. and De Robertis, E. M. (1997). *Cerberus-like* is a secreted factor with neutralizing activity expressed in the anterior primitive endoderm of the mouse gastrula. Mech. Develop. 68, 45-57.

Beyer,T., Thumberger,T., Schweickert,A.,Blum,M. (2012). Connexin26-mediated transfer of laterality cues in Xenopus. Biol Open 1, 473–481.

Bisgrove, B. W. and Yost, H. J. (2001). Classification of left-right patterning defects in zebrafish, mice, and humans. Am. J. Med. Genet. 101, 315-323.

Blitz I. L., Biesinger J., Xie X. and Cho K. W. (2013). Biallelic genome modification in F0 Xenopus tropicalis embryos using the CRISPR/Cas system. Genesis 51, 827-834.

Bourillot, P.Y., Garrett, N., and Gurdon, J.B. (2002). A changing morphogen gradient is interpreted by continuous transduction flow. Development 129, 2167-2180.

Bray, S. and Furriols, M. (2001). Notch pathway: Making sense of Suppressor of Hairless. Curr. Biol. 11, R217-R221.

Brennan, J., Lu, C. C., Norris D. P., Rodriguez, T. A., Beddington, R. S. and Robertson, E. J. (2001). Nodal signalling in the epiblast patterns the early mouse embryo. Nature 411, 965-969.

Campione, M., Steinbeisser, H., Schweickert, A., Deissler, K., van Bebber, F., Lowe, L.A., Nowotschin, S., Viebahn, C., Haffter, P., Kuehn, M.R., and Blum, M. (1999). The homeobox gene *Pitx2*: mediator of asymmetric left-right signaling in vertebrate heart and gut looping. Development 126, 1225-1234.

Carneiro, K., Donnet, C., Rejtar, T., Karger, B. L., Barisone, G. A., Díaz, E., Kortagere, S., Lemire, J. M. and Levin, M. (2011). Histone deacetylase activity is necessary for left-right patterning during vertebrate development. BMC Dev. Biol. 11, 1-19.

Cha, Y. R., Takahashi, S. and Wright, C. V. (2006). Cooperative non-cell and cell autonomous regulation of Nodal gene expression and signaling by Lefty/Antivin and Brachyury in Xenopus. Dev. Biol. 290, 246-264.

Chalmers, A. D. and Slack, J. M. (2000). The Xenopus tadpole gut: fate maps and morphogenetic movements. Development 127, 381-392.

Chalmers, A. D. and Slack, J. M. (1998). Development of the gut in Xenopus laevis. Dev. Dyn. 212, 509-521.

Chen, G. and Courey, A. J. (2000). Groucho/TLE family proteins and transcriptional repression. Gene 249, 1-16.

Chen, C. and Shen, M. M. (2004). Two modes by which Lefty proteins inhibit Nodal signaling. Curr. Biol. 14, 618-624.

Chen, X., Rubock, M. J., and Whitman, M. (1996). A transcriptional partner for MAD proteins in TGF-β signaling. Nature 383, 691-696.

Chen, X., Weisberg, E., Fridmacher, V., Watanabe, M., Naco, G. and Whitman, M. (1997). Smad4 and FAST-1 in the assembly of activin-responsive factor. Nature 389, 85-89.

Cheng, A. M., Thisse, B., Thisse, C. and Wright, C. V. (2000). The lefty-related factor Xatv acts as a feedback inhibitor of nodal signaling in mesoderm induction and L-R axis development in Xenopus. Development 127, 1049-1064.

Cinnamon, E. and Paroush, Z. (2008). Context-dependent regulation of Groucho/TLE-mediated repression. Curr. Opin. Genet. Dev. 18, 435-440.

Collignon, J., Varlet, I. and Robertson, E. J. (1996). Relationship between asymmetric *nodal* expression and the direction of embryonic turning. Nature 381, 155-158.

Conlon, F. L., Barth, K. S. and Robertson E. J. (1991). A novel retrovirally induced embryonic lethal mutation in the mouse: assessment of the developmental fate of embryonic stem cells homozygous for the 413.d proviral integration. Development 111, 969-981.

Conlon, F. L., Lyons, K. M., Takaesu, N., Barth, K. S., Kispert, A., Herrmann, B. and Robertson, E. J. (1994). A primary requirement for *nodal* in the formation and maintenance of the primitive streak in the mouse. Development 120, 1919-1928.

Constam, D. B. and Robertson, E. J. (2000). SPC4/PACE4 regulates a TGFb signaling network during axis formation. Genes Dev. 14, 1146-1155.

Dahle, Ø., Kumar, A. and Kuehn, M. R. (2010). Nodal signaling recruits the histone demethylase Jmjd3 to counteract Polycomb-mediated repression at target genes. Sci. Signal. 3, 1-8.

Daniels, D. L. and Weis, W. I. (2005). β-catenin directly displaces Groucho/TLE repressors from Tcf/Lef in Wnt-mediated transcription activation. Nat. Struct. Mol. Biol. 12, 364-371.

Davis, N.M., Kurpios, N.A., Sun, X., Gros, J., Martin, J.F., and Tabin, C.J. (2008). The chirality of gut rotation derives from left-right asymmetric changes in the architecture of the dorsal mesentery. Dev. Cell 15, 134-145.

Datto, M. B., Frederick, J. P., Pan, L., Borton, A. J., Zhuang, Y. and Wang, X. F. (1999). Targeted Disruption of Smad3 Reveals an Essential Role in Transforming Growth Factor beta-Mediated Signal Transduction. Mol. Cell Biol. 19, 2495-2504.

Deimling, S. J. and Drysdale, T. A. (2011). Fgf is required to regulate anterior-posterior patterning in the Xenopus lateral plate mesoderm. Mech. Dev. 128, 327-341.

DeRobertis, E. M., Larrain, J., Oelgeschläger, M. and Wessely, O. (200) The establishment of Spemann's organizer and patterning of the vertebrate embryo. Nat. Rev. Genet. 1, 171-181.

Derynck, R. and Miyazono, K. (2008). TGF-β and the TGF-β family. In *The TGF*-β *Family* (ed. R. Derynck and K. Miyazono), pp. 29-43. Cold Spring Harbor, NY: Cold Spring Harbor Laboratory Press.

de Sousa Lopes, S. M., Carvalho, R. L., van den Driesche, S., Goumans, M. J., ten Dijke, P. and Mummery, C. L. (2003). Distribution of phosphorylated Smad2 identifies target tissues of TGF beta ligands in mouse development. Gene Expr. Patterns 3, 355-360.

Di Guglielmo, G.M., Le Roy, C., Goodfellow, A. F. and Wrana, J. L. (2003). Distinct endocytic pathways regulate TGF-beta receptor signaling and turnover. Nat. Cell Biol. 5, 410-421.

Ding, J., Yang, L., Yan, Y., Chen, A., Desai, N., Wynshaw-Boris, A. and Shen, M. M. (1998). *Cripto* is required for correct orientation of the anterior–posterior axis in the mouse embryo. Nature 395, 702-707.

Downs, K. M. and Davies, T. (1993). Staging of gastrulating mouse embryos by morphological landmarks in the dissecting microscope. Development 118, 1255-1266.

Dyson, S. and Gurdon, J.B. (1998). The interpretation of position in a morphogen gradient as revealed by occupancy of activin receptors. Cell 93, 557-568.

Erter, C. E., Solnica-Krezel, L. and Wright, C. V. (1998). Zebrafish nodal-related 2 encodes an early mesendodermal inducer signaling from the extraembryonic yolk syncytial layer. Dev Biol 204, 361–372.

Faure, S., Lee, M.A., Keller, T., ten Dijke, P., and Whitman, M. (2000). Endogenous patterns of TGFβ superfamily signaling during early *Xenopus* development. Development 127, 2917-2931.

Fukumoto, T. Kema, I. P. and Levin, M. (2005). Serotonin Signaling Is a Very Early Step in Patterning of the Left-Right Axis in Chick and Frog Embryos. Cur. Biol. 15, 794-803.

Gage, P. J., Suh, H. and Camper, S. A. (1999). Dosage requirement of *Pitx2* for development of multiple organs. Development 126, 4643-4651.

Gaio, U., Schweickert, A., Fischer, A., Garratt, A. N., Müller, T., Ozcelik, C., Lankes, W., Strehle, M., Britsch, S., Blum, M. and Birchmeier, C. (1999). A role of the *cryptic* gene in the correct establishment of the left-right axis. Curr. Biol. 9, 1339-1342.

Germain, S., Howell, M., Esslemont, G. M. and Hill, C. S. (2000). Homeodomain and winged-helix transcription factors recruit activated Smads to distinct promoter elements via a common Smad interaction motif. Gene Dev. 14, 435-451.

Granier, C., Gurchenkov, V., Perea-Gomez, A., Camus, A., Ott, S., Papanayotou, C., Iranzo, J., Moreau, A., Reid, J., Koentges, G., Sabéran-Djoneidi, D. and Collignon, J. (2011). Nodal cis-regulatory elements reveal epiblast and primitive endoderm heterogeneity in the peri-implantation mouse embryo. Dev. Biol. 349, 350-362.

Gurdon, J. B., Harger, P., Mitchell, A. and Lemaire P. (1994). Activin signaling and response to a morphogen gradient. Nature 371, 487-492.

Gurdon, J.B., Mitchell, A., and Mahony, D. (1995). Direct and continuous assessment by cells of their position in a morphogen gradient. Nature 376, 520-521.

Hansen, C. S., Marion, C. D., Steele, K., George, S. and Smith, W. C. (1997). Direct neural induction and selective inhibition of mesoderm and epidermis inducers by Xnr3. Development 124, 483–492.

Harvey, S.A. and Smith, J.C. (2009). Visualisation and quantification of morphogen gradient formation in the zebrafish. PLoS Biol. 7, e1000101.

Hayhurst, M. and McConnell, S. K. (2003). Mouse models of holoprosencephaly. Curr. Opin. Neurol. 16, 135-141.

Henry, G. L. and Melton, D. A. (1998) *Mixer*, a homeobox gene required for endoderm development. Science 281, 91–96.

Hoodless, P. A., Pye, M., Chazaud, C., Labbé, E., Attisano, L., Rossant, J. and Wrana, J.L. (2001). FoxH1 (Fast) functions to specify the anterior primitive streak in the mouse. Gene. Dev. 15, 1257-1271.

Horne-Badovinac, S., Rebagliati, M. and Stainier, D. Y. (2003). A cellular framework for gut-looping morphogenesis in zebrafish. Science 302, 662-665.

Inman, G.J., Nicolás, F. J. and Hill C. S. (2002). Nucleocytoplasmic shuttling of Smads 2, 3, and 4 permits sensing of TGF-beta receptor activity. Mol. Cell 10, 283-294.

James, D., Levine, A. J., Besser, D., and Hemmati-Brivanlou, A. (2005). TGFβ/activin/nodal signaling is necessary for the maintenance of pluripotency in human embryonic stem cells. Development 132, 1273-1282.

Jennings, B. H. and Ish-Horowicz, D. (2008). The Groucho/TLE/Grg family of transcriptional co-repressors. Genome Biol. 9, 205.1-205.7.

Jennings, B. H., Pickles, L. M., Wainwright, S. M., Roe, S. M., Pearl, L. H. and Ish-Horowicz, D. (2006). Molecular recognition of transcriptional repressor motifs by the WD domain of the Groucho/TLE corepressor. Mol. Cell 22, 645-655.

Jiménez, G., Verrijzer, C. P. and Ish-Horowicz, D. (1999). A conserved motif in Goosecoid mediates Groucho-dependent repression in *Drosophila* embryos. Mol. Cell. Biol. 19, 2080-2087.

Jones, C. M., Kuehn, M. R., Hogan, B. L. M., Smith, J. C. and Wright, C. V. E. (1995). Nodal-related signals induce axial mesoderm and dorsalize mesoderm during gastrulation. Development 121, 3651-3662.

Joseph, E.M. and Melton, D. A. (1997). Xnr4: A Xenopus nodal-related gene expressed in the Spemann organizer. Dev. Biol. 184, 367–372.

Jullien, J. and Gurdon, J. (2005). Morphogen gradient interpretation by a regulated trafficking step during ligand-receptor transduction. Gene. Dev. 19, 2682-2694.

Koop, K. E., MacDonald, L., M. and Lobe, C. G. (1996). Transcripts of *Grg4*, a murine *Groucho*-related gene, are detected in adjacent tissues to other murine neurogenic gene homologues during embryonic development. Mech. Develop. 59, 73-87.

Kunwar, P. S., Zimmerman, S., Bennett, J. T., Chen, Y., Whitman, M. and Schier, A. F. (2003). Mixer/Bon and FoxH1/Sur have overlapping and divergent roles in Nodal signaling and mesendoderm induction. Development 130, 5589-5599.

Kurpios, N.A., Ibañes, M., Davis, N.M., Lui, W., Katz, T., Martin, J.F., Belmonte, J.C., and Tabin, C.J. (2008). The direction of gut looping is established by changes in the extracellular matrix and in cell:cell adhesion. PNAS 105, 8499-8506.

Kurth, T., Weiche, S., Vorkel, D., Kretschmar, S. and Menge, A. (2012). Histology of plastic embedded amphibian embryos and larvae. Genesis 50, 235-250.

Labbé, E., Sivestri, C., Hoodless, P. A., Wrana, J. L. and Attisano, L. (1998). Smad2 and Smad3 Positively and Negatively Regulate TGFb-Dependent Transcription through the Forkhead DNA-Binding Protein FAST2. Mol. Cell 2, 109-120.

Lei Y. , Guo X. , Liu Y. , Cao Y. , Deng Y. , Chen X. , Cheng C. H. , Dawid I. B. , Chen Y. and Zhao H. (2012). Efficient targeted gene disruption in Xenopus embryos using engineered transcription activator-like effector nucleases (TALENs). Proc Natl Acad Sci U S A. 109, 17484-17489.

Lenhart, K. F., Lin, S. Y., Titus, T. A, Postlethwait, J. H. and Burdine, R. D. (2001) Two additional midline barriers function with midline lefty1 expression to maintain asymmetric Nodal signaling during left-right axis specification in zebrafish. Development 138, 4405-4410.

Leon, C. and Lobe, C. G. (1997). *Grg3*, a murine *Groucho*-related gene, is expressed in the developing nervous system and in mesenchyme-induced epithelial structures. Dev. Dynam. 208, 11-24.

Leonard, M., Zhang, L., Zhai, N., Cader, A., Chan, Y., Nowak, R. B., Fowler, V. M., Menko, A. S. (2011). Modulation of N-cadherin junctions and their role as epicenters of differentiation-specific actin regulation in the developing lens. Dev. Biol. 349, 363-377.

Levin, M., Johnson, R. L., Stern, C. D., Kuehn, M. and Tabin, C. (1995). A Molecular Pathway Determining Left-Right Asymmetry in Chick Embryogenesis. Cell 82, 803-814.

Levin, M., Thorlin, T., Robinson, K. R., Nogi, T. and Mercola, M. (2002). Asymmetries in H^+/K^+-ATPase and Cell Membrane Potentials Comprise a Very Early Step in Left-Right Patterning. Cell 111, 77-89.

Licona, P., Chimal-Monroy, J. and Soldevila, G. (2006). Inhibins are the major Activin ligands expressed during early thymocyte development. Dev. Dyn. 235, 1124-1132.

Licona-Limón, P. and Soldevila, G. (2007). The role of TGF-beta superfamily during T cell development: new insights. Immunol. Lett. 109, 1-12.

Liu, B., Dou, C., Prabhu, L. and Lai, E. (1999). FAST-2 is a mammalian winged-helix protein which mediates transforming growth factor β signals. Mol. Cell. Biol. 19, 424-430.

Liu, C., Liu, W., Lu, M., Brown, N. A. and Martin, J. F. (2001). Regulation of left-right asymmetry by thresholds of Pitx2c activity. Development 128, 2039-2048.

Logan, M., Pagán-Westphal, S.M., Smith, D.M., Paganess,i L. and Tabin, C. J. (1998). The transcription factor Pitx2 mediates situs-specific morphogenesis in response to left-right asymmetric signals. Cell 94, 307-317.

Long, S., Ahmad, N. and Rebagliati, M. (2003). The zebrafish nodal-related gene southpaw is required for visceral and diencephalic left–right asymmetry. Development 130, 2303–2316.

Lowe, L. A., Supp, D. M., Sampath, K., Yokoyama, T., Wright, C. V. E., Potter, S. S., Overbeek, P. and Kuehn, M. R. (1996). Conserved left-right asymmetry of nodal expression and alterations in murine *situs inversus*. Nature 381, 158-161.

Lu, C. C., Brennan, J. and Robertson, E. J. (2001). From fertilization to gastrulation: axis formation in the mouse embryo. Curr. Opin. Genet. Dev. 11, 384-392.

Marjoram, L. and Wright, C. (2011). Rapid differential transport of Nodal and Lefty on sulfated proteoglycan-rich extracellular matrix regulates left-right asymmetry in *Xenopus*. Development 138, 475-485.

Marques, S., Borges, A. C., Silva, A. C., Freitas, S., Cordenonsi, M. and Belo, J.A. (2004). The activity of the Nodal antagonist Cerl-2 in the mouse node is required for correct L/R body axis. Genes Dev. 18, 2342-2347.

Massagué, J., Seoane, J. and Wotton, D. (2005). Smad transcription factors. Genes Dev. 19, 2783-2810.

McLin, V.A., Henning, S. J. and Jamrich, M. (2009). The role of the visceral mesoderm in the development of the gastrointestinal tract. Gastroenterology 136, 2074-2091.

Meno, C., Gritsman, K., Ohishi, S., Ohfuji, Y., Heckscher, E., Mochida, K., Shimono, A., Kondoh, H., Talbot, W. S., Robertson, E. J. et al. (1999). Mouse Lefty2 and zebrafish Antivin are feedback inhibitors of Nodal signaling during vertebrate gastrulation. Mol. Cell 4, 287-298.

Meno, C., Saijoh, Y., Fujii, H., Ikeda, M., Yokoyama, T. Yokoyama, M., Toyoda, Y. and Hamada, H. (1996). Left-right asymmetric expression of the TGFβ-family member *lefty* in mouse embryos. Nature. 381, 151-155.

Meno, C., Shimono, A., Saijoh, Y., Yashiro, K., Mochida, K., Ohishi, S., Noji, S., Kondoh, H. and Hamada, H. (1998). *Lefty-1* is required for left-right determination as a regulator of *lefty-2* and *nodal*. Cell 94, 287-297.

Meno, C., Takeuchi, J., Sakuma, R., Koshiba-Takeuchi, K., Ohishi, S., Saijoh, Y., Miyazaki, J., ten Dijke, P., Ogura, T. and Hamada, H. (2001). Diffusion of Nodal signaling activity in the absence of the feedback inhibitor Lefty2. Dev. Cell 1, 127-138.

Mine, N., Anderson, R. M. and Klingensmith, J. (2008). BMP antagonism is required in both the node and lateral plate mesoderm for mammalian left-right axis establishment. Development 135, 2425-2434.

Morckel, A.R., Lusic, H., Farzana, L., Yoder, J. A., Deiters, A. and Nascone-Yoder, N. M. (2012). A

photoactivatable small-molecule inhibitor for light-controlled spatiotemporal regulation of Rho kinase in live embryos. Development 139, 437-442.

Moustakas, A. and Heldin, C. (2009). The regulation of TGFβ signal transduction. Development 136, 3699-3714.

Muller, J.K., Prather, D.R., and Nascone-Yoder, N.M. (2003). Left-right asymmetric morphogenesis in the *Xenopus* digestive system. Dev. Dynam. 228, 672-682.

Müller, P., Rogers, K. W., Jordan, B. M., Lee, J. S., Robson, D., Ramanathan, S. and Schier, A. F. (2012). Differential diffusivity of Nodal and Lefty underlies a reaction-diffusion patterning system. Science 336, 721-724.

Nakamura, T. and Hamada, H. (2012). Left-right patterning: conserved and divergent mechanisms. Development 139, 3257-3262.

Nakamura, T., Saito, D., Kawasumi, A., Shinohara, K., Asai, Y., Takaoka, K., Dong, F., Takamatsu, A., Belo, J.A., Mochizuki, A. and Hamada, H. (2012). Fluid flow and interlinked feedback loops establish left-right asymmetric decay of Cerl2 mRNA. Nat. Commun. 3:1322. doi: 10.1038/ncomms2319.

Nakamura, T., Mine, N., Nakaguchi, E., Mochizuki, A., Yamamoto, M., Yashiro, K., Meno, C. and Hamada, H. (2006). Generation of robust left-right asymmetry in the mouse embryo requires a self-enhancement and lateral-inhibition system. Dev. Cell 11, 495-504.

Nakayama T., Fish M. B., Fisher M., Oomen-Hajagos J., Thomsen G. H. and Grainger R.M. (2013). Simple and efficient CRISPR/Cas9-mediated targeted mutagenesis in Xenopus tropicalis. Genesis 51, 835-843.

Nandadasa, S., Tao, Q., Menon, N.R., Heasman, J. and Wylie, C. (2009). N- and E-cadherins in Xenopus are specifically required in the neural and non-neural ectoderm, respectively, for F-actin assembly and morphogenetic movements. Development 136, 1327-1338.

Nieuwkoop, P. D. and Faber, J. (1967). Normal table of *Xenopus Laevis*. Amsterdam, The Netherlands: North Holland Publishing Co.

Norris, D. P. and Robertson, E. J. (1999). Asymmetric and node-specific nodal expression patterns are controlled by two distinct cis-acting regulatory elements. Genes Dev. 13, 1575-1588.

Norris, D. P., Brennan, J., Bikoff, E. K. and Robertson, E. J. (2002). The Foxh1-dependent autoregulatory enhancer controls the level of Nodal signals in the mouse embryo. Development 129, 3455-3468.

Oh, S. P. and Li, E. (1997). The signaling pathway mediated by the type IIB activin receptor controls axial patterning and lateral asymmetry in the mouse. Genes Dev 11, 1812–1826.

Ohi, Y. and Wright, C. V. E. (2007). Anteriorward shifting of asymmetric *Xnr1* expression and contralateral communication in left-right specification in *Xenopus*. Dev. Biol. 301, 447-463.

Okada, Y., Takeda, S., Tanaka, Y., Izpisúa Belmonte, J. C. and Hirokawa, N. (2005). Mechanism of nodal flow: a conserved symmetry breaking event in left-right axis determination. Cell 121, 633-44.

Oki, S., Hashimoto, R., Okui, Y., Shen, M. M., Mekada, E., Otani, H., Saijoh, Y. and Hamada, H. (2007). Sulfated glycosaminoglycans are necessary for Nodal signal transmission from the node to the left lateral plate in the mouse embryo. Developmnet 134, 3893-3904.

Okumura, T., Fujiwara, H., Taniguchi, K., Kuroda, J., Nakazawa, N., Nakamura, M., Hatori, R., Ishio, A., Maeda, R. and Matsuno, K. (2010). Left-right asymmetric morphogenesis of the anterior midgut depends on the activation of a non-muscle myosin II in Drosophila. Dev. Biol. 344, 693-706.

Osada, S., Saijoh, Y., Frisch, A., Yeo, C., Adachi, H., Watanabe, M., Whitman, M., Hamada, H. and Wright, C. V. E. (2000). Activin/Nodal responsiveness and asymmetric expression of a *Xenopus nodal*-related gene converge on a FAST-regulated module in intron 1. Development 127, 2503-2514.

Papanayotou, C., Benhaddou, A., Camus, A., Perea-Gomez, A., Jouneau, A., Mezger, V., Langa, F., Ott, S., Sabéran-Djoneidi, D. and Collignon, J. (2014). A novel *Nodal* enhancer dependent on pluripotency factors and Smad2/3 signaling conditions a regulatory switch during epiblast maturation. PLoS Biol. 12, e1001890.

Patel, S. R., Bhumbra, S. S., Paknikar, R. S. and Dressler, G. R. (2012). Epigenetic mechanisms of Groucho/Grg/TLE mediated transcriptional repression. Mol. Cell 45, 1-11.

Perea-Gomez, A., Vella, F. D. J., Shawlot, W., Oulad-Abdelghani, M., Chazaud, C., Meno, C., Pfister, V., Chen, L., Robertson, E., Hamada, H. et al. (2002). Nodal antagonists in the anterior visceral endoderm prevent the formation of multiple primitive streaks. Dev. Cell 3, 745-756.

Persson, U., Izumi, H., Souchelnytskyi, S., Itoh, S., Grimsby, S., Engström, U., Heldin, C. H., Funa, K. and ten Dijke, P. (1998). The L45 loop in type I receptors for TGF-beta family members is a critical determinant in specifying Smad isoform activation. FEBS Lett. 434, 83-87.

Piedra, M. E., Icardo, J. M., Albajar, M., Rodriguez-Rey, J. C. and Ros, M. A. (1998). Pitx2 participates in the late phase of the pathway controlling left-right asymmetry. Cell 94, 319-324.

Plageman, T.F. Jr., Zacharias, A. L., Gage, P. J. and Lang, R. A. (2011). Shroom3 and a Pitx2-N-cadherin pathway function cooperatively to generate asymmetric cell shape changes during gut morphogenesis. Dev. Biol. 357, 227-234.

Randall, R. A., Germain, S., Inman, G. J., Bates, P. A. and Hill, C. S. (2002). Different Smad2 partners bind a common hydrophobic pocket in Smad2 via a defined proline-rich motif. EMBO 21, 145-156.

Ramsdell, A. F. and Yost, H. J. (1999). Cardiac looping and the vertebrate left-right axis: antagonism of left-sided Vg1 activity by a right-sided ALK2-dependent BMP pathway. Development 126, 5195-5205.

Reid, C. D., Steiner, A. B., Yaklichkin, S., Lu, Q., Wang, S., Hennessy, M. and Kessler, D. S. (2014). FoxH1 mediates a Grg4 and Smad2 dependent transcriptional switch in Nodal signaling during *Xenopus* mesoderm development. Under review.

Robertson, E. J. (2014). Dose-dependet Nodal/Smad signals pattern the early mouse embryo. Semin. Cell Dev. Biol. (in press).

Rodriguez, C. I., Buchholz, F., Galloway, J., Sequerra, R., Kasper, J., Ayala, R., Stewart, A. F. and Dymecki, S. M. (2000). High-efficiency delete mice show that FLPe is an alternative to Cre-loxP. Nat. Genet. 25, 139-140.

Ryan, A.K., Blumberg, B., Rodriguez-Esteban, C., Yonei-Tamura, S., Tamura, K., Tsukui, T., de la Peña, J., Sabbagh, W., Greenwald, J., Choe, S., Norris, D.P., Robertson, E.J., Evans, R.M.,

Rosenfeld, M.G., and Belmonte, J.C. (1998). Pitx2 determines left-right asymmetry of internal organs in vertebrates. Nature 394, 545-551.

Saijoh, Y., Adachi, H., Mochida, K., Ohishi, S., Hirao, A. and Hamada, H. (1999). Distinct transcriptional regulatory mechanisms underlie left-right asymmetric expression of *lefty-1* and *lefty-2*. Genes Dev. 13, 259-269.

Saijoh, Y., Adachi, H., Sakuma, R., Yeo, C., Yashiro, K., Watanabe, M., Hashiguchi, H., Mochida, K., Ohishi, S., Kawabata, K. et al. (2000). Left-Right asymmetric expression of *lefty2* and *nodal* is induced by a signaling pathway that includes the transcription factor FAST2. Mol. Cell 5, 35-47.

Saijoh, Y., Oki, S., Tanaka, C., Nakamura, T., Adachi, H., Yan, Y., Shen, M. M. and Hamada, H. (2005). Two Nodal-responsive enhancers control left-right asymmetric expression of *Nodal*. Dev. Dynam. 232, 1031-1036.

Saka, Y., Hagemann, A.I., Pipenburg, O., and Smith, J.C. (2007). Nuclear accumulation of Smad complexes occurs only after the midblastula transition in *Xenopus*. Development 134, 4209-4218.

Sampath, K., Rubinstein, A. L., Cheng, A. M., Liang, J. O., Fekany, K., Solnica-Krezel, L., Korzh, V., Halpern, M.E. and Wright C. V. (1998). Induction of the zebrafish ventral brain and floorplate requires cyclops/nodal signalling. Nature 395, 185–189.

Schier, A. F. (2009). Nodal morphogens. Cold Spring Harb. Perspect. Biol. 1(5):a003459.

Schier, A. F. and Shen, M. M. (1999). Nodal signaling in vertebrate development. Nature 403, 385-389.

Schohl, A. and Fagotto, F. (2002). B-catenin, MAPK and Smad signaling during early *Xenopus* development. Development 129, 37-52.

Schweickert, A., Campione, M., Steinbeisser, H. and Blum, M. (2000). Pitx2 isoforms: involvement of Pitx2c but not Pitx2a or Pitx2b in vertebrate left-right asymmetry. Mech. Dev. 90, 41-51.

Shen, M. M. and Schier, A. F. (2000). The EGF-CFC gene family in vertebrate development. Trends Genet. 16, 303-309.

Shi, Y. and Massagué, J. (2003). Mechanisms of TGF-β Signaling Review from Cell Membrane to the Nucleus. Cell 133, 658-700.

Shinohara, K., Kawasumi, A., Takamatsu, A., Yoshiba, S., Botilde, Y., Motoyama, N., Reith, W., Durand, B., Shiratori, H. and Hamada, H. (2012). Two rotating cilia in the node cavity are sufficient to break left-right symmetry in the mouse embryo. Nat. Commun. 3:622. doi: 10.1038/ncomms1624.

Shiratori, H., Sakuma, R., Watanabe, M., Hashiguchi, H., Mochida, K., Sakai, Y., Nishino, J. Saijoh, Y., Whitman, M. and Hamada, W. (2001). Two-step regulation of left-right asymmetric expression of *Pitx2*: initiation by Nodal signaling and maintenance by Nkx2. Mol. Cell 7, 137-149.

Simpson, E. H., Johnson, D. K., Hunsicker, P., Suffolk, R., Jordan, S. A. and Jackson, I. J. (1999). The mouse *Cer1* (*Cerberus related* or *homologue*) gene is not required for anterior pattern formation. Dev. Biol. 213, 202-206.

Smith, W. C., McKendry, R., Ribisi, S. and Harland, R. M. (1995). A *nodal*-related gene defines a physical and functional domain within the Spemann organizer. Cell 82, 37-46.

Spiller, C. M., Feng, C., Jackson, A., Gillis, J. M., Rolland, A. D., Looijenga, L. H. J., Koopman, P. and Bowles, J. (2012). Endogenous Nodal signaling regulates germ cell potency during mammalian testis development. Development 139, 4123-4132.

Stephen, L. A., Johnson, E. J., Davis, G. M., McTeir, L., Pinkham, J., Jaberi, N. and Davey, M. G. (2014). The chicken left right organizer has nonmotile cilia which are lost in a stage-dependent manner in the talpid(3) ciliopathy. Genesis 52, 600-613.

Strizzi, L., Hardy, K. M., Kirschmann, D. A., Ahrlund-Ritchter, L. and Hendrix, M. J. C. (2012). Nodal expression and detection in cancer: Experience and Challenges. Cancer Res. 72, 1915-1920.

Takahashi, S., Yokota, C., Takano, K., Tanegashima, K., Onuma, Y., Goto, J. and Asashima, M. (2000). Two novel nodal-related genes initiate early inductive events in Xenopus Nieuwkoop center. Development 127, 5319–5329.

Tanaka, C., Sakuma, R., Nakamura, T., Hamada, H. and Saijoh, Y. (2007). Long-range action of Nodal requires interaction with GDF1. Genes Dev. 21, 3272-3282.

Vincent, S. D., Dunn, N. R., Hayashi, S., Norris, D. P. and Robertson, E. J. (2003). Cell fate decisions within the mouse organizer are governed by graded Nodal signals. Genes Dev. 17, 1646-1662.

Viotti, M., Niu, L., Shi, S.H. and Hadjantonakis, A. K. (2012). Role of the gut endoderm in relaying left-right patterning in mice. PLoS Biol. 10(3):e1001276.

Waldrip, W. R., Bikoff, E. K., Hoodless, P. A., Wrana, J. L. and Robertson, E. J. (1998). Smad2 signaling in extraembryonic tissues determines anterior-posterior polarity of the early mouse embryo. Cell 92, 797-808.

Watabe, T. and Miyazono, K. (2009). Roles of TGF-β family signaling in stem cell renewal and differentiation. Cell Res. 19, 103-115.

Wei, Q. and Adelstein, R.S. (2002). Pitx2a espression alters actin-myosin cytoskeleton and migration of HeLa cells through Rho GTPase signaling. Mol. Biol. Cell 13, 683-697.

Weisberg, E., Winnier, G. E., Chen, X., Farnsworth, C. L., Hogan, B. L. H. and Whitman, M. (1998). A mouse homologue of FAST-1 transduces TGFβ superfamily signals and is expressed during early embryogenesis. Dev. Dynam. 79, 17-27.

Welsh, I.C., Thomsen, M., Gludish, D.W., Alfonso-Parra, C., Bai, Y., Martin, J. F. and Kurpios, N.A. (2013). Integration of left-right Pitx2 transcription and Wnt signaling drives asymmetric gut morphogenesis via Daam2. Dev. Cell 26, 629-644.

Wheat, J. C., Krause, D. S., Shin, T. H., Chen, X., Wang, J., Ding, D., Yamin, R. and Sweetser, D. A. (2014). The corepressor Tle4 is a novel regulator of murine hematopoiesis and bone development. PLoS One 9(8):e105557.

Whitman, M. (2001). Nodal Signaling in Early Vertebrate Review Embryos: Themes and Variations. Dev. Cell 1, 605-617.

Wrana, J. L. (2002). Phosphoserine-dependent regulation of protein-protein interactions in the Smad pathway. Structure 10, 5-7.

Wrana, J. L. and Attisano, L. (2000). The Smad pathway. Cytokine Growth F. R. 11, 5-13.

Wu, J. W., Hu, M., Chai, J., Seoane, J., Huse, M., Li, C., Rigotti, D. J., Kyin, S., Muir, T. W., Fairman, R., Massagué, J. and Shi, Y. (2001). Crystal structure of a phosphorylated Smad2. Recognition of phosphoserine by the MH2 domain and insights on Smad function in TGF-beta signaling. Mol. Cell 8, 1277-1289.

Wu, M. Y. and Hill, C. S. (2009). TGF-β superfamily signaling in embryonic development and homeostasis. Dev. Cell 16, 329-343.

Xu, C., Liguori, G., Persico, M. G. and Adamson, E. D. (1999). Abrogation of the Cripto gene in mouse leads to failure of postgastrulation morphogenesis and lack of differentiation of cardiomyocytes. Development 126, 483-494.

Yaklichkin, S., Vekker, A., Stayrook, S., Lewis, M. and Kessler, D. S. (2007a). Prevalence of the EH1 Groucno interaction motif in the metazoan Fox family of transcriptional regulators. BMC Genomics 8, 1-17.

Yaklichkin, S., Steiner, A. B., Lu, Q. and Kessler, D. S. (2007b). FoxD3 and Grg4 physically interact to repress transcription and induce mesoderm in *Xenopus*. J. Biol. Chem. 282, 2548-2557.

Yamamoto, M., Meno, C., Sakai, Y. Shiratori, H., Mochida, K., Ikawa, Y., Saijoh, Y. and Hamada, H. (2001). The transcription factor FoxH1 (FAST) mediates Nodal signaling during anterior-posterior patterning and node formation in the mouse. Genes. Dev. 15, 1242-1256.

Yamamoto, M., Mine, N., Mochida, K., Sakai, Y., Saijoh, Y., Meno, C. and Hamada, H. (2003). Nodal signaling induces the midline barrier by activating *Nodal* expression in the lateral plate. Development 130, 1795-1804.

Yan, Y., Gritsman, K., Ding, J., Burdine, R. D., Corrales, J. D., Price, S. M., Talbot, W. S., Schier, A. F. and Shen, M. M. (1999). Conserved requirement for *EGF-CFC* genes in vertebrate left-right axis formation. Genes Dev. 13, 2527-2537.

Yan, Y., Liu, J., Luo, Y., E, C., Haltiwanger, R. S., Abate-Shen, C. and Shen, M. M. (2002). Dual Roles of Cripto as a Ligand and Coreceptor in the Nodal Signaling Pathway. Mol. Cell. Biol. 22, 4439-4449.

Yang, Z., Roberts, E. A. and Goldstein, L., S., B. (2001). Functional analysis of mouse C-terminal kinesin motor KifC2. Mol. Cell. Biol. 21, 2463-2466.

Yeo, C. and Whitman, M. (2001). Nodal Signals to Smads through Cripto-Dependent and Cripto-Independent Mechanisms. Mol. Cell 7, 949-957.

Yoshiba, S., Shiratori, H., Kuo, I. Y., Kawasumi, A., Shinohara, K., Nonaka, S., Asai, Y., Sasaki, G., Belo, J. A., Sasaki, H., Nakai, J., Dworniczak, B., Ehrlich, B. E., Pennekamp, P. and Hamada H. (2012). Cilia at the node of mouse embryos sense fluid flow for left-right determination via Pkd2. Science 338, 226-231.

Yost, H. J. (1990). Inhibition of proteoglycan synthesis eliminates left-right asymmetry in Xenopus laevis cardiac looping. Development 110, 865-874.

Young, J. J. and Harland, R. M. Targeted gene disruption with engineered zinc-finger nucleases (ZFNs).

Yu, X., St Amand, T. R., Wang, S., Li, G., Zhang, Y., Hu, Y. P., Nguyen, L., Qiu, M.S. and Chen, Y. P. (2001). Differential expression and functional analysis of Pitx2 isoforms in regulation of heart looping in the chick. Development 128, 1005-1013.

Zakin, L., Reversade, B., Virlon, B., Rusniok, C., Glaser, P., Elelouf, J. and Brûlet, P. (2000). Gene expression profiles in normal and *Otx2*$^{-/-}$ early gastrulating mouse embryos. P. Natl. Acad. Sci. USA. 97, 14388-14393. Methods Mol Biol. 917, 129-141.

Zhang, J. et al. (1998). The role of maternal VegT in establishing the primary germ layers in *Xenopus* embryos. Cell 94, 515–524.

Zhou, X., Sasaki, H., Lowe, L., Hogan, B. L. M. and Kuehn, M. R. (1993). *Nodal* is a novel TGF-β-like gene expressed in the mouse node during gastrulation. Nature 361, 543-547.

Zhu, Y., Richardson, J. A., Parada, L. F. and Graff, J. M. (1998). *Smad3* Mutant Mice Develop Metastatic Colorectal Cancer. Cell 94, 703-714.